JOINT INSTITUTE FOR AERONAUTICS AND ACOUSTICS

National Aeronautics and
Space Administration
Ames Research Center

JIAA TR - 97

Stanford University

NCC2-55

Controlled Vortical Flow on Delta Wings Through Unsteady Leading Edge Blowing

By

K. T. Lee and Leonard Roberts

Stanford University
Department of Aeronautics and Astronautics
Stanford, CA 94305

January 1990

ABSTRACT

The vortical flow over a delta wing contributes an important part of the lift - the so called nonlinear lift. Controlling this vortical flow with its favorable influence would enhance aircraft maneuverability at high angle of attack. Several previous studies have shown that control of the vortical flow field is possible through the use of blowing jets. The present experimental research studies vortical flow control by applying a new blowing scheme to the rounded leading edge of a delta wing; this blowing scheme is called "Tangential Leading Edge Blowing(TLEB)". Vortical flow response both to steady blowing and to unsteady blowing is investigated. It is found that TLEB can redevelop stable, strong vortices even in the post-stall angle of attack regime. Analysis of the steady data shows that the effect of leading edge blowing can be interpreted as an "effective change in angle of attack". The examination of the fundamental time scales for vortical flow re-organization after the application of blowing for different initial states of the flow field is studied. Different time scales for flow re-organization are shown to depend upon the effective angle of attack. A faster response time can be achieved at angles of attack beyond stall by a suitable choice of the initial blowing momentum strength. Consequently, TLEB shows the potential of controlling the vortical flow over a wide range of angles of attack; i.e. in both for pre-stall and post-stall conditions.

TABLE OF CONTENTS

-

LIST OF FIGURES

LIST OF TABLES

NOMENCLATURE

A_j	blowing slot area
c	wing root chord
C_L	wing lift coefficient
C_N	wing normal force coefficient
C_n	sectional normal force coefficient
C_l	sectional rolling moment coefficient
$\tilde{C}_n$	upper surface sectional normal force coefficient
$\tilde{C}_{n_v}$	upper surface sectional normal force coefficient by the vortex contribution
$\tilde{C}_l$	upper surface sectional rolling moment coefficient
$\tilde{C}_{l_v}$	upper surface sectional rolling moment coefficient by the vortex contribution
$\tilde{C}_n^*$	maximum upper surface sectional normal force coefficient
$\tilde{C}_{n_o}^*$	maximum upper surface sectional normal force coefficient without blowing
$\tilde{C}_{n_v}^*$	maximum upper surface sectional normal force coefficient by the vortex contribution with blowing

$\tilde{C}_{n_{v_o}}$	upper surface sectional normal force coefficient by the vortex contribution without blowing
$\tilde{C}_{n_{linear}}$	upper surface sectional normal force coefficient of the attached (or linear) flow contribution
$\tilde{C}_{l_{linear}}$	upper surface sectional rolling moment coefficient of the attached (or linear) flow contribution
$C_{p_{linear}}$	upper surface averaged pressure coefficient of the attached (or linear) flow contribution
C_p	pressure coefficient
c_p	specific heat of air at constant pressure
C_μ	blowing momentum coefficient
$C_{\mu i}$	initial blowing momentum coefficient during transient blowing
$C_{\mu f}$	final blowing momentum coefficient during transient blowing
$\dot{C}_\mu$	rate of blowing momentum coefficient change with time
$\dot{m}$	mass flow rate from the blowing slot
P_a	static air pressure far from the model in the test section
P_i	gauge pressure at model plenum
q_∞	free stream dynamic pressure
R	gas constant
R_e	Reynolds number
s	wing semi-span
S_{ref}	wing reference area (semi-span planform area)

T_a	air temperature far from the model in the test section
T_i	air temperature at model plenum
t	time
U_∞	free stream speed
V_j	jet velocity from the blowing slot
x,y,z	Cartesian coordinates fixed relative to the apex of the wing

α	angle of attack
α_g	geometric angle of attack
α_e	vortex effective angle of attack
α^*	angle of attack at maximum normal force
$\alpha_o{}^*$	angle of attack at maximum normal force without blowing
ϵ	semi-apex angle of delta wing
γ	ratio of specific heats
Γ	vortex strength
π	3.141592654.....
ρ_∞	free stream density
τ	time constant

CHAPTER 1
INTRODUCTION

1.1 General Background

The advent of the delta wing three decades ago has enabled aircraft to perform efficiently at supersonic cruise conditions while retaining acceptable low speed performance. The higher level of lift achieved by the delta wing has also allowed greater maneuverability and has extended the limits of the flight envelope for combat aircraft. It is known that the short range combat capabilities of military fighter aircraft strongly depend on their unsteady maneuver performance in the low subsonic speed regime[1]. Maneuvers typically include operations at angles of attack beyond the point of maximum lift. The low aspect ratio delta planform wing is typical of that used for such highly maneuverable aircraft, and consequently there has been considerable interest in the development of aerodynamic techniques to enhance the controllability of aircraft of this planform, particularly in the context of subsonic post-stall maneuverability.

The aerodynamic performance of delta wings is enhanced by the presence of large scale organized vortices on the leeward side of the wing which occur at moderate to high angles of attack. Thus, leading edge separation and the resulting development of strong, stable leading edge vortices over the wing is desirable at high angles of attack. However, for slender delta wings, two types of high angle of attack problems occur due to separation: leading edge vortex breakdown (or burst) and the occurrence of asymmetric leading edge vortices[2,3,4,5] before vortex

breakdown. Both these phenomena can cause abrupt changes of the wing aerodynamic coefficients. The vortex asymmetry on the wing may take the form of non-symmetric vortex burst locations leading to asymmetric forces and moments on the wing. As the angle of attack increases beyond the stall angle, the vortex flow ceases to be organized and steady and is replaced by unsteady shedding. This causes a loss in lift and the onset of unsteady loads and moments on the wing.

At this point, it is useful to review the flow regimes for a delta wing as a function of angle of attack[6] to provide some understanding of the performance envelope. The flow pattern about a delta wing can, in general, be classified into four regimes as follows:

(I) At very low angle of attack, the flow on the leeward side of the wing remains attached and vortex-free. The lift increases linearly with angle of attack.

(II) At moderate to high angles of attack, the boundary layer on the lower surface flows outward and separates at the leading edge resulting in a free shear layer. This free shear layer rolls up in a spiral fashion to form a pair of vortices on the leeward side of the wing, figure 1.1. These vortices are characterized by being both stable and symmetric. A noticeable difference with regime (I), as illustrated in figure 1.2, is that the lift increases nonlinearly as angle of attack increases, due to the additional low pressure on the wing upper surface induced by the leading edge vortices. This is the so-called "non-linear lift".

(III) At very large angles of attack, breakdown of the vortex structure moves upstream and can pass the trailing edge. Position of vortex breakdown depends on the apex angle of the wing as well as angle of

attack. It may be accompanied by an asymmetric and unsteady flow pattern. An indication of vortex breakdown is an abrupt increase in the cross-sectional area of the vortex and the turbulence level within the vortex core. We can also have asymmetric, unburst vortices at these angles of attack in the case of a very slender delta wing. With further increase in angle of attack, the vortex breakdown progresses further upstream and eventually the vortex system is burst over the entire wing. The adverse effects of both vortex breakdown and asymmetric vortices result in large, unfavorable changes in forces and moments on the wing, and thereby lead to loss of control.

(IV) At extremely large angles of attack (up to 90^{o}), the flow on the leeward side is characterized by an unsteady wake and periodic vortex shedding. As a result, the forces acting on the wing are very unpredictable.

Highly maneuverable aircraft operate primarily in the flow regimes (II) and (III), where the "non-linear" vortex lift can be used to aerodynamic advantage. Since the vortex flow for a delta wing plays such an important role in determining lift in these flow regimes, it is desirable to control these vortices and thereby enhance the controllability and maneuverability of the aircraft.

Previous studies[7-19,24] have shown that control of the vortex flow field is possible through the use of blowing jets. A number of blowing techniques have been investigated, each technique having its own advantages and disadvantages. Partial success in delaying the occurrence of the vortex burst and improving both lift and controllability has been achieved with these techniques.

1.2 Previous Work

Recent studies conducted at Stanford University have shown promise in achieving vortical flow control by applying a new blowing scheme to the rounded leading edge of a delta wing; this blowing scheme is called "Tangential Leading Edge Blowing(TLEB)". However, before discussing the detailed aspects of TLEB, previous work on other blowing schemes will be briefly reviewed in this section. The blowing techniques that have been studied in the past may be categorized as follows: (a) spanwise blowing from the leading edge, (b) blowing parallel to the leading edge, (c) core blowing and (d) tangential leading edge blowing. This terminology is used here to clarify the different concepts and distinguish the means by which they attempt to modify and control the flow field. Figure 1.3 shows a schematic of each blowing scheme.

1.2.1 Spanwise blowing from the leading edge

First attempts to modify the leading edge vortex flow on delta wings by blowing employed spanwise blowing[7,8,9,10]. A blowing slot extends along each leading edge of the delta wing and the blowing air is ejected in the spanwise direction (see figure 1.3a). As a result, thin jet sheets are formed which emanate from each leading edge of the wing in the plane of the wing. Experimental tests have been conducted by Alexander(19-63), Trebble(1966) and Spillman and Goodridge(1972) on the effects of this type of blowing.

Alexander[7,8] conducted a series of experiments on a 70^{o} swept delta wing and a cropped delta wing with blowing for $\alpha = 0^{o}$ to 25^{o}. The results

revealed that this form of blowing increases the size and strength of the leading edge vortices and moves the core outboard and upward. The increase in lift was mainly due to an increase in the nonlinear vortex contribution. In addition, suppression of the secondary separation through entrainment of the leading edge jet was observed in the experiment.

Preliminary experiments by Trebble[9] on a 70^{o} swept delta wing in the angle of attack range of 0^{o} to 16.4^{o} have also shown that lift gains are obtainable by ejecting a high momentum jet in the spanwise direction from the leading edge of the wing. The lift was measured by a force-balance and the results demonstrated that there was no appreciable Reynolds number effect in the range from 10^{5} to 10^{6}. Five different jet slot shapes were tested and the optimum slot shape proved to be a tapered slot; this was expected to give a momentum distribution consistent with the preservation of conical flow.

These experiments on the effects of spanwise blowing have shown that a lift increment was possible for moderate angles of attack. But large drag penalties resulted if the jet was not directed with the minimum possible forward component and the increments in lift coefficient were much smaller than expected. At low angle of attack, the lift gains were less than the applied blowing momentum. Lift increments with spanwise blowing result from increasing the size and strength of the leading edge vortices at a given angle of attack and corresponds to an effective enlargement of the wing span. However, the blowing also causes vortex breakdown at a lower angle of attack. The angle of attack envelope of the wing is thereby reduced and it is, therefore, not a desirable technique in terms of improving maneuverability.

1.2.2 Blowing parallel to the leading edge

More positive results have been obtained when the jet was ejected in a direction parallel to the leading edge [11,12,13,14,15,16]. The blowing nozzle is located over the wing's upper surface at the junction of wing and fuselage or at some point on the wing leading edge(see figure 1.3b). The basic idea was that the high-speed jet could provide suction on the upper surface of the wing because of its entrainment effects. In other words, blowing a high velocity jet parallel to the leading edge would cause the flow to act like a line sink parallel to the leading edge. Therefore, it can maintain the attachment of the vortex to the wing surface and avoid vortex burst.

Experiments were conducted by Bradley and Wray[11] on half-span flat plate models to study blowing as a means of lift enhancement. Four possible benefits of leading edge blowing were outlined. First, an increase in vortex lift could be obtained by an augmentation of the natural vortex lift on highly swept wings and aid in vortex formation on wings with little or no vortex flow present. Second, vortex breakdown could be delayed, which would improve buffet characteristics. Third, an improvement in directional stability was possible by avoiding the adverse effects of vortex breakdown in the vicinity of the vertical and horizontal tail surfaces. Finally, an increase in the effective aspect ratio, due to the blowing, would increase the lift. Their tests were conducted on a half-span, 60^0-swept, flat plate delta wing. A convergent nozzle was used to direct the air jet. Nozzle position was held at one nozzle diameter above the wing surface. Preliminary tests suggested that a chordwise location of 0.1 chord and a direction parallel to the leading edge as the best position. Angle of incidence was varied from 5^0 to 30^0 at a Mach

number of 0.3 and a Reynolds number of 1.8×10^5 per foot. Flow visualization revealed a tightening of the core and quite large increases in the vortex lift were seen from the force balance data.

Campbell[12,13] investigated the effects of blowing on a trapezoidal wing-body model. Experimental force and pressure data were obtained at a Mach number of about 0.2 for sweep angles of 30^o and 45^o. Full vortex suction lift in terms of Polhamus' suction analogy[23] was achieved with low rates of blowing, but an increase in the blowing rate was required at increased spanwise locations to maintain the same lift increments. Smaller sweep angles showed a larger lift gain, presumably since highly swept wings already have a well developed vortex flow. Increases of the blowing rate decreased the lifting efficiency of the blowing scheme, however this trend of decreasing efficiency is typical of most jet augmentation systems. That this is attributed to jet decay (the effects of the jet decrease substantially away from the nozzle exit) is suggested, implying that the vortex development and resulting incremental lift are very dependent upon the local jet properties, vortex flow properties, and even the free stream velocity. Blowing was also seen to improve the drag polars, by increasing the maximum lift to drag ratio, and to extend the linear pitching moment to higher lift. The objective of these leading edge blowing schemes was to artificially induce spanwise flow gradients similar to those that appear naturally on highly swept wings[20,21,22,23]. The flow gradients resulting from this blowing scheme are favorable for the formation and control of leading edge vortices[24].

Anglin et al.[14] conducted an investigation very similar to Campbell's to determine the effects of leading edge blowing on two configurations representative of current fighter airplanes with 60^0 leading edge sweep. The wind tunnel tests included measurement of static

and forced oscillation aerodynamic data, and visualization of the airflow changes over the wing created by the leading edge blowing. The results indicated that the use of leading edge blowing created and/or enhanced vortex lift at moderate-to-high angles of attack, and increased the maximum lift coefficient but did not affect the angle of attack at which maximum lift occurred. Use of blowing inhibited a wing rock experienced by the basic configuration at about 20^0 angle of attack.

Iwanski[15] investigated the vortex flow field over a 70^o delta wing, with external jet blowing parallel to and at the leading edge, visually and quantitatively. The jet blowing moved vortex breakdown farther downstream from its natural position and influenced the characteristics of the breakdown. The outer core swirl angle was 40^o at vortex breakdown for both the natural flow and with jet blowing. The blowing jet was entrained into the outer vortical flow, which increased the overall size of the vortex and decreased the peak velocity components. The relative strength of the vortex was reduced by the jet blowing and thus led to a delay in breakdown.

Visser[16] performed a wind-tunnel evaluation to quantify the effects of a jet on the leading edge vortices generated by a 70^o-swept, sharp edged delta wing at low Reynolds numbers. Effects were made to optimize the jet nozzle position with respect to maximum lift increments. Two angles of attack were investigated, 30^o and 35^o, at Reynolds numbers of $1.5x10^5$ and $2.0x10^5$. Aerodynamic enhancement, including lift and drag gains of about 20% and 17% respectively, were measured. Results indicate an optimum jet nozzle location to be close to the leading edge, tangent to the upper wing surface and in a direction aligned parallel to the leading edge. Nozzle interference effects, especially near the apex, were not negligible.

1.2.3. Core blowing

The third blowing scheme is "core blowing"[4]. A jet from a blowing nozzle, located at or near the wing apex, is ejected in the vortex core direction(see figure 1.3c). The problem with this scheme is that the blowing direction, i.e., the core direction, must be pre-determined before blowing is applied.

Qualitative results from Malcolm et al.[4] on blowing to enhance leading edge extension(LEX) vortices indicate that effective breakdown position control cannot be fully achieved by disturbing the vortex core at the leading edge extension apex. Manipulation of the vortex downstream, after it was fully formed, seemed to be most effective, since continual vortex generation along the leading edge extension surface tends to overcome any disturbance initiated at the apex.

1.2.4 Tangential leading edge blowing

In most cases the primary effects of blowing have been; to delay the occurrence of the burst phenomenon, to re-energize the vortex, to stabilize its position or to control vortical asymmetries. Generally, the techniques have required some advance information on the position of the vortex, and the amounts of blowing required have been significant. Previous blowing schemes, i.e., spanwise or leading edge blowing, tried to modify the inviscid vortex flow field through the use of jet momentum. Jets which directly interact with the vortical flow structure are dependent upon their aerodynamic stiffness to produce variations in the pressure field around the vortex. In simple terms, the momentum of the

jets must be sufficient to balance a pressure difference across the jet sheet while maintaining a minimum of jet curvature. Thus these schemes may be described as inertial or inviscid type interactions which are inherently inefficient. It has been suggested that a far more efficient technique for modification of a global flow field is by interaction with the viscous flow that produces the separated regions. Since the leading edge is the region where the vortices originate, it is logical to attempt direct control over the vortical flow at its source. Thus the fourth and the most recent blowing scheme is termed "tangential leading edge blowing". The blowing slot extends along the leading edge as with the "spanwise blowing". The direction of blowing from the slot, however, is tangential to the rounded leading edge surface in the cross flow direction. This interaction may be considered to be almost entirely viscous in nature and the transfer of momentum between the flows is more efficient. If strong convex surface curvature is present a high momentum jet will attach to the surface via the Coanda effect and the mixing with the exterior flow will be greatly enhanced.

Recent research[26,27,28] at Stanford University has described the development of a method for controlling the vortical flow over a rounded leading edge delta wing at high angles of attack(flow regimes III and IV in section 1.1). Previous blowing schemes were effective in enhancing the lift characteristics in terms of maximum lift or lift-to-drag ratio only at low to moderate angles of attack(flow regime II in section 1.1), and a slight increase in stall angle of attack was possible in some cases. But TLEB can redevelop stable, strong vortices even at post-stall angles of attack. Thus TLEB has the potential to resolve the problems caused by the two types of separation-induced discontinuities at high angles of attack, i.e., vortex breakdown and vortex asymmetry. A detailed description of TLEB will be introduced in the next chapter.

1.3 Motivation for Present Work

The primary motivation for this study is both to understand vortical flows associated with delta wings at high angle of attack and to devise an approach to regulate the flow or provide active control. Previous experimental studies have shown that TLEB is capable of strongly influencing and reorganizing the steady vortical flow over a delta wing over a wide range of angles of attack. Naturally the next question concerns the transient characteristics of vortical flow with TLEB. If the time required for vortical flow re-organization by changing the blowing level is too long, TLEB cannot provide a means for active flow control for a real aircraft. So the examination and identification of the unsteady response of the vortical flow with TLEB is essential. Particularly important is the identification of the fundamental time scales for vortical flow re-organization after the application of blowing for different initial states of the flow field. This is necessary to formulate an approach to various methods of control for delta wings.

1.4 Objectives

As previously stated, this study concerns the influence of unsteady TLEB on the vortical flow field over a delta wing. Since TLEB has been shown to have significant effects on the vortical flow at various steady state testing conditions, the main objective of this study is to acquire a physical understanding of the transient process of vortex re-organization with TLEB. More specifically, the objectives of present study are to:

(1) examine the unsteady response of vortical flow re-organization with TLEB over a broad range of angles of attack

(2) identify the fundamental time scales related to vortical flow re-organization

(3) provide aerodynamic information about TLEB to permit the design of active flow control schemes

In order to achieve these objectives, the following steps are required: first, the unsteady response of the blowing supply system and the unsteady response of vortical flow re-organization due to transient blowing must be examined. Second, the fundamental time scales associated with vortical flow re-organization over a wide range of angles of attack must be identified to provide the very basic aerodynamic information for the design of vortical flow control schemes. Such control schemes would offer the possibility of an aircraft's performing dynamic maneuvers into the post-stall regime and permit steady state post-stall operations.

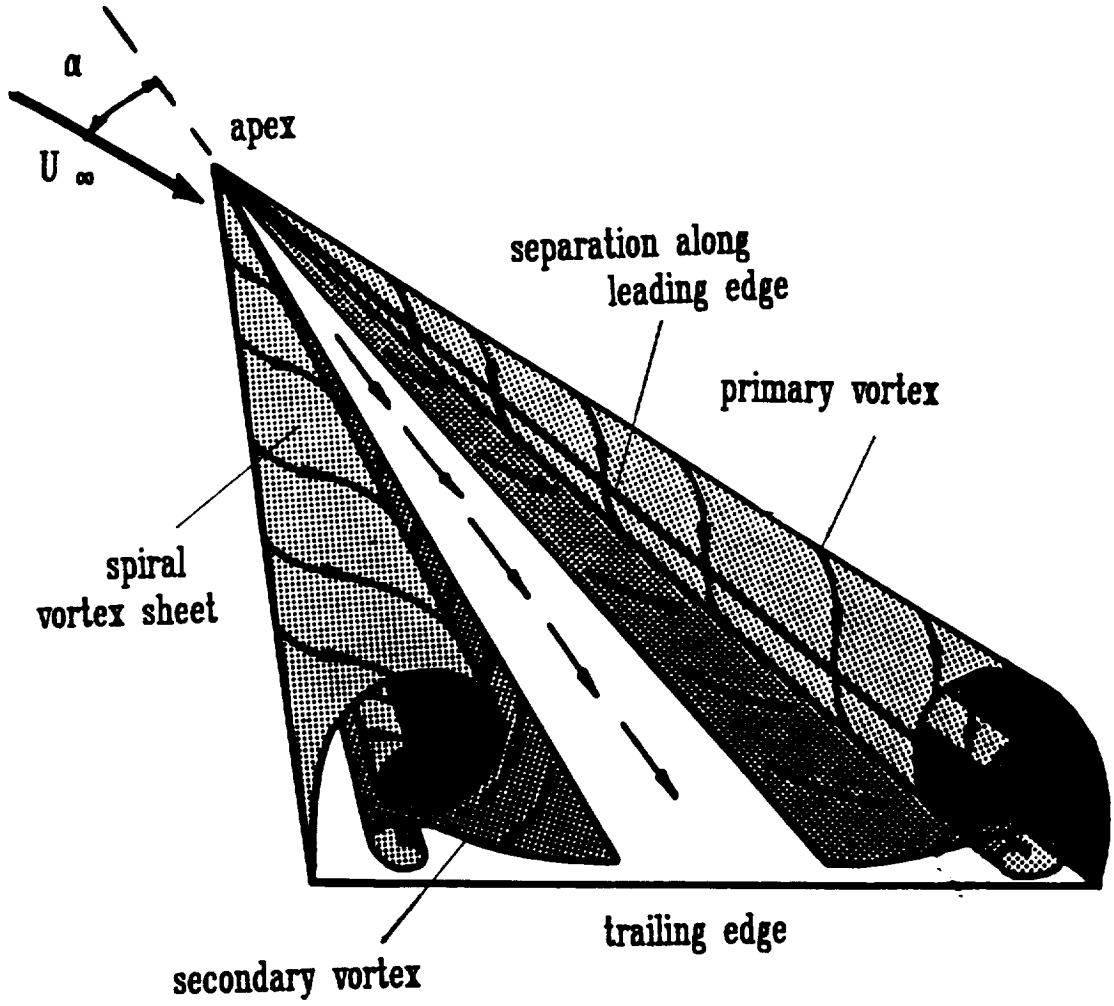

Figure 1.1 Illustration of vortex flow over a delta wing (Iwanski,Ref.15)

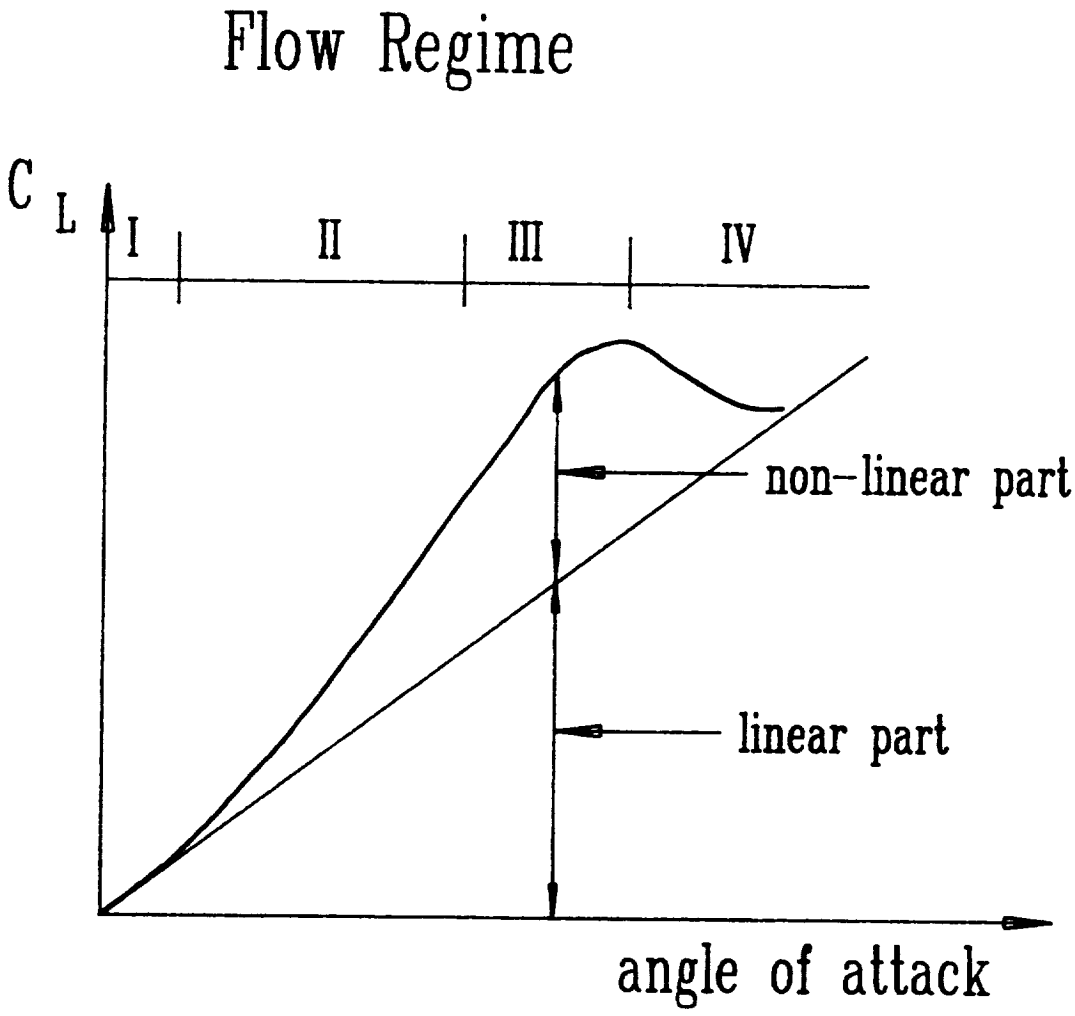

Figure 1.2 Schematic representation of the lift characteristics of a delta wing(Hummel,Ref.34)

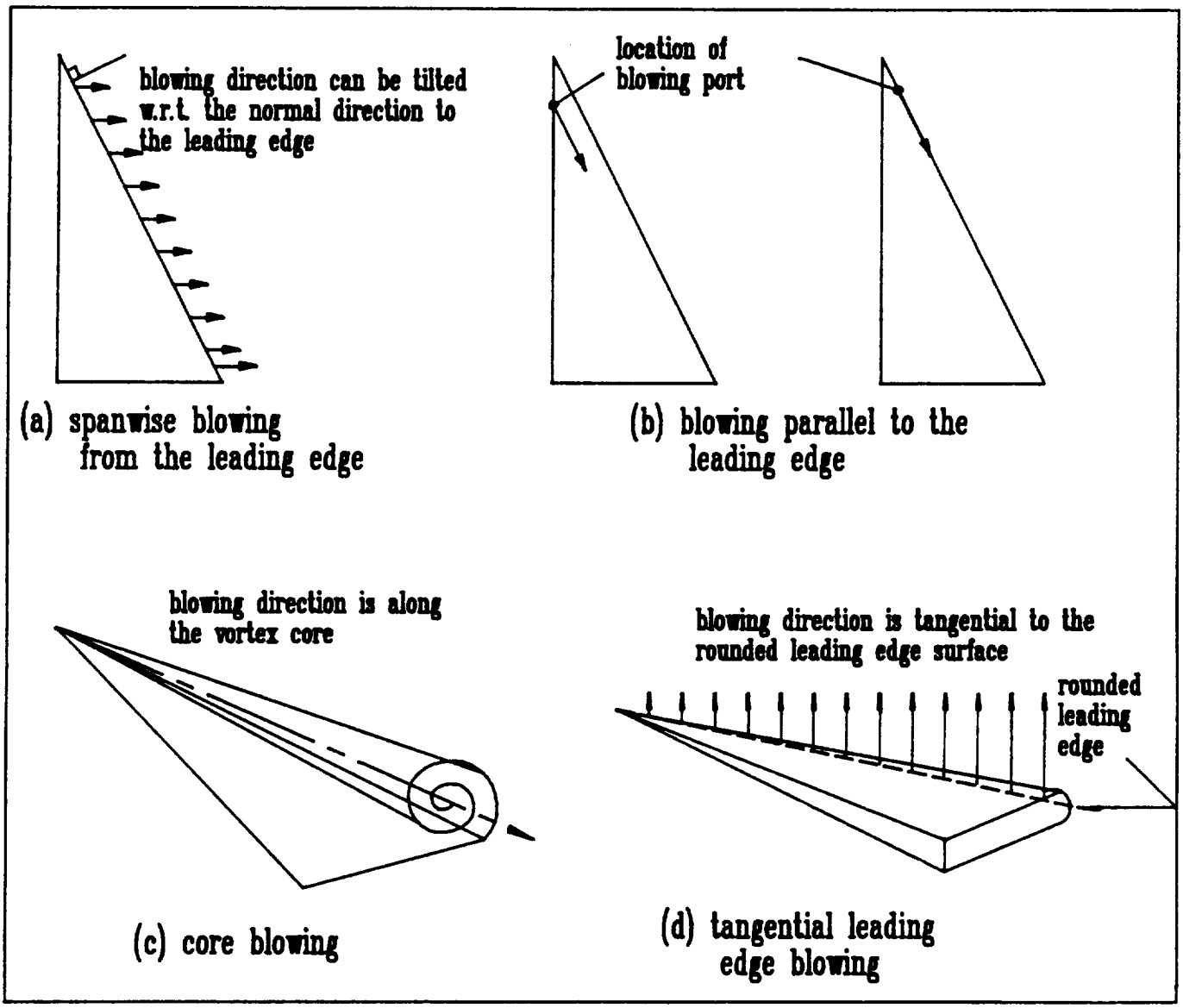

Figure 1.3 Classification of blowing schemes

CHAPTER 2

TANGENTIAL LEADING EDGE BLOWING

2.1 The Concept of Vortex Equilibrium

2.1.1 Equilibrium of leading edge vortex

The flow considered is that over a delta wing at angle of attack, figure 1.1. Separation occurs on the leading edge and produces two spiral vortex feeding sheets across which the pressure is continuous but the tangential velocity is discontinuous. Within the limits of slender body theory, the model in figure 1.1 is applicable to subsonic flows. The only contribution of viscosity in these flows is to fix the separation point at the leading edge for reasons exactly analogous to those justifying the use of the Kutta condition at subsonic trailing edges. Since the strength of these vortices must grow in the chordwise direction for a conical flow field, they must be continuously supplied with vorticity from the leading edge. This conical model can be a good approximation for the well-organized, stable leading edge vortex system at low angles of attack.

The vortex system in the cross flow plane is governed by a 'force-free' condition since only the wing and not the fluid can sustain forces. This force-free condition determines the resulting vortex strength, vortex core location, and shape of the feeding sheet. This is called the state of "vortex equilibrium" for a given angle of attack, free stream condition and leading edge separation point.

For a delta wing with given leading edge sweep, there are three parameters associated with the state of vortex equilibrium, i.e., the vortex strength, vortex core location and separation point. When one of these parameters is modified, the others must respond to establish the new state of vortex equilibrium. The idea of TLEB originates from this concept of vortex equilibrium.

2.1.2 TLEB as a device for vortex equilibrium modification

The separation point is fixed at the leading edge for a conventional sharp leading edge delta wing. Therefore, only two parameters are available to change the state of vortex equilibrium (strength,position). All previous blowing schemes for leading edge vortex control were attempts to modify the state of vortex equilibrium by changing these two parameters.

By contrast, control of flow separation on two dimensional airfoils is a viscous interaction and results in large changes in the global inviscid flow field. The concept of circulation control utilizes a thin, high velocity, tangential jet of fluid to control the location of the rear separation points on a rounded trailing edge airfoil. Gains in lift coefficient have been observed over a wide range of operational conditions[25]. Thus the possibility exists to consider the use of separation control for delta wings as a cross flow plane device to modify the trajectory of the ensuing vortices. This of course requires the cross section of a delta wing to have a rounded leading edge in contrast to the usual sharp configuration. It is possible to control the leading edge

vortex flow (i.e., the location and strength of the vortex and its feeding sheet) by controlling the location of primary separation around the rounded leading edge in accordance with the vortex equilibrium arguments discussed earlier. Moreover, it is expected that such an approach would be very effective in that a relatively small change in the location of boundary layer separation will have a large influence on the strength and position of the resulting vortex.

In the TLEB scheme, this separation modification is accomplished through the use of a thin wall jet placed along the leading edge and blowing tangentially inward on the wing upper surface. The jet energizes the boundary layer as it flows around the leading edge and across the upper surface of the wing, figure 2.1. The wall jet is more robust than the original boundary layer and remains attached to the rounded leading edge by the Coanda effect. This causes a delay in separation which, in turn, influences the entire flow field. The vortex and its feeding sheet must relocate and the vortex strength is modified such that equilibrium of the cross flow is maintained.

2.2 Steady State Behaviour of Vortical Flow with TLEB

Previous work with a 60^0-swept, conical delta wing model, figure 2.2, has clearly demonstrated the ability of TLEB to control the vortical flow over a wide range of angles of attack. It is useful to review the previous steady state results to better understand the unsteady flow characteristics.

The overall effect of steady co-flowing TLEB on wing normal force is shown in figure 2.3[26] for constant increments of blowing strength. The

co-flowing configuration is defined as that where the jet issues towards the upper surface, i.e., co-flowing with the cross flow. It is immediately apparent that increments in both angle of attack at maximum normal force and the maximum normal force coefficient may be realized. The unblown results have been compared with those from Küchemann[30], showing the data from previous experiments on sharp leading edge wings. The effect of the rounded leading edge and the increasing thickness of the wing appears to be consistent with previous observations, the total normal force of the 60^0 sweep, rounded leading edge delta wing being approximately 60 % of that produced by an equivalent sharp leading edge delta wing. Two aspects are apparent in figure 2.3; at low angles of attack(below the point of maximum normal force, i.e., at pre-stall angles of attack) there appears to be little change in the normal force with blowing; at high angles of attack(beyond the point of maximum normal force, i.e., post-stall angles of attack) the normal force is increased for even small amounts of blowing momentum. It is beneficial to consider the two regimes separately and to examine the effects of the blowing on the spanwise pressure distributions on the wing surface.

2.2.1 Low angle of attack behaviour

Figure 2.4[27] illustrates the effect of TLEB on the spanwise pressure distribution for the low angle of attack condition. While the integrated results for normal force showed little dependence on the blowing strength for this angle of attack, the spanwise pressure distributions are much more sensitive to the effects of TLEB. Two primary effects can be observed. First, the strength and location of the vortex, as signified by the inboard peak in the upper surface suction distribu-

tion, is clearly seen to move toward the wing root while the intensity of that suction peak diminishes. Second, the suction around the leading edge of the wing is seen to increase both in intensity and extent. This represents the increasing extent of the wall jet attachment and the delayed separation of the cross flow boundary layer. Since the overall integrated normal force showed little dependence upon the blowing momentum, figure 2.3, it can be observed that the effects of the jet attachment and the vortex displacement are offsetting.

The primary effect of TLEB for low angles of attack is to reduce the strength of the vortical flow and relocate the vortex inboard while maintaining nearly constant wing normal force. It may be demonstrated experimentally that, in the limit, the cross flow separation point can be relocated all the way to the wing midspan thereby eliminating any vortical flow. For that case the pressure distribution confirms to that expected from the 'R.T.Jones'[41] or 'attached flow' case.

2.2.2 High angle of attack behaviour

Figure 2.5[27] illustrates the effects of blowing momentum on the spanwise pressure distribution at the same chordwise location as figure 2.4 but for an angle of attack 45^0. The effects now are apparently quite different. For the zero blowing case, the upper surface pressure distribution is flat indicating the apparent absence of a vortical flow. As the blowing momentum is initially increased, the entire upper surface pressure reduces until a pressure signature, characteristic of the presence of a vortical flow, is observed. With increasing blowing, the

lateral position of the vortex is controlled by the blowing strength, as is the increased suction around the leading edge of the wing. Therefore, up to some level of the blowing, both the influence of the re-established vortical flow and the leading edge suction are additive, producing significant increases in the integrated normal force coefficient. Flow visualization studies have indicated a strong stabilization of the flow in this case.

At some blowing strength, a point of maximum normal force is reached, beyond which the flow characteristics revert to those seen at lower angles of attack. In this regime, changes in the contributions to normal force by the vortical flow and the leading edge jet offset each other, thus producing a nearly constant normal force with increasing blowing momentum. This corresponds exactly to those effects observed at low angles of attack.

2.3 Outline of Present Approach

Low speed wind tunnel measurements have been performed to examine the dynamics of vortical flow control over a rounded leading edge delta wing by TLEB. Of particular interest in the present work is the investigation of the time response of the vortical flows to time varying blowing strengths over a range of angles of attack, both pre- and post-stall. It is intended to verify that TLEB is capable of transient operation by the identification of fundamental time scales related to vortical flow re-

organization. Flow visualization, i.e., surface-oil flow, tufts and smoke visualization by laser light sheet, were used to compare the flowfields for both steady and unsteady conditions. The results will confirm the application of such an approach for post-stall conditions.

This work is divided into five chapters. A description of the experiment is presented in Chapter 3. Chapter 4 gives details of the results and discusses the steady and unsteady measurements. Finally, Chapter 5 summarizes the results, presents conclusions and discusses recommendations for future work.

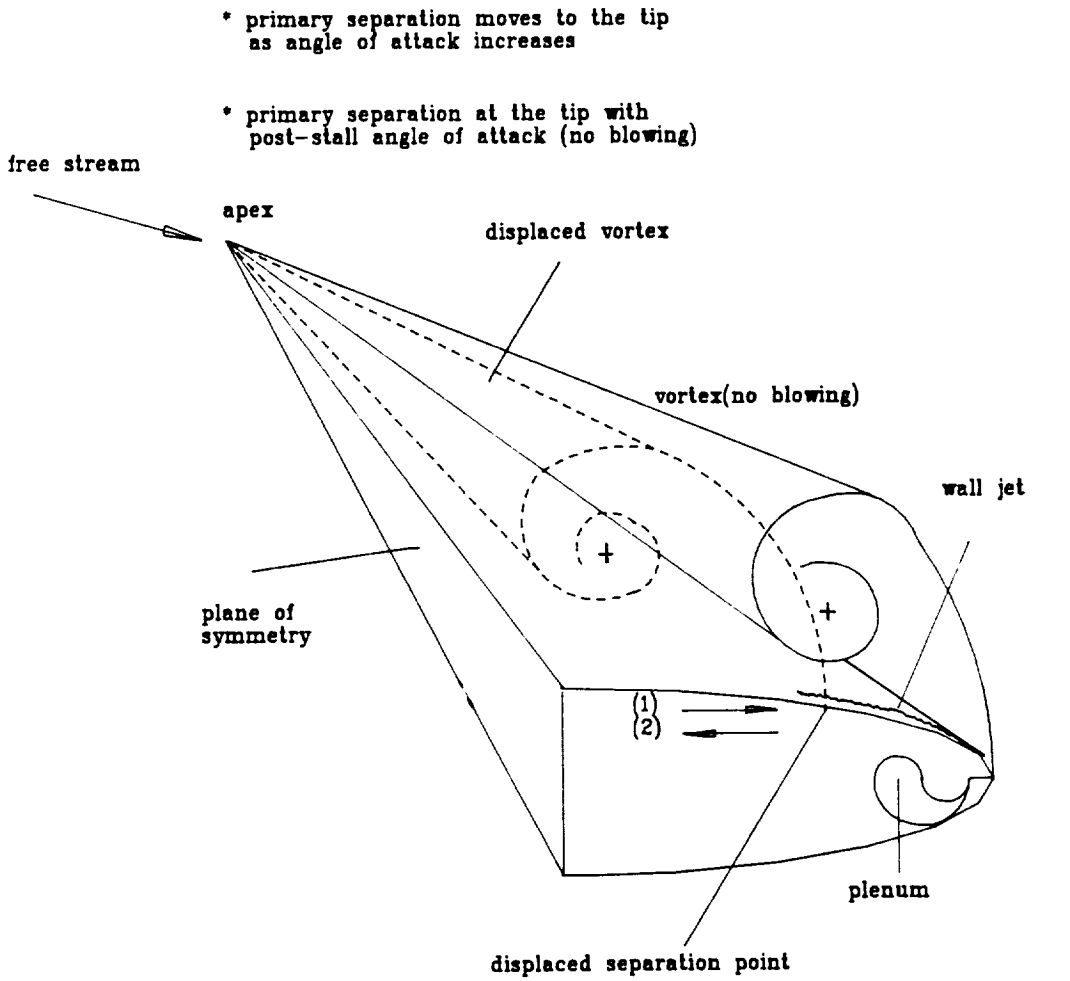

Figure 2.1 Schematic representation of the concept of tangential leading edge blowing

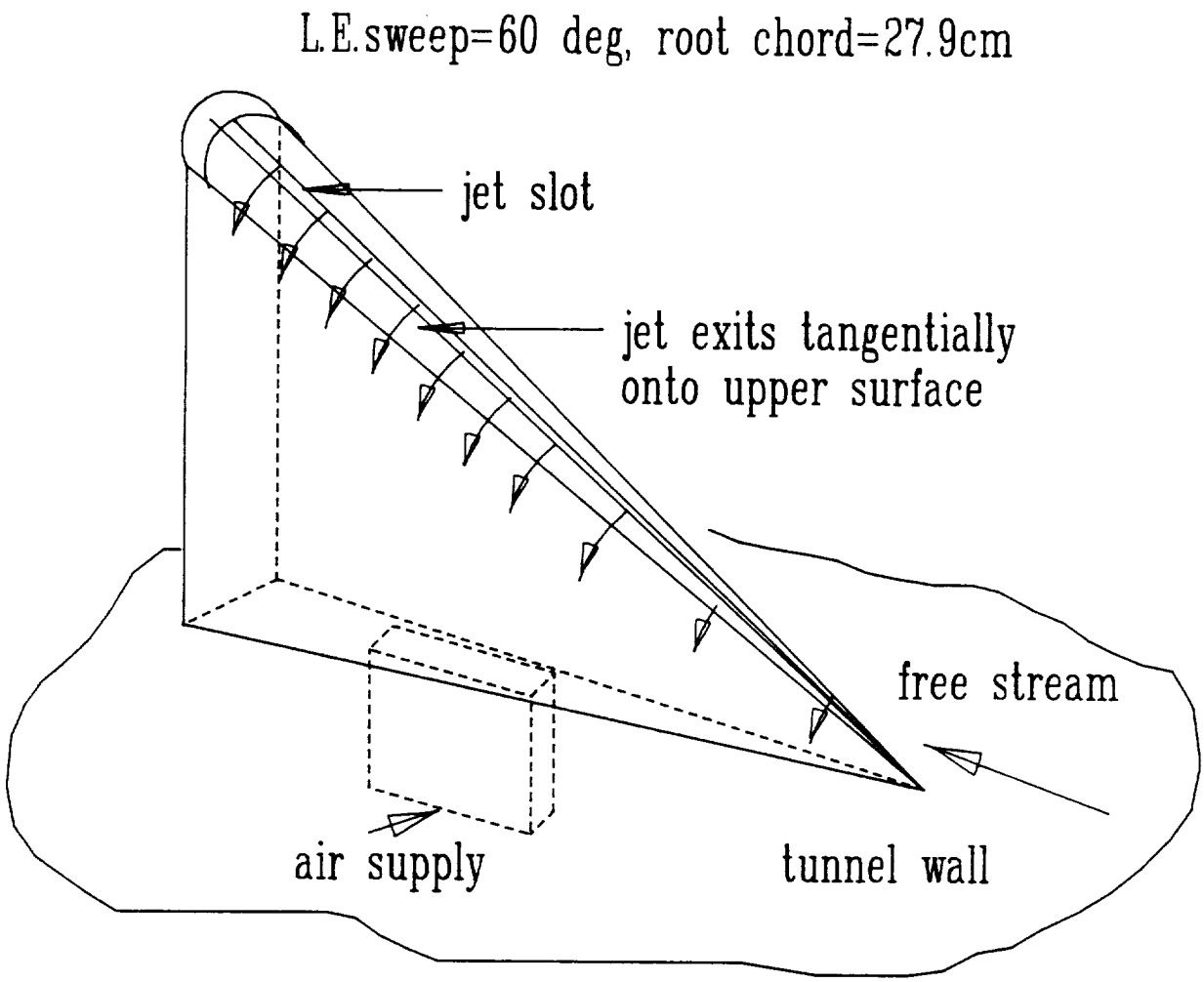

Figure 2.2 Schematic of 60 deg.-swept conical delta wing model

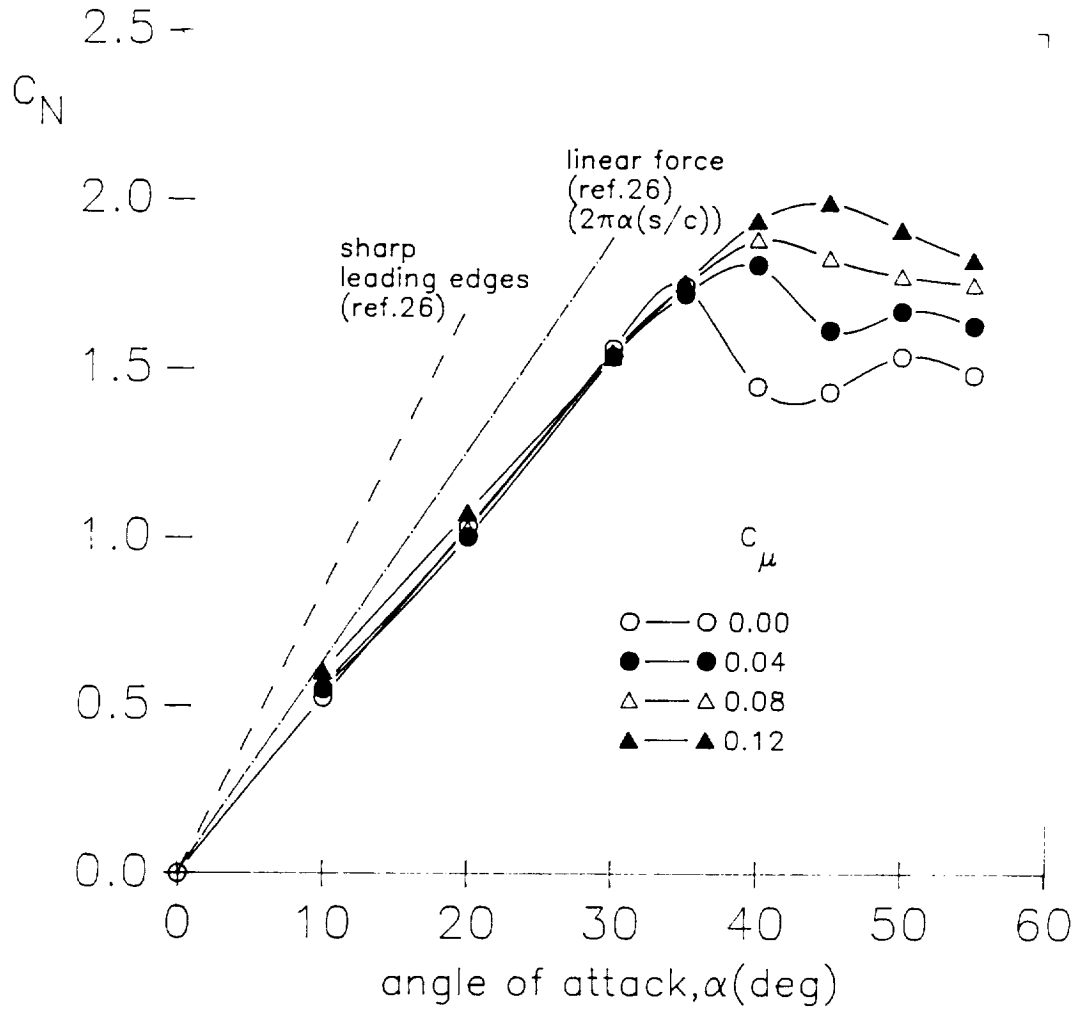

Figure 2.3 Normal force increments for changes in blowing strength (Ref.26)

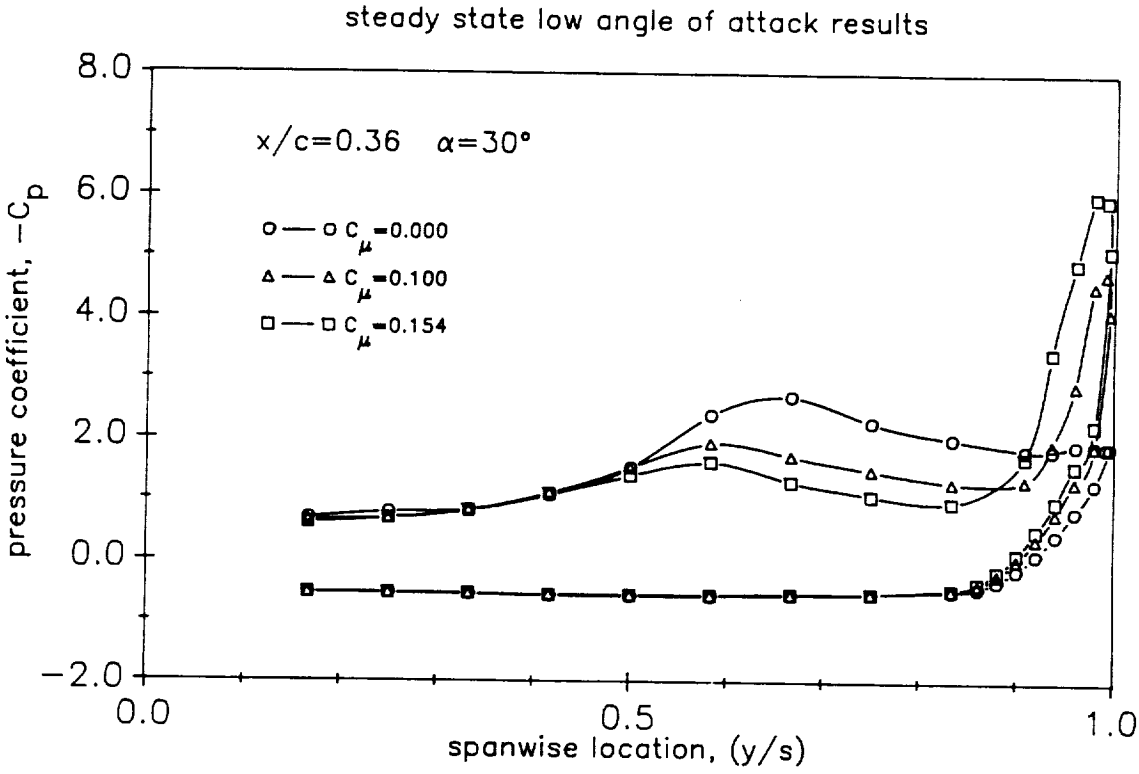

Figure 2.4 Spanwise pressure distribution with TLEB
(steady state low angle of attack results,Ref.27)

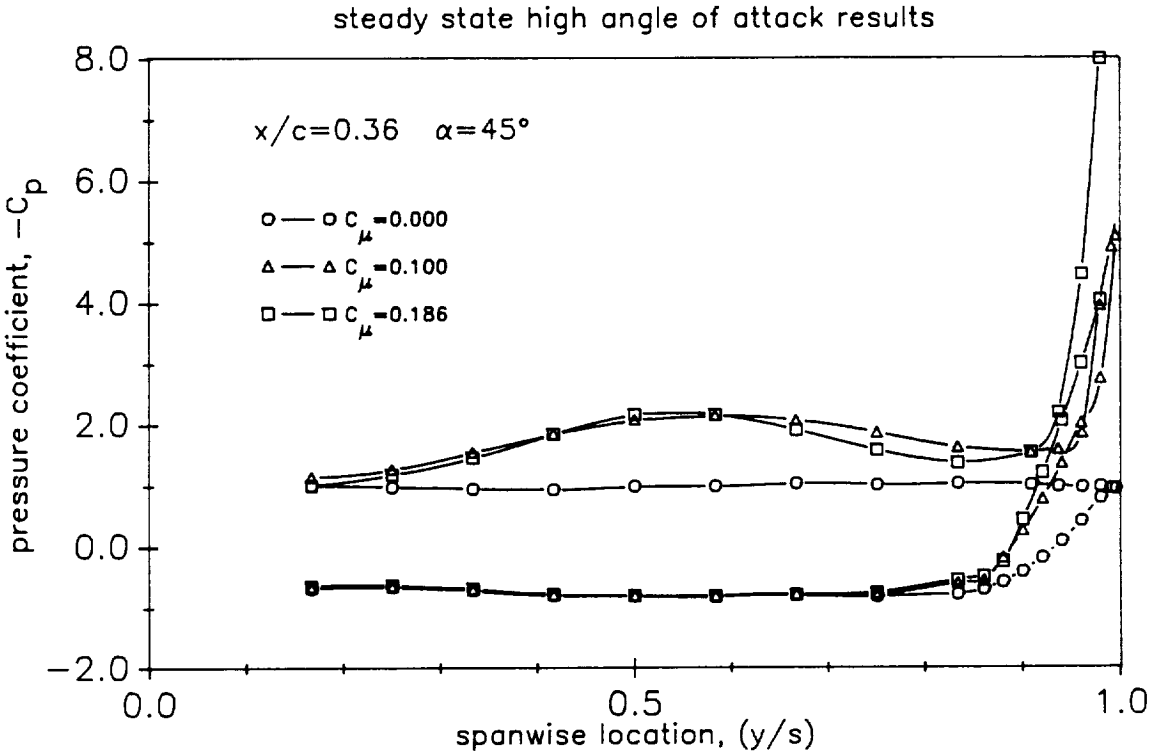

Figure 2.5 Spanwise pressure distribution with TLEB
(steady state high angle of attack results,Ref.27)

CHAPTER 3
EXPERIMENTAL APPARATUS AND TECHNIQUES

3.1 Wind Tunnel

3.1.1 Tunnel characteristics

The experiments were performed in the 18" x 18" test section of the Stanford Low Speed Wind Tunnel. The tunnel has a maximum centerline free stream speed of 57 m/sec and is capable of continuous operation. Speeds in the range of 20 to 40 m/sec were used here, and this variation provided a mechanism for expansion of the range of blowing momentum coefficients that were achievable. The typical free stream speed for most of the measurements was 23 m/sec ($Re = 4.66 \times 10^5$ based on model root chord length). Centerline velocities were monitored through a reference static pressure difference from two stations in the contraction, which had previously been calibrated against a pitot static tube and shown to be free of interference due to the presence of the model.

A continuous-operation centrifugal flow compressor was used as the source of compressed air for the blowing. This compressor is capable of delivering a maximum of 450 cfm at approximately 2 psi. The mass flow supplied to the model was calculated from direct measurement of the model internal plenum pressure.

3.1.2 Modification of the test section

A semi-span delta wing configuration was chosen to allow the scale of the model to be increased relative to a full-span model and to simplify the ducting required for the blowing air supply. The model was mounted on a turn table in the test section floor with the span oriented normal to the floor.

A problem associated with semi-span models is the effect of the wall boundary layer. Part of the delta wing model, especially near the apex, is immersed in the boundary layer and this situation may affect the vortical flow structure on the delta wing. It is necessary to modify the model set-up in the test section to remove the effects of the wall boundary layer for a better simulation of the vortical flow structure of a full-span delta wing. When the boundary layer thickness is too large relative to the model semi-span, the quantitative results regarding the leading edge vortex flow may be unreliable. Consequently the test section was modified to remove the wall boundary layer on the test section floor.

The semi-span wing model was mounted on a splitter plate offset from the tunnel wall in order to remove the boundary layer. The gap height between the leading edge of the plate and the original test section floor was determined from boundary layer thickness measurements. The edges of the splitter plate were manufactured as sharp as possible.

Figure 3.1 represents the modification of the test section to remove the boundary layer. There was a measureable difference in the vortical flow pattern above the wing, with and without the splitter plate. The general trend was for larger normal force with removal of the boundary

layer. This was apparently due to a more uniform flow resulting in increased shedding of vorticity near the apex. This fact could be confirmed from the spanwise pressure distribution data at several different chordwise stations. Another aspect of this modification was an approximately constant rate of increase in the vortex strength (circulation) along the chord at a fixed angle of attack, before vortex breakdown. The difference of the vortex strength along the chordwise direction reflects the fact that additional shed vorticity from the region near the apex is recovered by the removal of the boundary layer.

In summary, it is beneficial to eliminate the boundary layer developed on the test section floor through the use of a splitter plate when one is investigating leading edge separation and the vortical flow structure for semi-span delta wing model configurations.

3.2 Wind Tunnel Model

A semi-span configuration was chosen for simplicity of construction and relative scale in the test section. The wing model has a 6.25 % constant thickness relative to the wing root chord and has a 50^0 leading edge sweep angle, figure 3.2. The model is a cropped delta wing configuration and the trailing edge thickness is made finite by the inclusion of a simple dual trailing edge flap system which may be later used to determine the effectiveness of mechanical flap devices at high angles of attack in the presence of TLEB. The leading edge blowing slot extends over

most of the leading edge and the slot gap can be varied by adjustment of the location of the cylinder that forms the upper surface leading edge. For the present experiments, a nearly conical slot geometry was used with the slot gap linearly varying from 0.004" at the apex to 0.020" at the end of wing leading edge. A constant slot gap was investigated in a preliminary test and was shown to produce a vortical flow field that was highly three-dimensional and very complicated to analyze. The optimum blowing slot shape proved to be a tapered slot as determined previously in Trebble's spanwise blowing measurement[9] because the linearly varying momentum distribution was appropriate to preserve conical flow. The vortex strength along the chord increases linearly for conical flow. To preserve the conical nature of the delta wing leading edge vortices with any kind of blowing scheme, the local blowing strength based on the local spanwise dimension at any chordwise station should be constant. That means the blowing jet momentum chordwise distribution, and therefore the slot gap, should increase linearly.

The model can be configured for either unsteady or steady pressure measurement or a combination of both. Facility was provided for two rows of pressure instrumentation at the 32.5 % and 54.5 % chordwise locations. For steady pressure measurement, a total number of 27 and 24 tappings respectively were included, with the most outward locations being 79 % and 84 % of the semi-span. For unsteady measurement, a total number of 4 and 5 Kulite miniature unsteady pressure transducers were included extending to 76 % and 80 % of the semi-span. Detailed pressure tapping locations in non-dimensional spanwise coordinates are shown in the table 3.1 and 3.2. The model is floor mounted in a turntable arrangement to provide angle of attack variation up to 50^0. Typical measurements were performed at tunnel free stream speed of 20 - 30 m/sec and Reynolds numbers of 4.05 - 6.07 x 10^5 based on the wing root chord.

3.3 Definition of Parameters

3.3.1 Blowing momentum coefficient

The blowing momentum coefficient is defined as follows

$$C_\mu = \frac{\dot{m}\, V_j}{q_\infty\, S_{ref}} \tag{3.1}$$

In the absence of compressibility, $\rho_\infty = \rho_j$,the above expression becomes;

$$C_\mu = 2 \left(\frac{V_j}{V_\infty}\right)^2 \left(\frac{A_j}{S_{ref}}\right) \tag{3.2}$$

The jet velocity was determined from measurement of the internal pressure of the model plenum and the isentropic relations.

$$\frac{P_a + P_i}{P_a} = \left(\frac{T_i}{T_a}\right)^{\frac{\gamma}{\gamma-1}} \tag{3.3}$$

$$\frac{T_i}{T_a} = 1 + \frac{V_j^2}{2\, c_p\, T_a} \tag{3.4}$$

$$c_p = \frac{\gamma}{\gamma-1} R \tag{3.5}$$

From equations (3.3) - (3.5), the following relation for the jet velocity, V_j, can be obtained.

$$V_j = \sqrt{2\ R\ T_i\ \frac{\gamma}{\gamma-1}\left(\ 1\ -\ \left(\frac{P_a}{P_a+P_i}\right)^{\frac{\gamma-1}{\gamma}}\right)} \qquad (3.6)$$

The blowing momentum coefficient can be determined at each testing condition from measurements of the atmospheric pressure, model plenum internal pressure, air temperature in the model plenum, and free stream speed.

In the unsteady measurements, C_μ is a function of time. Two types of blowing waveform were used to examine the time response of the vortical flow. The first is increasing the blowing strength with time. This is called 'positive $\dot{C}_\mu$ operation' or 'normal operation'. The second is decreasing the blowing strength and is called 'negative $\dot{C}_\mu$ operation' or 'reverse operation'.

3.3.2 Transition times and time constant

The re-organization process of the leading edge vortices from one equilibrium state to another was traced by measurement of the surface pressure during the transition. There are two different transition times involved: first is the internal pressure transition time and second is the surface pressure transition time. The end states of the vortical flow on the delta wing, particularly the pressure distribution on the surface under the vortex, is known from the steady state measurements.

The blowing momentum coefficient was controlled by a change of plenum pressure which was achieved by an unsteady blowing control valve. A

typical pattern of pressure response with ramp change of blowing input is shown in figure 3.3. Time $t = t_0$ is the reference time that represents the time when the internal pressure starts to change. At $t=t_1$ the internal pressure transition is completed. The surface pressure starts to change at $t = t_2$ and the surface pressure response generally shows a very short initial delay, $t_2 - t_0 \approx 0$. At $t = t_3$ the surface pressure reaches another steady state. Here $t_1 - t_0$ is called the internal pressure transition time and $t_3 - t_2$ is called the surface pressure transition time. The initial delay of surface pressure response, $t_2 - t_0$, is not a constant for all cases. That means the initial delay of surface pressure response may be related to the vortex re-organization but the trend of this initial delay is not clear due to limitation of the measurement resolution. The initial delay of surface pressure is very short compared to the surface pressure transition time and the trend of this quantity is very irregular. But it appears that the initial delay of surface pressure response cannot be excluded from the vortex re-organization process.

The time constant ($\tau = t_3-t_0$) can be defined as the sum of the initial delay and surface pressure transition time (see figure 3.3) which represents a characteristic time scale for vortex re-organization with a ramp change of blowing input.

3.4 Unsteady Blowing Control

3.4.1 Unsteady blowing control system

To provide transient blowing, a servo controlled rotary pneumatic valve system was developed. A simple ramp change of internal pressure was

determined to be the most practical form of input, both from pneumodynamic and time constant derivation considerations. It was anticipated that multiple time scales would be present for the vortex re-organization process. It is thought that the long time scale may be related to the downstream convection of the wing wake. Therefore, sinusoidal or other periodic variations of internal pressure would tend to obscure these effects, except in the case when the period of internal pressure variation input is long compared to the long time scale.

Figure 3.4 shows the control hardware for the half-span delta wing model. As can be seen in figure 3.4, the low moment of inertia rotary valve is activated by a brushless DC motor and the angular displacement of the rotary valve is sensed by a linear potentiometer. The electronics in figure 3.4 is for the feedback control of the rotary valve angular displacement which is directly related to the air mass flow into the model plenum. The blowing momentum strength corresponding to the internal pressure was pre-calibrated for a broad range of internal pressure. The initial closed-loop response of the valve motion was underdamped. A lead compensation network was used to provide the desired damped response, figure 3.5. A minimum ramp time of the order of 5 milliseconds has been achieved with little overshoot. For any settings of required initial and final positions of the rotary valve, which correspond to initial and final values of blowing momentum, the ramp time and the ramp pattern of the rotary valve motion were similar. This was done to isolate the possible valve-characteristic effects from different internal pressure transition patterns. It was found that the optimum configuration of the rotary valve location in the air supply line was as close to the model plenum as possible in order to eliminate the time lag due to the pressure wave propagation from the valve to the model plenum. Figure 3.6 shows a schematic of the unsteady blowing control system.

3.4.2 Transient responses of internal pressure

Figure 3.7 - 3.10 show examples of the plenum internal pressure response to operation of the rotary valve system. The selected examples are typical of those for representing various testing conditions. The pattern and smoothness of the internal pressure transition were found to be a weak function of the speed of rotary valve operation, the pressure difference between the states and the direction of valve rotation, i.e. increasing or decreasing the blowing momentum with respect to time. In all cases, an overshoot in normal operation and an undershoot in reverse operation were observed and the magnitude of the overshoot or undershoot was found to be primarily a function of the pressure difference between the end states. The servo rotary valve system was designed to provide the shortest internal pressure transition time in order to catch the most rapid change of vortex re-organization. Any oscillations in the blowing supply appear to directly affect the external aerodynamics, i.e. the vortex re-organization process, so that smooth transitions are important if time differences are to be accurately determined. As mentioned in the previous section, the ability to measure time scale accurately was the basic requirement of the unsteady blowing control system in this experiment. As shown in figures 3.7 - 3.10, the internal pressure transition has patterns showing slight overshoot without any severe oscillations in all cases. A mean internal pressure transition time is approximately 26 milliseconds for all cases.

3.5 Surface Pressure Measurement

3.5.1 Steady measurement

For the steady pressure measurements a standard Scanivalve multi-pressure measuring system was used. The steady pressure tappings on the model were monitored by a 4 barrel, 48 port Scanivalve pressure scanning system that was controlled by an IBM AT computer. The Scanivalve was equipped with -2.5/+2.5 psid pressure transducers which were conditioned to give 10 volts response per 1 psi of pressure. The sampling rate was 1 Khz for each pressure port and 100 samples during 0.1 seconds were averaged to represent the time averaged static pressure on the wing surface at each tapping position. Graphical displays of the individual spanwise pressure distributions were available on-line. The temperature of the supplied air from the blower increased over a period of time and the difference between the free stream temperature and the air temperature in the model plenum could be more than 20^0C. This could cause a 6 % difference of the air densities between the free stream and the air blown from the slot. Also the heat transfer from the hot air in the plenum to the unsteady pressure transducers caused a shift in the reference reading, which were very sensitive to ambient temperature. A heat exchanger was installed to cool the supplied air before the model plenum and this could reduce the temperature difference to 10^0C. A schematic for steady pressure measurement is shown in figure 3.11.

3.5.2 Unsteady measurement

To measure the transient pressures on the wing it was required to measure the unsteady response of individual Kulite miniature pressure

transducers mounted just below the wing surface. Data acqusition software capable of sampling a maximum of 16 channels of analog information with an aggregate sampling rate of 130 Khz was developed. During typical operation, only 9 channels were sampled with an individual rate of 3 Khz. This corresponds to 3 samples per millisecond and was judged to be sufficient. The maximum sample time was 5 seconds and this sample time period was determined from the preliminary test runs which showed that 1 second was enough to record the transient response of surface pressure even for extremely high angles of attack. Four cycles of positive and negative $\dot{C}_\mu$ ramps were performed during each sample time to check repeatability and to compare the difference of normal and reverse operation. Post-processing of the digital signals was used to smooth the signals to enable improved assessment of the transition and delay times. An example of a typical surface pressure response to transient blowing is shown in figure 3.12. The smoothing algorithm was obtained from reference [29], and examples for different data windows are shown. A value of 10 to 20 points was typical, depending upon the signal fluctuations. This particular smoothing scheme has the advantage of preserving the time base, compared to analog filtering, for example. A certain degree of oscillation was still present in the pressure signals, and in some cases this could be correlated with the internal pressure fluctuations. It was assumed that these fluctuations were a characteristic of the blowing supply system and not an instability in the vortex control. This is supported by the observation that the oscillations become more prevalent at the higher blowing rates regardless of the angle of attack. The results from unsteady surface and internal pressure measurements during vortex re-organization provided accurate measurements of the time constants and phase relationships involved in TLEB. A schematic of the unsteady pressure measurement is shown in figure 3.13.

	Spanwise Location, y/s	
# of tap	row #1 (x/c=0.325)	row #2 (x/c=0.545)
1	0.0293	0.0350
2	0.0586	0.0700
3	0.0880	0.1050
4	0.1174	0.1400
5	0.1467	0.1750
6	0.1761	0.2099
7	0.2054	0.2449
8	0.2347	0.2799
9	0.2641	0.3149
10	0.2934	0.3499
11	0.3228	0.3849
12	0.3521	0.4199
13	0.3815	0.4549
14	0.4108	0.4899
15	0.4401	0.5249
16	0.4695	0.5598

* Table 3.1 is continued in the next page.

# of tap	row #1 (x/c=0.325)	row #2 (x/c=0.545)
17	0.4988	0.5948
18	0.5282	0.6298
19	0.5575	0.6648
20	0.5869	0.6998
21	0.6162	0.7348
22	0.6455	0.7698
23	0.6749	0.8048
24	0.7042	0.8398
25	0.7336	
26	0.7629	
27	0.7923	

Table 3.1 Non-dimensional spanwise locations of steady pressure tappings

wing root : y/s=0
wing tip : y/s=1

	Spanwise Location, y/s	
# of tap	row #1 (x/c=0.325)	row #2 (x/c=0.545)
1	0.2347	0.2449
2	0.4107	0.3849
3	0.5868	0.5249
4	0.7628	0.6648
5		0.8048

Table 3.2 Non-dimensional spanwise locations of unsteady pressure tappings

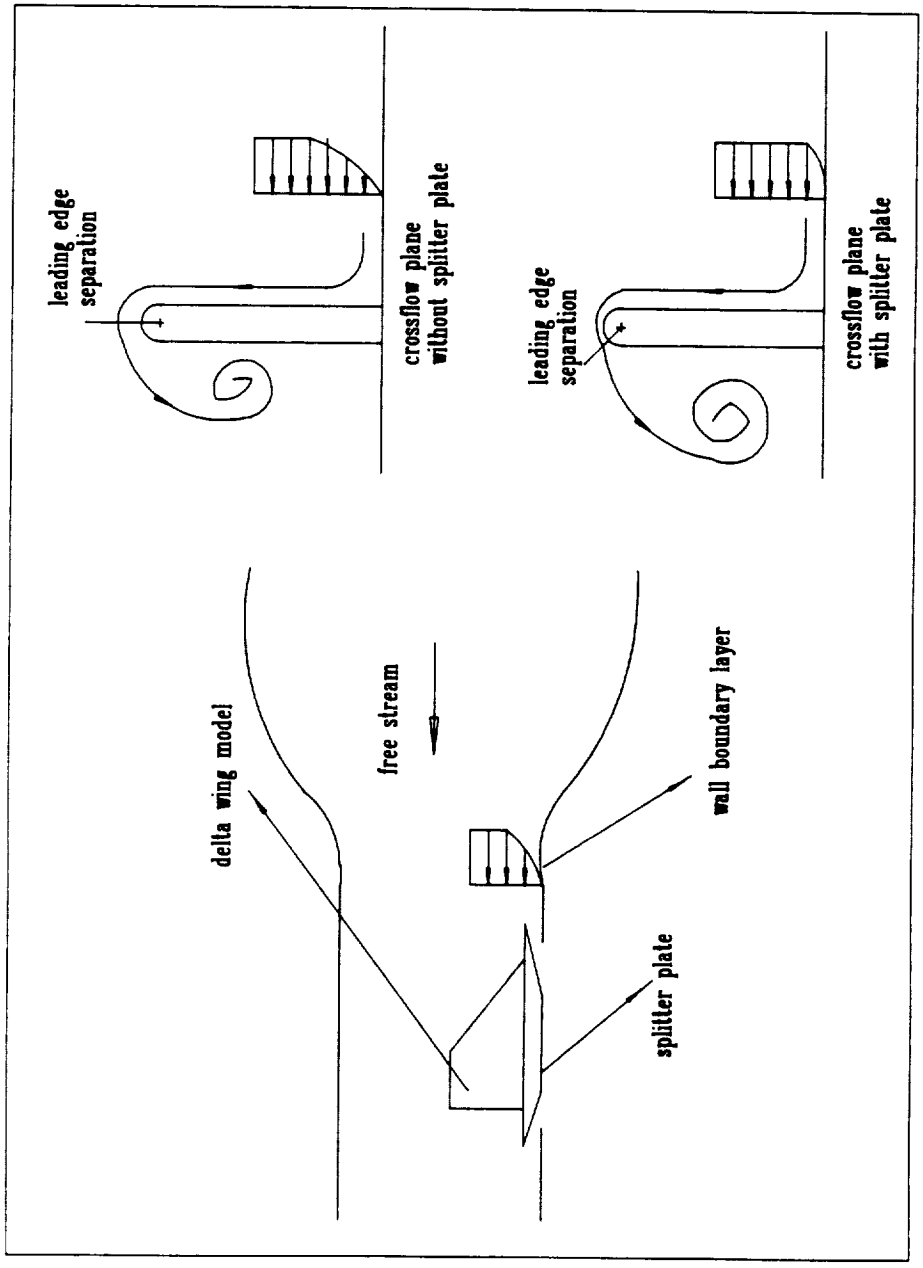

Figure 3.1 Schematic of test section modification with splitter plate for removal of wall boundary layer

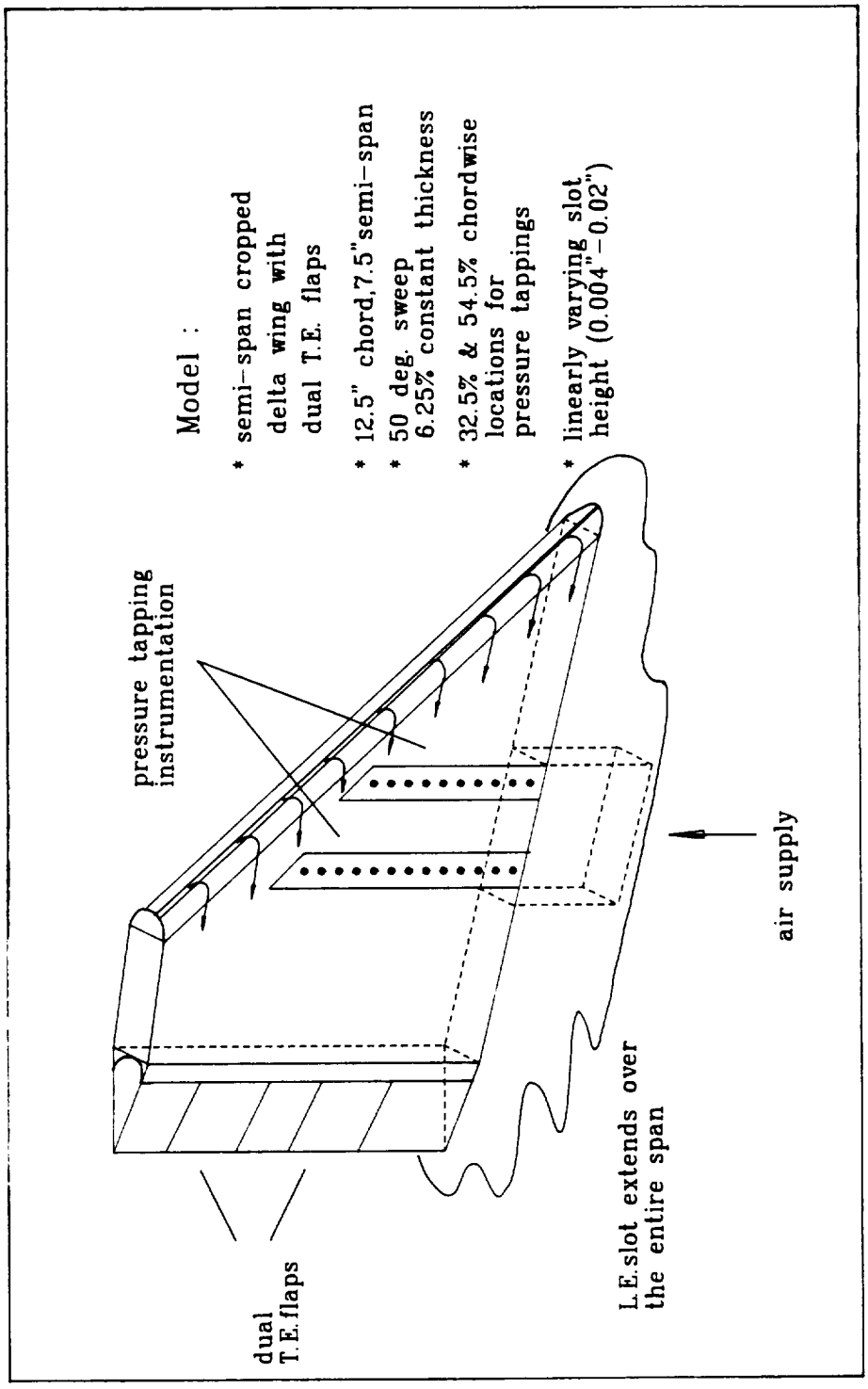

Figure 3.2 Configuration of wind tunnel model

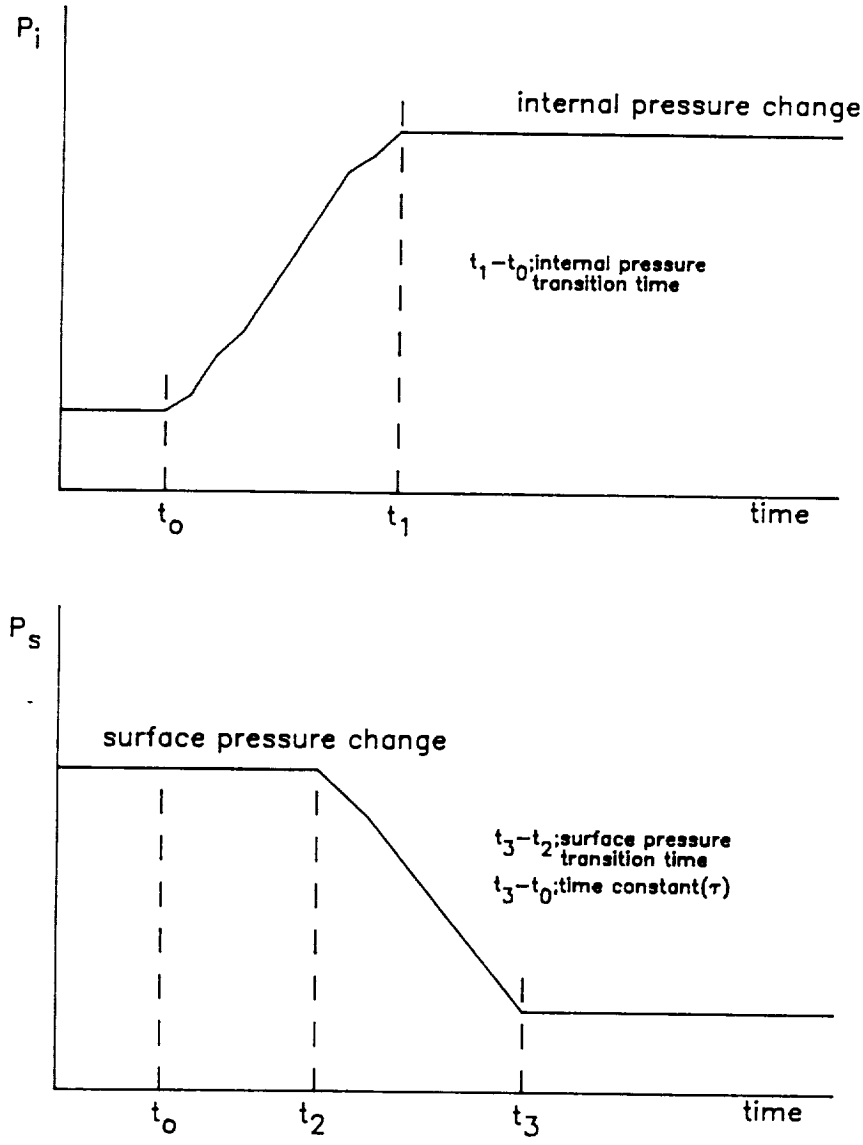

Figure 3.3 Definitions of internal and surface pressure transition times and time constant

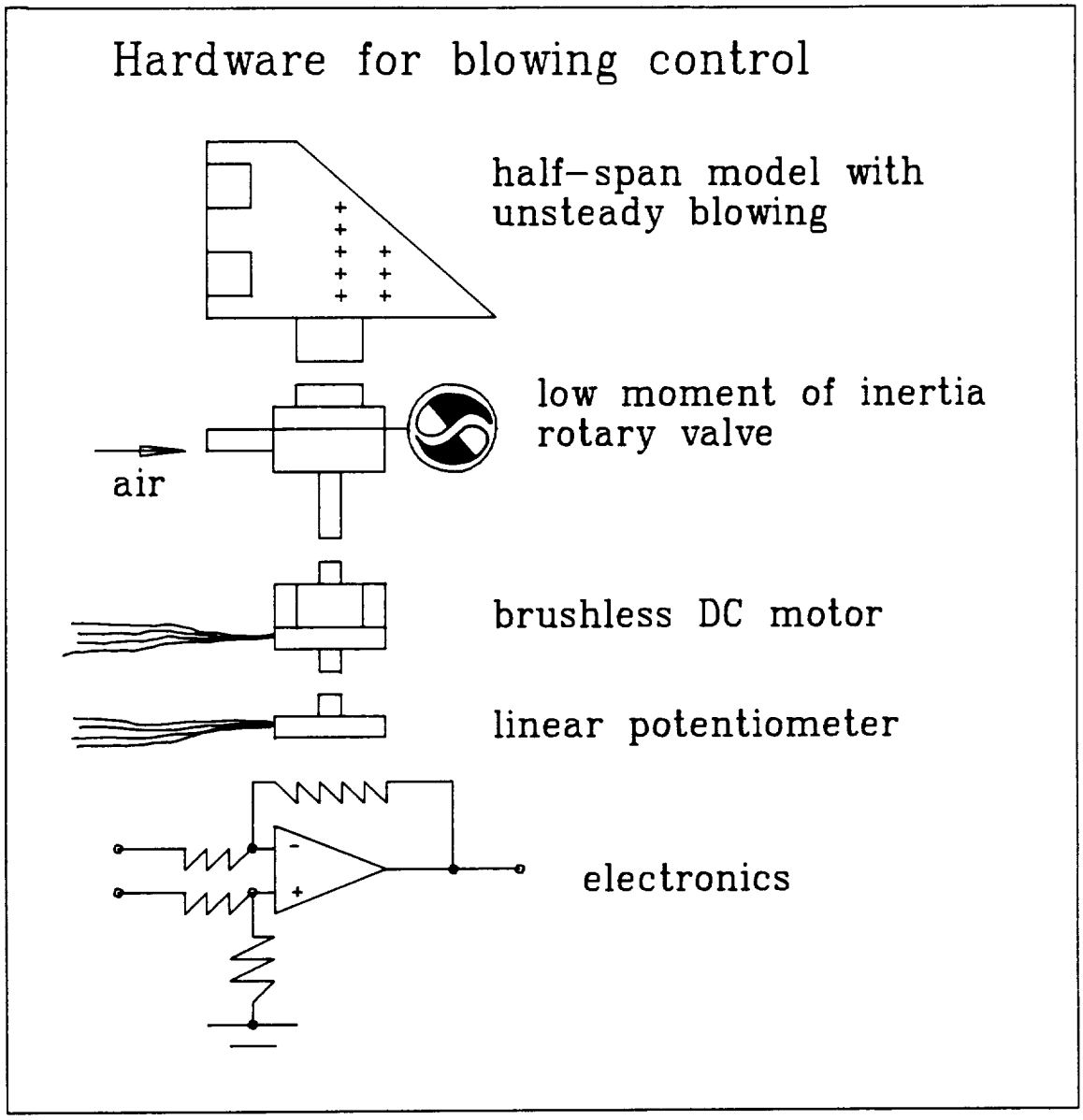

Figure 3.4 Blowing control valve system hardware

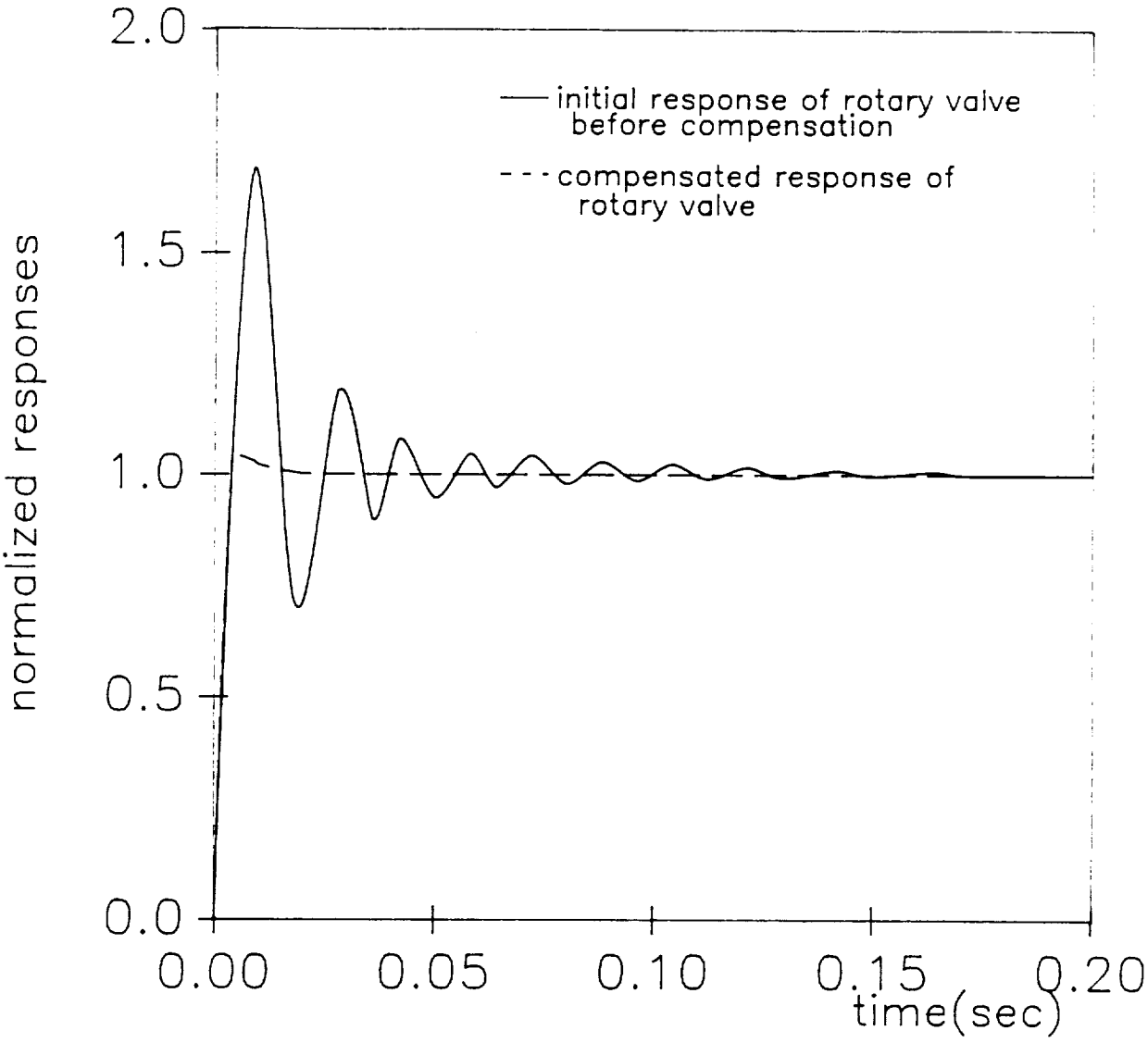

Figure 3.5 Responses of rotary valve motion

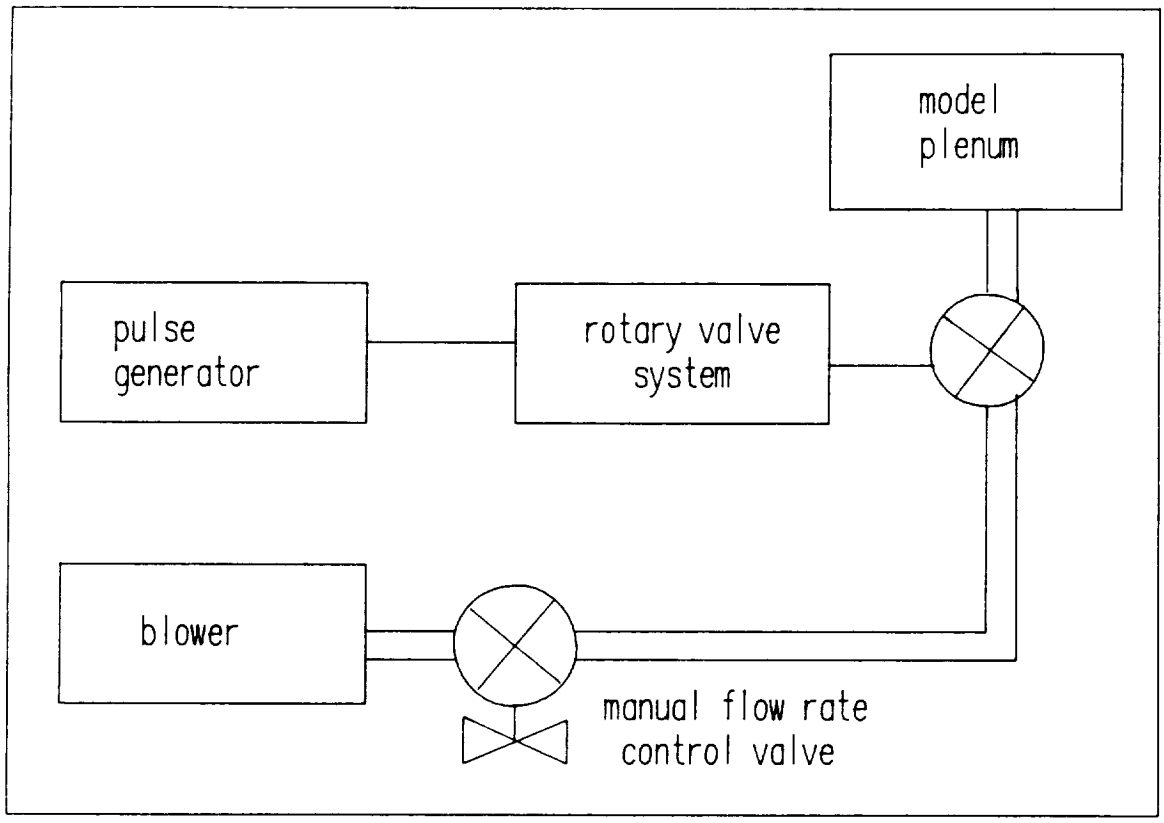

Figure 3.6 Schematic representation of unsteady blowing control system

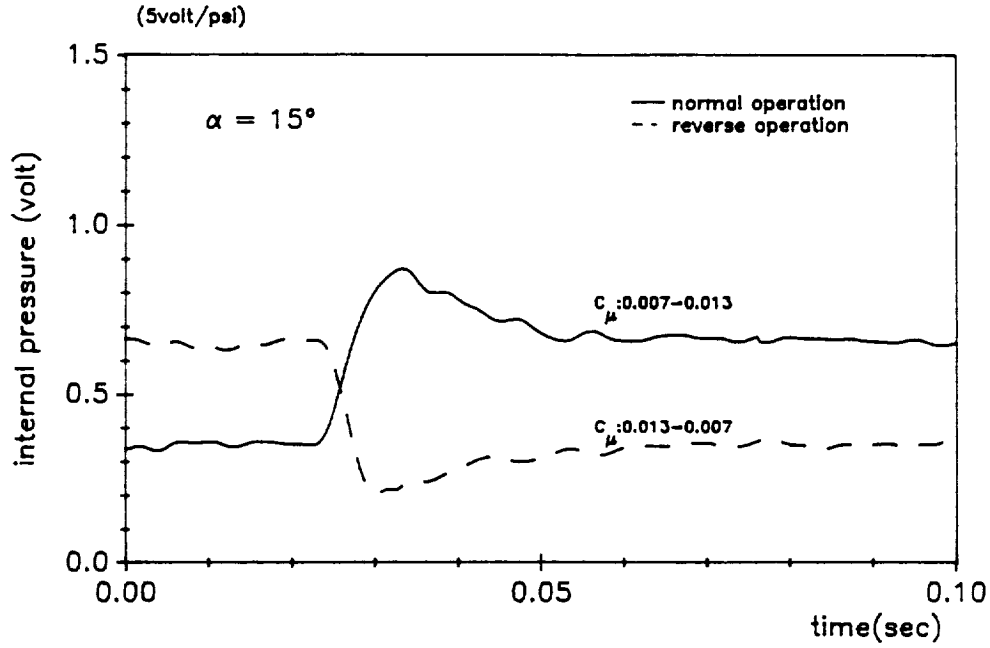

Figure 3.7 Internal pressure transition pattern
(pre-stall at low α_g case)

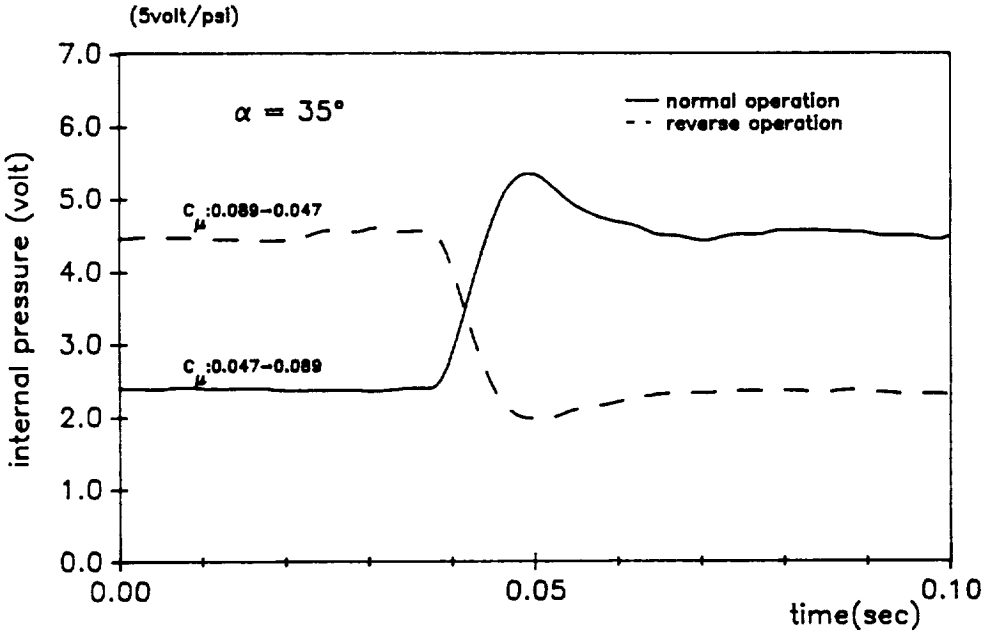

Figure 3.8 Internal pressure transition pattern
(pre-stall at high α_g case)

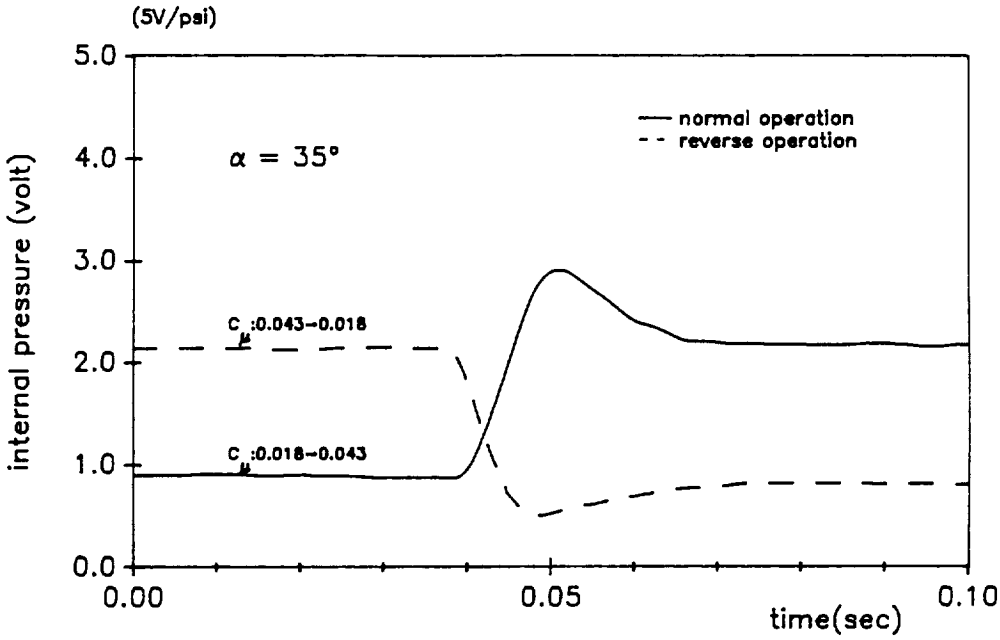

Figure 3.9 Internal pressure transition pattern
(post-stall at high α_g case)

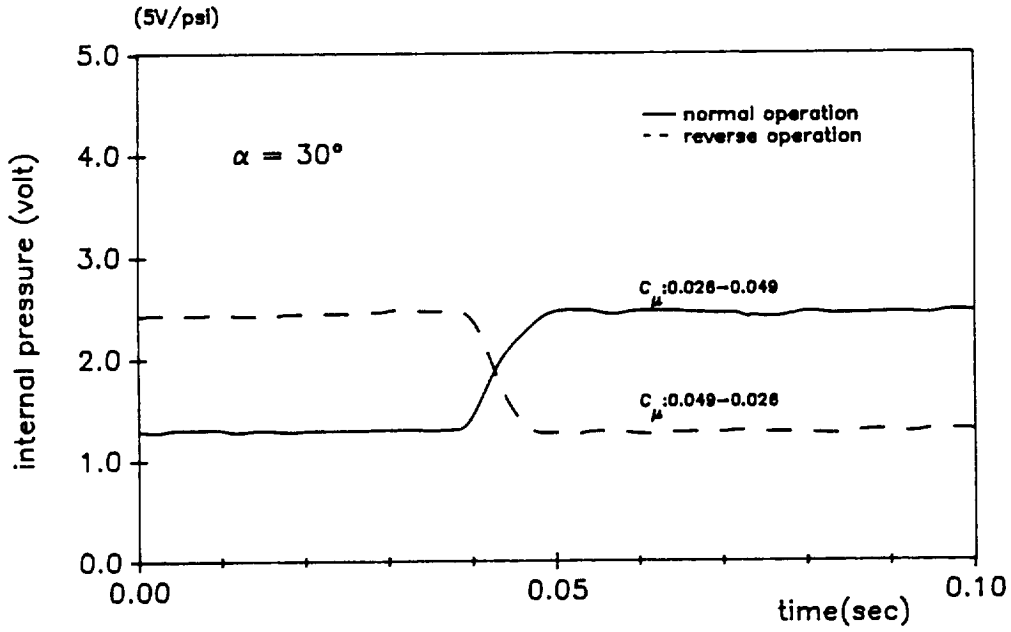

Figure 3.10 Internal pressure transition pattern
(trans-stall at high α_g case)

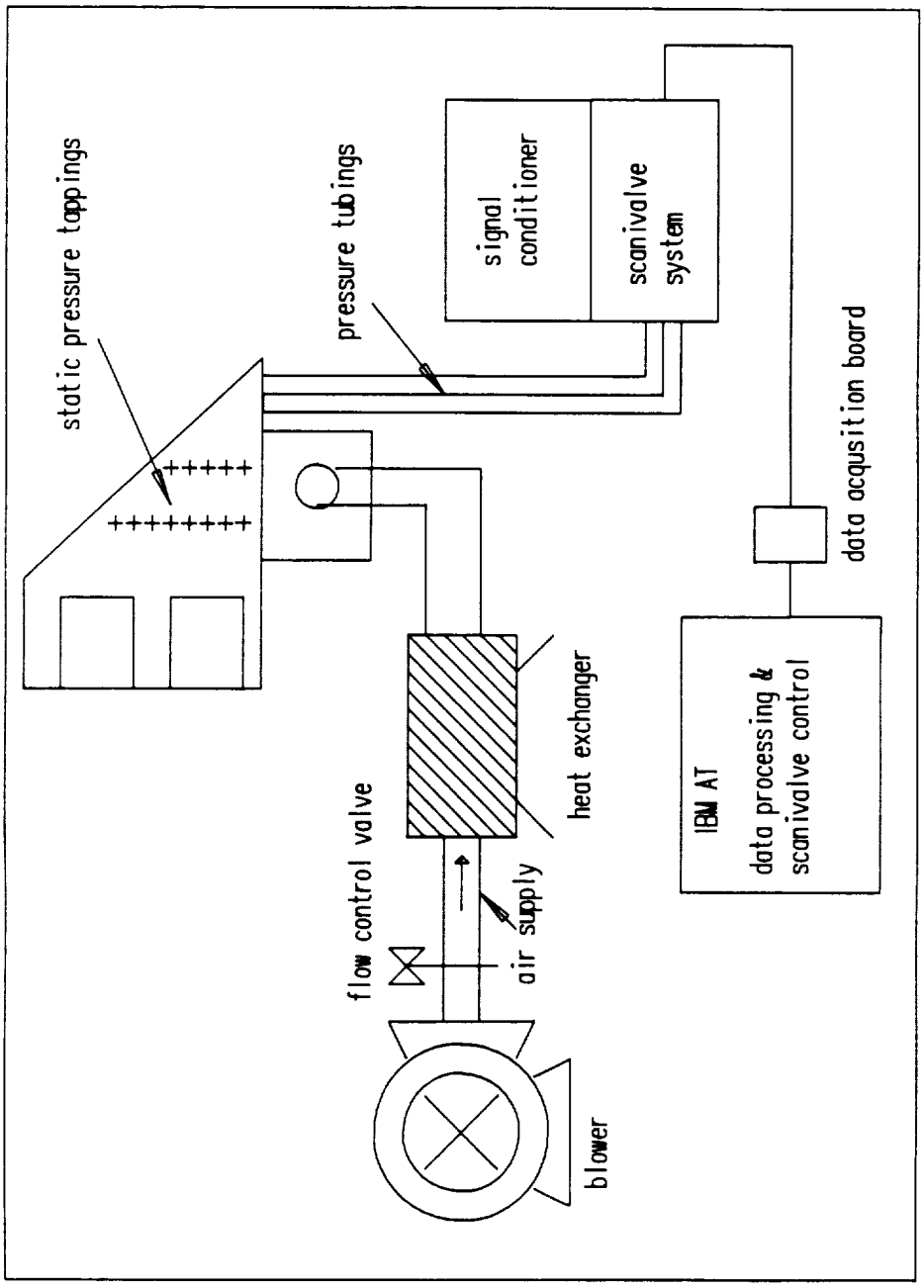

Figure 3.11 Steady surface pressure measurement

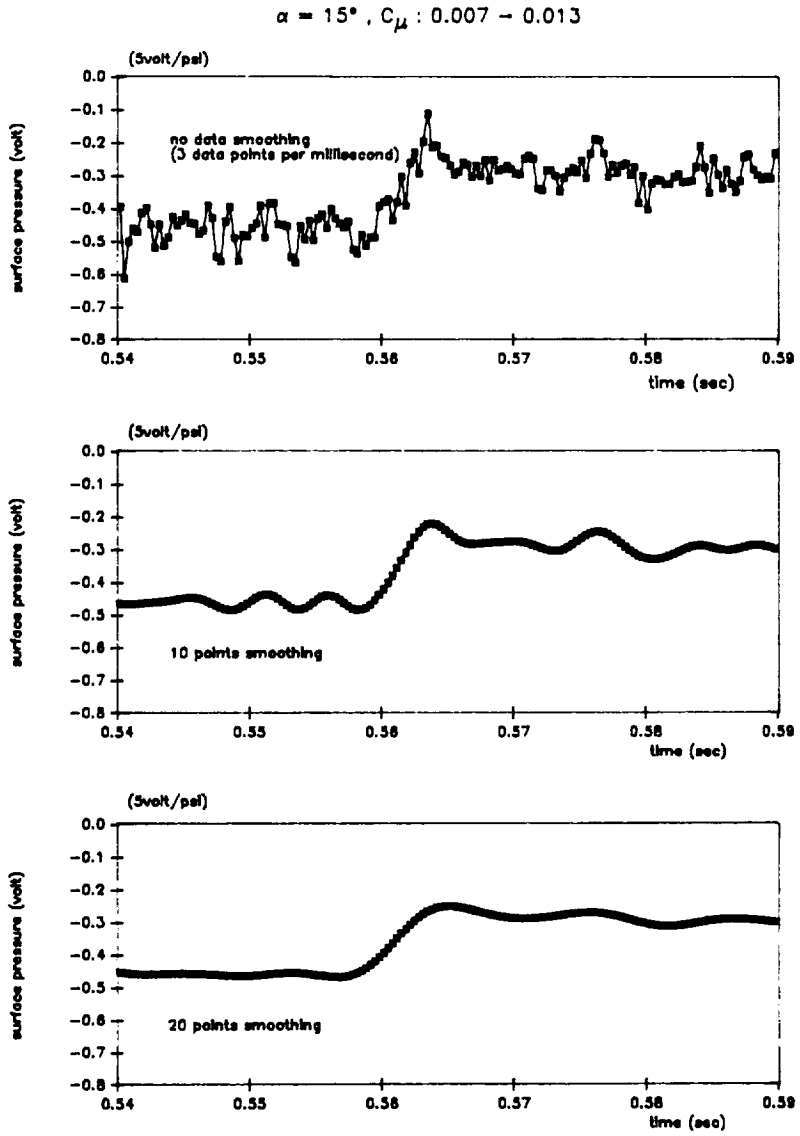

Figure 3.12 Typical unsteady surface pressure response with varying degrees of data smoothing

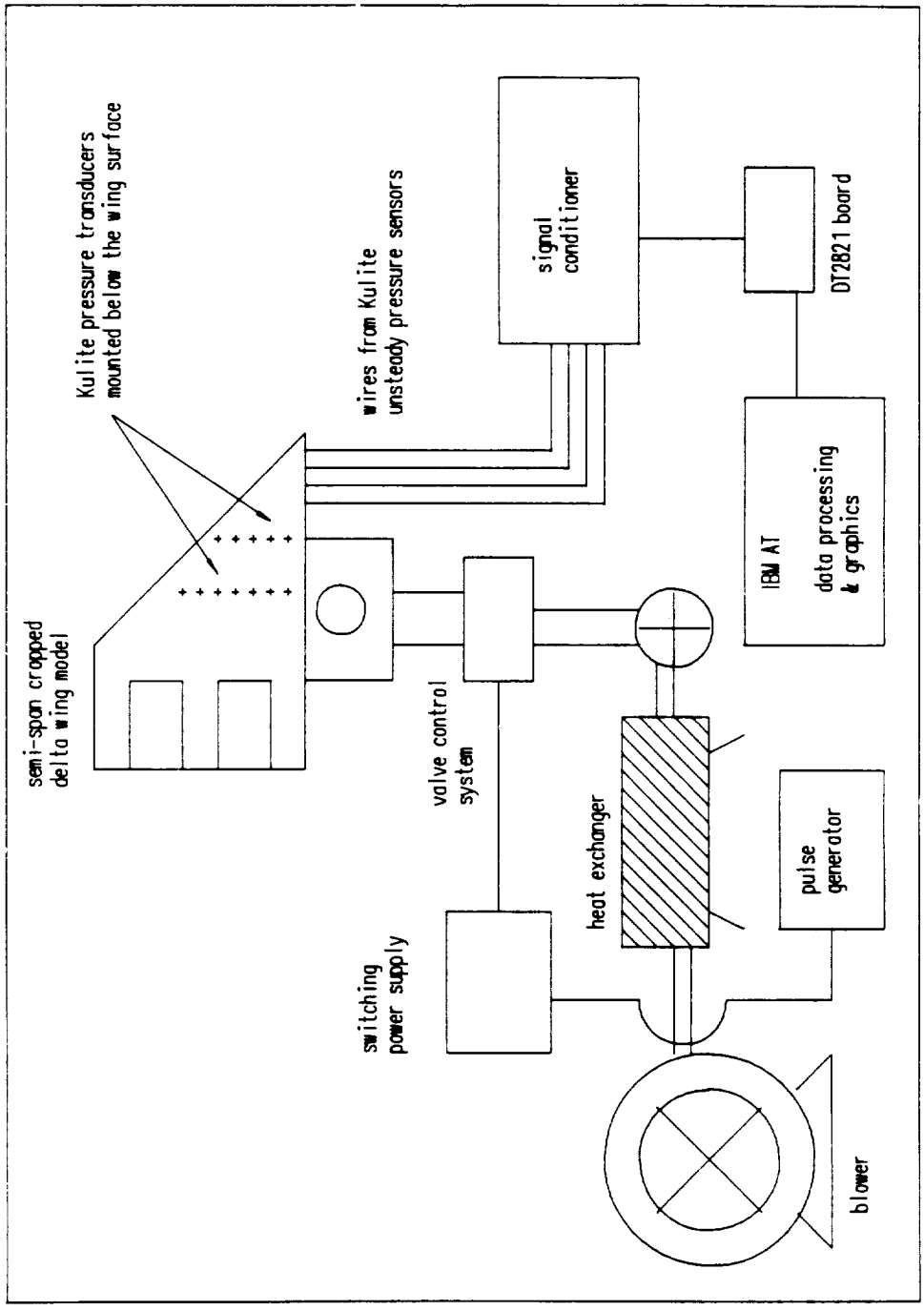

Figure 3.13 Schematic of unsteady pressure measurement system

CHAPTER 4
EXPERIMENTAL RESULTS AND DISCUSSION

4.1 Steady State Behaviour

To confirm that the measurements on the 50^0-swept cropped delta wing model were consistent with previous TLEB results[26,27], a series of steady state measurements was performed. The wing upper surface pressure distributions were measured for various angles of attack and blowing strengths. Two different regimes of angle of attack were observed to show the different behaviours of the vortical flow. The first was at angles of attack below the point of maximum normal force (referred to as 'low' or 'pre-stall' angle of attack) and the second was at angles of attack beyond the point of maximum normal force (referred to as 'high' or 'post-stall' angle of attack).

4.1.1 Spanwise pressure distribution

Surface spanwise pressure distributions were measured at two chordwise stations, 32.5 % and 54.5 %. Due to the limited amount of pressure instrumentation mounted on the model no actual measurements or integrations for normal force are available. It is not clear how to define the angle of attack for maximum total normal force just from upper surface pressure distribution measurement at two chordwise stations, but decreasing vortex strength could be observed from the pressure distribu-

tion data at around 25^0 angle of attack. The onset of vortex breakdown and the abrupt increase in flow unsteadiness could be observed above 25^0 angle of attack from the tuft visualization surveys. Strictly speaking, the stall angle of attack in this case corresponds to the angle of attack where vortex breakdown occurs at the chordwise station where the spanwise pressure distributions were measured.

Figures 4.1 - 4.2 illustrate the spanwise pressure distributions without blowing at 32.5 % and 54.5 % chordwise stations for several angles of attack. The movement of the vortex core (which approximately corresponds to the suction peak position) with increasing angle of attack is clearly demonstrated. The inboard movement of the vortex core and the increase in scale of the vortex motion with increasing angles of attack can be observed (this can be represented by the vortex core height from the wing surface and is approximately proportional to the half width of the spanwise vortex pressure distribution[26]). These results are typical of vortex flow on sharp leading edge delta wings[31].

The angle of attack representing 'low angle of attack' (pre-stall) behaviour was chosen at 15^0 : for 'high angle of attack' (post-stall), 35^0. Figures 4.3 - 4.8 illustrate the spanwise pressure distributions at various blowing strengths from 15^0 to 40^0 angles of attack. Figure 4.3 shows the typical low angle of attack behaviour with various blowing strengths at 32.5 % chordwise station. The reduction of vortex influence and the movement of the vortex with increasing blowing strength are clearly demonstrated. The leading edge suction representing the attached wall jet is assumed to be present and would offset the reduced vortex influence on normal force[26,27]. Figure 4.7 shows the equivalent results for the typical high angle of attack case. The enhanced nature of the vortical flow is evident. There is no vortical flow without blowing at

this post-stall angle of attack but the vortical flow is redeveloped with only a small amount of blowing momentum. This redeveloped vortical flow is strengthened and stabilized with increasing blowing momentum up to C_μ = 0.043. The vortex influence is reduced for large values of blowing momentum coefficient. Thus the behaviour of the vortical flow for $C_\mu >$ 0.043 is similar to that at low angle of attack. Notice that the values of the blowing momentum coefficient are significantly less than for the previous 60^0-swept, conical delta wing test results, figures 2.4 and 2.5 in section 2.2. This is probably a direct effect of the smaller blowing slot height that was used on the present model. Previous work on other wall jet blowing schemes such as circulation control airfoils has suggested that efficient boundary layer control may be achieved with slot heights as small as 1/100th of the local boundary layer thickness[32,33]. The higher velocities from the blowing slot for a given C_μ, i.e., the smaller slot height, promote more rapid mixing between the jet and the boundary layer. It is likely that a value of that order has not yet been reached on the present configuration and therefore that further improvement may be possible. As previously discussed, all results are consistent with the general steady characteristics of TLEB discussed in section 2.2.

4.1.2 Interpretation of steady vortex behaviour

A more complete interpretation of the previous experimental data has yielded a fundamental result regarding the nature of the flow field with TLEB. This is the definition of a "vortex effective angle of attack".

First of all, it is convenient to define several quantities to aid in the explanation of the effects of TLEB on the vortical flow. Since there are no pressure tappings around the rounded leading edge or the

lower surface (due to the limited installation space in the model), the actual sectional force and rolling moment cannot be obtained from integration of the surface pressure distributions. But quantities which behave in a similar way to the sectional normal force and rolling moment can be defined from the upper surface spanwise pressure distribution. These quantities, $\tilde{C}_n$ and $\tilde{C}_l$, are shown as functions of α for several values of the blowing coefficient C_μ in figure 4.9 and 4.10. All upper ~ quantities are force or moment coefficients about midspan experienced by the half a delta wing. Futhermore, the results suggest that they may be expressed in the form

$$\tilde{C}_n = \tilde{C}_{n_{linear}} + \tilde{C}_{n_v} \tag{4.1}$$

and

$$\tilde{C}_l = \tilde{C}_{l_{linear}} + \tilde{C}_{l_v} \tag{4.2}$$

where

$$\tilde{C}_{n_{linear}} = \int_{upper} [-C_{p_{linear}}] d\left(\frac{y}{s}\right) \tag{4.3}$$

and

$$\tilde{C}_{l_{linear}} = \int_{upper} [-C_{p_{linear}}] \frac{y}{s} d\left(\frac{y}{s}\right) \tag{4.4}$$

are the attached flow contributions (linear in α) to the sectional upper surface force and rolling moment coefficients;
and

$$\tilde{C}_{n_v} = \int_{upper} [-(C_p - C_{p_{linear}})] \; d\left(\frac{y}{s}\right) \tag{4.5}$$

$$\tilde{C}_{l_v} = \int_{upper} [-(C_p - C_{p_{linear}})] \frac{y}{s} d\left(\frac{y}{s}\right) \tag{4.6}$$

are the vortex force contributions (non-linear in α). The linear contributions $\bar{C}_{n_{linear}}$ and $\bar{C}_{l_{linear}}$ can be determined approximately from the constant level of spanwise pressure distribution near the wing root region and represent the contribution from the attached flow.

It is clear from these figures that the maximum value, $\bar{C}_n^*$, and the angle of attack at which this occurs (stall angle) both increase with C_μ. If the non-linear vortex contribution is isolated, as shown in figure 4.11 and 4.12, the influence of blowing becomes clear: the non-linear normal force is shifted in α with increasing C_μ.

With $\bar{C}_{n_v}^*$, the maximum value of $\bar{C}_{n_v}$, occuring at $\alpha = \alpha^*$, it is found that $\bar{C}_{n_v}^*$ is approximately constant and that α^* is a linear function of C_μ as shown in figure 4.13 and 4.14.

$$\bar{C}_{n_v}^* = 0.525 \tag{4.7}$$

$$\begin{aligned} \alpha^* &= \alpha_o^* + k\, C_\mu \\ &= 0.4887 + 3.7815\, C_\mu \quad (\alpha \text{ in rad.}) \end{aligned} \tag{4.8}$$

Furthermore, if the relationship between $\bar{C}_{n_v}$ and α for no blowing is expressed as

$$\bar{C}_{n_v} = \bar{C}_{n_v}^* f\left(\frac{\alpha}{\alpha_o^*}\right) \tag{4.9}$$

It is found that, with blowing, the results may be expressed in the form

$$\bar{C}_{n_v} = \bar{C}_{n_v}^* f\left(\frac{\alpha - kC_\mu}{\alpha_o^*}\right)$$

$$= \tilde{C}_{n_v}^{*} \quad f\left(\frac{\alpha - 3.7815 C_\mu}{0.4887}\right) \qquad (4.10)$$

The result is shown in figure 4.15 which clearly identifies the pre-stall and post-stall regimes in the presence of blowing. Thus, the behaviour of 'f' can describe the vortex contribution to normal force for any combination of angle of attack and blowing strength for this configuration. The constants $\tilde{C}_{n_v}^{*}$, α_0^{*}, and k are expected to vary with the geometry. From this interpretation, the new variable, α - k C_μ , can be defined and this is termed "vortex effective angle of attack".

$$\alpha_e = \alpha - k\, C_\mu \quad , \; k = 3.7815 \text{ (rad.)} \qquad (4.11)$$

where α : angle of attack

α_e : vortex effective angle of attack

This analysis is carried out using only the upper surface pressure distribution data at a given chordwise station. But the behaviour of the true sectional normal force, which includes the contribution from the lower surface pressure distribution, is approximately unchanged by angle of attack and blowing strength. Furthermore, the behaviour of the sectional characteristics like C_n, C_l, etc will be the same as the behaviour of the total characteristics (such as C_N) when the flow field is approximately conical.

For a rounded leading edge delta wing at a pre-stall angle of attack, the primary separation point moves outboard around the leading edge as the angle of attack increases, figure 2.1. This motion of the primary separation point, coupled through the vortex equilibrium, modifies the

vortex strength and the vortex location. As shown in figure 2.1, the vortex strength increases with increasing angle of attack (before stall) in the zero blowing configuration. When blowing is applied, the primary separation point moves toward the wing root and the corresponding vortex strength is decreased with increasing blowing strength and has the same effect as reducing the angle of attack for the vortical flow.(see eq.4.10)

At high angles of attack without blowing, there is only a very weak vortical flow structure on the wing due to vortex burst. The primary separation point is at the leading edge tip in this situation. When sufficient blowing is applied to displace the primary separation inboard on the rounded leading edge, a vortical flow structure redevelops and is similar to the vortical flow field formed at the lower geometric angle of attack without blowing. For example, the spanwise pressure distribution measured at 30^{o} with some blowing strength resembled that measured at 10^{0},15^{0}, and 20^{0} angles of attack without blowing, figure 4.16. Some lateral translation is observed due to different vortex core locations, but otherwise the vortical flows appear similar. The vertical translation of flat region of pressure distribution is due to the different geometric angle of attack, i.e., different linear part of the lift. This observation was a general trend for the experimental data at high angles of attack. Similar vortical flow, having the same vortex contribution to normal force (or vortex strength), can be reproduced by applying blowing at high angles of attack. In other words, a vortical flow field with TLEB at some fixed angle of attack has very similar characteristics to another vortical flow field without blowing at a lower angle of attack.

It has been shown (figure 4.9 and 4.10) that the vortex lift due to blowing is decoupled from the attached flow lift which is independent of blowing under the conical flow assumption. Figure 4.17 clarifies the

decoupling hypothesis. Observations from spanwise pressure distribution data at a fixed chordwise station shows the decoupling behaviour of the linear and non-linear force contributions. The total normal force behaviour, figure 2.3, from the integration of spanwise pressure distribution measurements obscured this hypothesis, the reason being that the contribution of leading edge suction due to the attached jet compensates the reduction of the vortex force at pre-stall angle of attack[26].

Previous results[30,41] for the normal force, without blowing, have been expressed in the form when α is normalized by ϵ.

$$\frac{C_N}{\epsilon^2} = 2\pi k_1\left(\frac{\alpha}{\epsilon}\right) + k_2\, g\left(\frac{\alpha}{\epsilon}\right) \tag{4.12}$$

where ϵ is the semi-apex angle of the delta wing.

Brown and Michael[41] derived an analytical expression of the form

$$\frac{C_L}{\epsilon^2} = 2\pi\left(\frac{\alpha}{\epsilon}\right) + 4.987\left(\frac{\alpha}{\epsilon}\right)^{5/3} + 1.322\left(\frac{\alpha}{\epsilon}\right)^{2/3} \tag{4.13}$$

and Smith[30], through a numerical method, found that

$$\frac{C_L}{\epsilon^2} = 2\pi\left(\frac{\alpha}{\epsilon}\right) + 4.9\left(\frac{\alpha}{\epsilon}\right)^{1.7} \tag{4.14}$$

for slender, thin, sharp leading edge delta wings.

The experimental results of the present work (only using the upper surface pressure distributions) when cast in the form of expression (4.12) give the constants $k_1 = 0.186$, $k_2 = 1.0805$

and
$$g\left(\frac{\alpha}{\epsilon}\right) = 6.5048\left(\frac{\alpha}{\epsilon}\right)^{7/2}\left(2.1 - 2\,\frac{\alpha}{\epsilon}\right)^{7/4} \tag{4.15}$$

where the form of $g(\alpha/\epsilon)$ has been chosen to give a maximum value of $g = 1$ which occurs at $\alpha/\epsilon = 0.7$ because the maximum vortex contribution to normal force without blowing occurs at $\alpha = 28^{o}$ and the semi-apex angle of the wing, ϵ, is 40^{o} for this configuration.

Because of the dependence of the vortex contribution on C_μ, as discussed previously, the more general result, which includes the effects of blowing can be expressed as

$$\frac{C_N}{\epsilon^2} = 2\pi k_1\left(\frac{\alpha}{\epsilon}\right) + k_2\, g\left(\frac{\alpha - kC_\mu}{\epsilon}\right) \tag{4.16}$$

Equation (4.16) reflects the fact that the attached flow contribution varies linearly with the angle of attack, α, whereas the vortex contribution is a non-linear function of the effective angle of attack, $\frac{\alpha - kC_\mu}{\epsilon}$. The contribution of the blowing jet i.e. the leading edge suction due to the attached flow around the rounded leading edge is not included in equation (4.16)

The effect of TLEB may be thought of as reducing the "vortex effective angle of attack" with increasing blowing strength. In the limit

the fully attached flow case for a given angle of attack represents a vortical flow with zero effective angle of attack. The decoupling of the linear and non-linear forces based on the effective angle of attack concept suggests that TLEB may be a practical solution for changing normal force without changing attitude.

4.1.3 Steady pressure behaviour at single location

Further insight into the steady state response of the surface pressure may be obtained from an examination of the results at a fixed single location on the wing as a function of blowing strength. Figures 4.18 - 4.21 illustrate the pressure coefficient, C_p, behaviour as a function of blowing strength at the various fixed spanwise locations at 32.5 % chordwise station. This very simple representation of the data clearly illustrates the different control of the vortex influence as a function of the angle of attack and blowing coefficient. Figure 4.18 is one of these C_p.vs.C_μ plots at a fixed location of 32.5 % chordwise and 76.3 % spanwise location. The chosen location in figure 4.18 coincides with the position of one of the Kulite unsteady pressure sensors. The behaviour of the vortical flow can be categorized by introducing the concept of vortex effective angle of attack which was discussed in the previous section.

It is important to explain why the steady pressure signal from a fixed location is so meaningful. The vortex effective angle of attack can identify the state of the vortical flow from the vortex strength. Detailed velocity field surveys in the cross flow plane could also provide information about the state of vortex flow but this is a very time

consuming procedure. As previously discussed, the spanwise pressure distribution can provide the same kind of information qualitatively. The existence of vortical flow, the spanwise core location, relative vortex core height from the wing surface, relative vortex strength, and the existence of a burst vortex before that chordwise station can be determined qualitatively just from the shape of the spanwise pressure distribution[26,27]. Figure 4.22 shows the steady state behaviour of the vortex contribution to sectional normal force and the pressure coefficient at a chosen location with respect to effective angle of attack. Two different regimes of vortex contribution to normal force (or vortex strength[26,27]) are clearly observed, figure 4.22. The first one is the region of decreasing vortex contribution to normal force with increasing C_μ. The second one is the region of increasing vortex contribution to normal force with increasing C_μ. The first region can exist in different angle of attack regions. That is to say, vortex flow on the wing is in the pre-stall region at low angles of attack and it can be also in the pre-stall region at high angles of attack with sufficient blowing strength. The behaviour of the vortical flows in the pre-stall region is the same although actual angles of attack (low or high) are different. This is because TLEB produces the same effective angle of attack of the vortex flow at different geometric angles of attack. The vortex strength shows the same behaviour of the function 'f' in section 4.1.2, figure 4.18 and 4.23. So the behaviour of the vortex strength or vortex contribution to normal force can be deduced from figure 4.15. The second region can exist only at high angles of attack, i.e. the angles of attack after stall without blowing. Figure 4.24 shows a way of deducing the behaviour of the vortex strength with respect to C_μ from figure 4.15. In the pre-stall angle of attack region, f (normalized function for vortex contribution to normal force) shows a decreasing behaviour when the angle of attack is fixed and C_μ is increased. This corresponds to the first region i.e.

pre-stall, low angle of attack. In the high angle of attack region, two types of behaviour can be observed. Function 'f' shows the increasing behaviour when the angle of attack is fixed and the C_μ is increased. This corresponds to the second region i.e. post-stall, high angle of attack. When the C_μ is increased further, then f shows the decreasing behaviour again with increasing C_μ, which means that the vortex flow is in the pre-stall regime. For the pre-stall regime, a well-organized, stable vortex flow exists over the wing and there is no vortex breakdown from the apex to the chordwise station being considered.

From the above observation it is possible to locate one spanwise position where the qualitative behaviour of the surface pressure is very similar to the behaviour of the vortex strength or the vortex contribution to normal force, figure 4.22. There is a close similarity between these two plots in figure 4.22. The local surface pressure is affected by two contributions, vortex strength and distance from the core. The steady surface pressure behaviour in figure 4.18 - 4.21 reflects the relative contributions of vortex strength and distance from the core to the local surface pressure at various locations. Increasing vortex strength is equivalent to decreasing surface pressure (i.e. greater suction) and decreasing vortex strength is equivalent to increasing surface pressure, figure 4.18. Thus, the local surface pressure behaviour in figure 4.18 represents the behaviour of the vortex strength or the vortex contribution to normal force (see figure 4.23). In regions where the local surface pressure is increasing with increasing blowing, a strong well defined vortex is present over the wing surface and the vortex strength is reducing. This corresponds to a pre-stall regime. In regions where the local surface pressure is decreasing with increasing blowing, the vortex strength is increasing and this corresponds to the post-stall regime. In this latter region, the degree of bursting of the vortex is being reduced

and the stability of the vortical flow is improved.

As discussed above, the state of the vortex and the magnitude of the vortex contribution to normal force can be represented by a C_p measurement at a suitably chosen spanwise position for each chordwise station. So the behaviour of the pressure coefficient at chosen location is a very good indicator for representing the state of the vortex flow (pre-stall or post-stall) at that chordwise station. As will be shown, this approach simplifies unsteady testing procedures.

4.1.4 Derivation of quasi steady response

Figures 4.18 - 4.21 illustrate the steady state response of the local surface pressure at various locations where Kulite pressure transducers are installed on the wing. For transient conditions, the unsteady pressure signals were measured in real time at several locations on the wing upper surface and model plenum. To better understand the unsteady response of the surface pressure some reference datum must be defined. This reference datum is called the 'quasi steady response' in the analysis of the unsteady data. It is possible to derive a quasi steady surface pressure response at every location from the internal pressure transition signal and the steady state response of the local surface pressure, figures 4.18 - 4.21. At a fixed angle of attack, the blowing momentum coefficient is a function of the internal pressure and the relationship between the internal pressure and the blowing momentum coefficient is pre-calibrated. The steady state results are known as a function of angle of attack and blowing strength. Therefore the quasi steady response of the surface pressure, which represents a vortical flow response with zero time lag,

can be deduced from the internal pressure transition signal and the corresponding steady state behaviour of the local surface pressure. This quasi steady response of the surface pressure is the ideal result which neglects any unsteady lag effects. The purpose of the quasi steady response is not to approximate the real unsteady surface pressure response but to act as a reference response for measuring the contribution of lag effects on the vortex flow re-organization. Figure 4.25 shows the way to produce a quasi steady response from the internal pressure transition signal and the steady results of the local surface pressure.

4.2 Transient Behaviour

4.2.1 Definition of test cases

For steady state measurement, two different regimes were observed; the pre-stall and post-stall regimes. The test cases were determined in the following way to examine the difference of vortex flow re-organization between those two regimes.

(i) pre-stall at low & high angle of attack
(ii) post-stall at high angle of attack
(iii) trans-stall at high angle of attack
(i.e. transition between pre- and post-stall)

Stall is defined as the angle of attack with maximum section normal force at each blowing strength.

As mentioned in section 4.1.3, the C_p.vs.C_μ behaviour for different angles of attack at certain locations on the wing surface can represent

the state of the vortical flow in terms of the vortex contribution to normal force. Therefore the C_p.vs.C_μ plots (figure 4.18 - 4.21) are a good reference to determine the two end states and to examine the characteristics of vortex re-organization for different effective angle of attack regimes. Figure 4.26 shows the test cases for the measurement of the transient surface pressure response. The sign of $\dot{C}_\mu$ plays an important role in the vortex transition process so both positive $\dot{C}_\mu$ and negative $\dot{C}_\mu$ were tested in each case.

The two end states, $C_{\mu i}$ and $C_{\mu f}$, were chosen so as to maximize the difference of the local surface pressure. The resolution for transient measurements is improved due to the relatively large surface pressure difference between the end states. In both low and high angle of attack operations, the surface pressure difference between two end states at the chosen location (y/s=0.763 at x/c=0.325) was kept constant within the capability of blowing control valve system. By keeping constant the internal pressure transition time and the increment of the surface pressure, it is possible to observe changes in the overall response time of the vortical flow as a function of the angle of attack and the initial blowing conditions. The constant increment of the local surface pressure at the chosen location is approximately equivalent to the change of vortex strength or vortex contribution to normal force at that chordwise station. For the trans-stall case the vortical flow on the wing surface passes the peak at which the vortex strength is maximum during the transition. Most of the discussion will focus on the transient local surface pressure response at the y/s=0.763 spanwise location.

4.2.2 Transient response in pre-stall regime

Figures 4.27 - 4.28 show typical unsteady surface pressure signals for the pre-stall case at angles of attack, namely 15^0 and 35^0. Although the number of unsteady pressure transducer locations was quite limited, it is possible to examine how the spanwise surface pressure distribution varies during the transition. Figures 4.29 - 4.30 show the time history of the spanwise pressure distribution. Figure 4.29 shows the case of the low angle of attack and figure 4.30 is for the high angle of attack case. As can be seen, the transitions from one state to another are quite smooth. There is some slight overshoot in the detailed time history due to the overshoot of the internal pressure. In general, the surface pressure transition i.e. vortex re-organization process, is well correlated with the internal pressure pattern for pre-stall angle of attack operations. As the blowing increases, the vortex influence reduces and the location of the vortex suction peak (determined approximately by the vortex core location) shifts inboard, figure 4.29 - 4.30.

Figures 4.31 - 4.36 show the comparisons between the surface pressure response and the quasi steady response (see section 4.1.4) at a single location in the pre-stall regime for various angles of attack. The time axis is non-dimensionalized by one convective time which is the time required for a particle travelling at the free stream speed to travel one chord length. For this particular configuration, one convective time is 13.8 milliseconds. Figure 4.31 - 4.33 represent the response at low angles of attack and figures 4.34 - 4.36 represent the responses of high angles of attack. Both the low angle of attack and high angle of attack are in the pre-stall regime because the values of α - k C_μ are less than the unblown stall angle of attack. The overall form of the surface pressure

transition agrees quite well with the internal pressure transition as represented by the quasi steady response. The longest time lag of the actual surface pressure signal from the quasi steady response appears to be of the order of 5 milliseconds (0.362 convective time) at 15^0 angle of attack (figure 4.31) and the general form of the correlation between the two signals is very good. It should be noted however that because of the apparent 'noise' on the actual surface pressure responses, it is difficult to discern any obvious time lags from each plot. Closer examination of the actual recorded time histories shows that the time lag between those two signals reduces with increasing angle of attack for the pre-stall case.

In the pre-stall regime, the time lags are less than one convective time scale. As expected, the local unsteady surface pressure response at this particular position (y/s=0.763) could also represent the unsteady behaviour of the vortex influence.

In summary, rapid vortex re-organization with a short time lag (less than one convective time scale) can be observed in this regime. The actual unsteady pressure response follows the quasi steady response with only a short time lag. This time lag is reduced with increasing geometric angle of attack.

4.2.3 Transient response in post-stall regime

Figure 4.37 shows the typical unsteady surface pressure signals for post-stall operations. At 35^0 angle of attack without blowing the vortical flow represents the post-stall condition. Similarly to section 4.2.2, the transient spanwise pressure distribution (figure 4.38) can be deduced from figure 4.37. Two major differences can be observed in the post-stall

operation. Compare the behaviour in figures 4.29 - 4.30 and 4.38. Note that the actual transition times for the internal pressure were similar for both pre-stall and post-stall operations (26 milliseconds) but that the time to reach steady state is nearly double in the post-stall case. Second, the steady vortex influence is increased with increasing blowing strength in the post-stall regime (figure 4.24) but the unsteady surface pressure distribution shows an initially decreasing vortex influence. After this initial undershoot of vortex influence, the unsteady vortex influence starts to approach the quasi steady behaviour.

The unsteady local surface pressure responses, figures 4.39 - 4.41, show the same trends. Notice how the transition time appears to be much longer although the transition time for the blowing strength was approximately constant. The time lag in figures 4.39 - 4.41 now appears to be several times one convective time scale. In this post-stall regime, the unsteady local surface pressure response does not follow the quasi steady response. In the initial stage of the vortex re-organization, the actual surface pressure response reacts the opposite way to the steady response (this was observed in figure 4.38, too). After this initial reverse reaction the local surface pressure response starts to follow the quasi steady response with a very long time lag. Closer examination of figures 4.39 - 4.41 shows this initial reverse response is fast and correlates with the initial internal pressure rise but in the reverse sense. In the later stage of vortex re-organization, after this initial reverse peak, the surface pressure shows relatively slow response and some oscillations. A long transition time and a long time lag are characteristics of vortex re-organization in the post-stall regime.

4.2.4 Transient response in trans-stall regime

Figure 4.42 shows an example of the unsteady local surface pressure response in the trans-stall regime. In this case the blowing range traverses the steady state peak in the surface pressure figure 4.18. The position was also 32.5 % chordwise station and 0.763 spanwise location. The lack of a significant difference between the end states makes it difficult to discern any time lags from the signals but the two stages of vortex re-organization i.e. initial fast, reverse response and the later slow, oscillating response, can be observed as in the post-stall regime. That means the pattern of the vortex re-organization depends on the initial state of the vortical flow, when the blowing is initiated. The source of noise on the pressure signals in the later stage after the reverse peak in figure 4.42 may be related with vortex streamwise unsteadiness particularly when bursting is present on the wing. This phenomenon of initial reverse behaviour when the starting point of blowing is in the post-stall regime will be discussed in the next section.

4.2.5 Fundamental time scales of vortex re-organization

From the observations in previous sections it is obvious that there are different fundamental time scales for vortex re-organization with TLEB which depend on the initial blowing conditions. One is the short characteristic time scale which is represented by a short transition time, short time lag and positive unsteady contribution with respect to the quasi-steady response (figure 4.31 - 4.36) for the pre-stall regime. The other is a long characteristic time scale which is represented by a long transition time, long time lag and negative unsteady contribution with

respect to the quasi-steady response (figure 4.39 - 4.41) for the post-stall regime.

A good starting point to understand the physics of the fundamental time scales is to examine the steady characteristics of the vortex flow in both the pre-stall and post-stall regimes. In the pre-stall regime, a well-organized, stable leading edge vortex flow exists on the wing and the vortex flow structure is approximately conical. In the post-stall regime, an unstable burst vortex flow exists and the vortex breakdown location moves toward the apex with increasing geometric angle of attack. As the blowing momentum increases the vortex breakdown location moves downstream, as a result, the overall stability of the vortex flow is increased. Further increases of the blowing momentum can remove the vortex breakdown past a given chordwise station; then the vortical flow at that chordwise station exhibits the pre-stall behaviour (figure 4.24).

Transient blowing changes the vortical flow from one steady state to another. In the pre-stall operation, this change of vortical flow structure occurs mainly in the lateral direction, in other words, the approximately conical vortex structure shifts spanwise in the cross flow plane according to the sign of $\dot{C}_\mu$. The characteristic time scale related to this change is short. Conicality of the flow field implies there is no longitudinal time scale involved during the transition. In the post-stall operation, the transient blowing modifies the longitudinal structure of the vortical flow, particularly the streamwise vortex breakdown location. Related to this three-dimensional vortex structure change, the concept of vortex equilibrium can be extended to three-dimensional burst vortex equilibrium. That is to say, the TLEB can modify the three-dimensional equilibrium of the burst vortex, which is represented by the longitudinal location of the vortex breakdown, and the characteristic time scale

related to this change is much longer than the short characteristic time scale as seen in the experimental observations.

It is suggested that the governing parameters involved in defining the vortex re-organization time scales for the pre-stall regime are the cross flow vortex dimension (which can be represented by the core height from the wing surface, for example), cross flow velocity ($U_\infty \sin\alpha$) and the convective length in the cross flow plane (which is the local semi-span length at a fixed chordwise station). The lateral structure of a steady conical vortex flow is governed by the cross flow velocity component, which increases with increasing angle of attack. The cross flow vortex dimension doesn't change much from one blowing strength to another[27] in the pre-stall regime. Therefore, the cross flow velocity ($U_\infty \sin\alpha$) and the convective length in the cross flow plane can play an important role in determining the rate of vortex re-organization represented by the short time scale. The cross flow velocity increases with increasing angle of attack but the convective length of the cross flow plane is constant. Therefore, the time scale derived from those two parameters should reduce with increasing angle of attack. The observed time lag from the quasi steady comparison does indeed reduce with increasing angle of attack in the pre-stall regime (see section 4.2.2). Therefore, the reduction of the unsteady lag must be related to the increase of the cross flow velocity component with increasing angle of attack.

The primary effect of transient blowing is to modify the vortex strength and the lateral position of the vortex core, not the size of the vortex. This hypothesis is only valid in the pre-stall regime because the flow can be approximated as conical, i.e. no vortex burst is present forward of the observation station. Therefore no characteristic time

scales related to the longitudinal modification of the vortex burst are present. It should also be stated that in this regime there is little change in the overall normal force acting on the wing (see section 2.1) and therefore little change in the wake strength or trajectory. One would therefore not expect to see long time lags associated with wake modification.

In the post-stall operation, the fact that the surface pressure signals no longer correlate with the internal pressure may in part be due to the condition of the vortical flow in this regime. As mentioned before, the vortex burst location is somewhere forward of the measurement station in this regime. Therefore the assumption of conicality can no longer be applied. The location of the vortex burst moves along the streamwise direction with changing blowing strength. When blowing strength is increased the location of the vortex burst moves downstream and vice versa. So the concept of vortex equilibrium in the cross flow plane can be extended to include vortex equilibrium in a three-dimensional sense in the post-stall regime. That is to say, the primary separation line around the leading edge, streamwise trajectory and shape of the feeding sheet, trajectory of the vortex core, and finally the location of vortex burst can be determined by the specific blowing strength at a fixed angle of attack.

The longitudinal characteristic time scale may be important to the vortex re-organization at post-stall conditions because of three-dimensional re-structuring of the vortex flow.

The convection of the burst position in the streamwise direction can be characterized by the longitudinal convection time parameter which is the time required for a particle to travel one chord length with the

chordwise component of the free stream velocity, $U_\infty \cos\alpha$. For increasing angle of attack, the chordwise component of the free stream velocity is reduced. From experimental observation, the time constant and time lag in the quasi steady comparison increase with increasing angle of attack just as the longitudinal convection time is increased. This indicates that vortex re-organization in the post-stall regime is governed by the longitudinal convection of the vortex burst position.

The surface pressure transition time and time lag of these post-stall cases are very long compared to the pre-stall operations, figure 4.39 - 4.41. The reverse flow in the core of the burst vortex may play an important role in defining the long transition time for the flow to reach another state of three-dimensional vortex equilibrium. Also, the total normal force on the wing is being significantly modified due to the additive effect of the vortex lift and leading edge suction lift due to the attached jet flow around the rounded leading edge[27]. This implies a modification to the wake strength and trajectory. This will also impart a longer characteristic time scale on the flow re-organization as the downwash induced by the wake may take several convective time scales to stabilize. In this regime, even small changes in the downwash could cause large changes in the surface pressure due to the sensitivity of the vortex burst location on the local pressure gradients.

Another characteristic of the vortex re-organization in the post-stall regime is the initial reverse behaviour of the vortex influence observed in section 4.2.3. It is necessary to examine the nature of TLEB to explain this phenomena. Figure 2.1 shows the behaviour of vortical flow due to TLEB. The primary separation point shift around the leading edge directly controls the change of the lateral structure of the vortex flow in the cross flow plane. The related characteristic time scale is

relatively short since it is governed by the cross flow plane parameters. The initial stage of burst vortex re-organization in a post-stall regime is still governed by this lateral change of vortex structure due to the rapid modification of the primary separation point in the cross flow plane. The vortex strength is modified initially according to the sign of C_μ, i.e., is in the reverse direction with respect to the steady behaviour, figure 2.1. After the adjustment of the primary separation point in the cross flow plane, the longitudinal vortex re-organization, i.e. the adjustment of vortex breakdown location, starts to satisfy the new three-dimensional equilibrium of the burst vortex. In the later stages of re-organization after the reverse behaviour, the vortex influence at a certain chordwise station starts to increase due to the downstream movement of vortex breakdown (for positive C_μ). In this later stage, the oscillation of the pressure signal reflects the local oscillation of the vortex breakdown location. As discussed, the initial nature of TLEB with positive C_μ operation is to reduce the vortex influence, even in case of a burst vortex. The main reason for this reverse behaviour in the initial stage of vortex re-organization is due to the initial rapid lateral change of the vortex structure. The longitudinal change of vortex breakdown position cannot follow this rapid transition. So when the internal pressure transition is carried out in the quasi steady manner, which means the internal pressure transition time is quite long compared to the characteristic longitudinal time scale, this initial reverse behaviour would disappear.

The point is that even a burst vortex must satisfy cross flow equilibrium initially before reaching the new state of three-dimensional equilibrium.

4.2.6 Discussion of transient response for negative $\dot{C}_\mu$ operation

The previous discussions was mainly about the transitional vortex flow behaviour when the blowing momentum increased, i.e. positive $\dot{C}_\mu$. The primary purpose of TLEB is to extend the angle of attack envelope for a delta wing geometry so the behaviour of the vortical flow with TLEB in the post-stall region is the principal interest. In the post-stall regime, positive $\dot{C}_\mu$ operation reduces the severity of the vortex bursting or removes the burst altogether. The 'reverse' operation, i.e. negative $\dot{C}_\mu$, is also interesting and may aid in understanding the behaviour of the transitional vortical flow. For all tests, normal and reverse operations were recorded to compare the response pattern of the vortex re-organization. The response patterns have some differences.

As mentioned in section 3.4.2, there is an overshoot in internal pressure for positive $\dot{C}_\mu$ and an undershoot for negative $\dot{C}_\mu$. The internal pressure transition patterns in both cases were quite symmetric.

Figures 4.43 - 4.44 show the case of pre-stall at low angle of attack. Figure 4.43 shows the quasi steady response and figure 4.44 shows the actual surface pressure responses of normal and reverse operations. Figures 4.45 - 4.46 show the case of pre-stall at high angle of attack. Finally, figures 4.47 - 4.48 show the case of post-stall at high angle of attack. As shown in figures 4.44 and 4.46, the transition patterns of the local surface pressure are quite symmetric for pre-stall operations. The time lag between the quasi steady response and the surface pressure response is very similar as is the transition time of the vortex flow. Thus, there is no dominant dynamic hysteresis between the normal and

reverse operations in the pre-stall regime. In this situation, the cross flow velocity component is the same due to the same angle of attack for both normal and reverse operations; the vortex flow is approximately conical so it can be claimed that the lateral changes of the vortex structure in the cross flow plane are quite reversible. But, in case of post-stall operation (figure 4.48), dynamic hysteresis can be clearly observed. In reverse operation, the transition time for vortex re-organization is much longer than that for normal operation and some characteristic frequencies can be observed during the transition especially after the peak in reverse operation.

Interestingly, the initial transition patterns before the peaks are quite symmetric. As discussed before, the initial transition of the vortex flow in the post-stall regime occurs in the cross flow plane, and is mainly due to the rapid change of the primary separation point. After the peaks, the longitudinal changes become dominant. In this phase, the sign of $\dot{C}_\mu$ can be very important because the positive $\dot{C}_\mu$ means increasing the stability of vortical flow, (i.e. reducing the severity of vortex burst) and negative $\dot{C}_\mu$ means increasing the severity of the vortex burst. So the transition time of the vortical flow may be much longer and the characteristic frequencies may be related to the local oscillations of the burst position. This dynamic hysteresis is another characteristic of post-stall operation with TLEB.

4.2.7 Summary of trends

Figure 4.49 shows the trends of the time constant, τ, for vortex re-organization with respect to angle of attack. The unsteady signals were smoothed to remove the high frequency oscillations but measurement error

may still exist due to the highly unsteady nature of the phenomenon. All measured values of the time constant from various spanwise positions are plotted on the same figure to show the qualitative trend in both the pre-stall and post-stall operations. Figure 4.49 represents the behaviour of the time constant at 32.5 % and 54.5 % chordwise stations for pre-stall and post-stall regimes. The sign of $\dot{C}_\mu$ is positive in all cases.

Note the different trends of the time constant for different vortex effective angle of attack. In the pre-stall regime, the time constant for vortex re-organization reduces with increasing angle of attack and the trend is reversed for the post-stall regime. This indicates two different vortex re-organization mechanisms, that is to say, two different time scales for re-organization are involved. As the angle of attack increases the cross flow component of the free stream, $U_\infty \sin\alpha$, which is the governing parameter for well-organized strong leading edge vortex flow on delta wings, is also increased. TLEB can redevelop a well-organized vortex flow even at high angles of attack so the cross flow component is still effective in this situation. The reverse trends of the time constant for the two different regimes (pre- or post-stall) suggests two different time scales i.e. a lateral time scale (equivalent to the short characteristic time scale) for the pre-stall condition and longitudinal time scale (equivalent to the long characteristic time scale) for the post-stall condition.

Figure 4.50 summarizes the results of the time lag behaviour between the actual surface pressure signal and the quasi steady response from the internal pressure transition. As can be seen, the behaviour of the unsteady time lag for the pre-stall operation is very similar to the behaviour of the cross flow convective time scale which is the time required for a particle to travel the semi-span with the cross flow

velocity. And the behaviour of the unsteady time lag for the post-stall condition has the same trend as the behaviour of the longitudinal convective time scale which is the time required for a particle to travel one chord length with the longitudinal component of the free stream velocity. This is a good indication of the two different mechanisms dominant in vortex re-organization. The cross flow parameter is important in the approximately conical vortex flow at pre-stall condition and the longitudinal convection of the vortex breakdown position is important for post-stall conditions.

The previous discussion about the vortex re-organization with TLEB implies that it takes significantly longer to modify a burst vortex than it does an unburst, well organized vortex. Previous studies on wing rock[3,35] have exibited time scales for the limit cycle oscillation of the order of 20 - 30 convective time lengths which should be controllable by TLEB. Divergent phenomena more likely to occur during post stall maneuvers and the contribution of unsteady vortex bursting is significant. For these cases, the ability to control the vortex flow to avoid vortex burst in a time of the order of one convective length may permit safe steady operation at both high yaw and pitch angles.

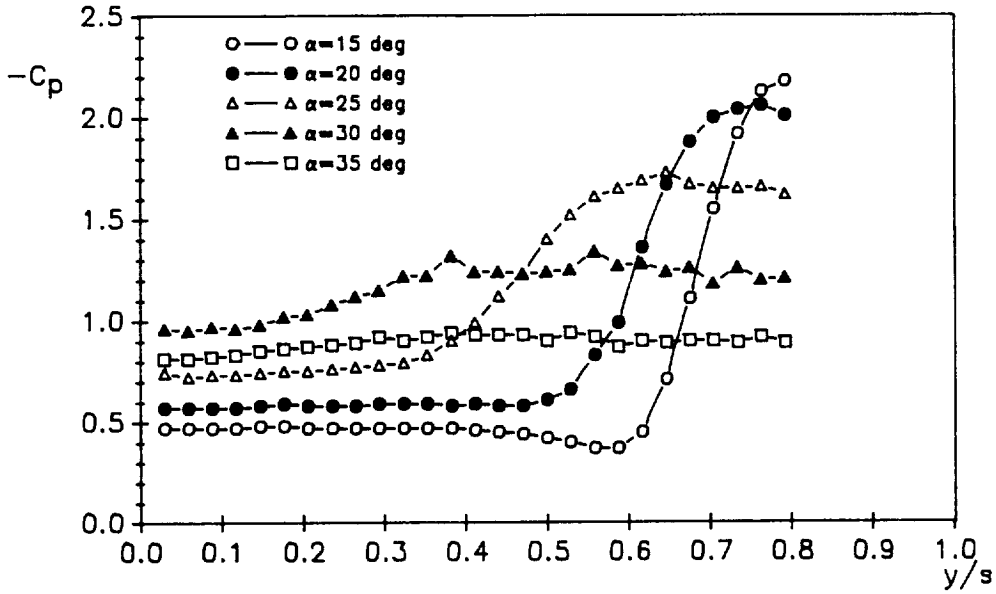

Figure 4.1 Upper surface spanwise pressure distribution without blowing (C_μ = 0.0, x/c = 0.325)

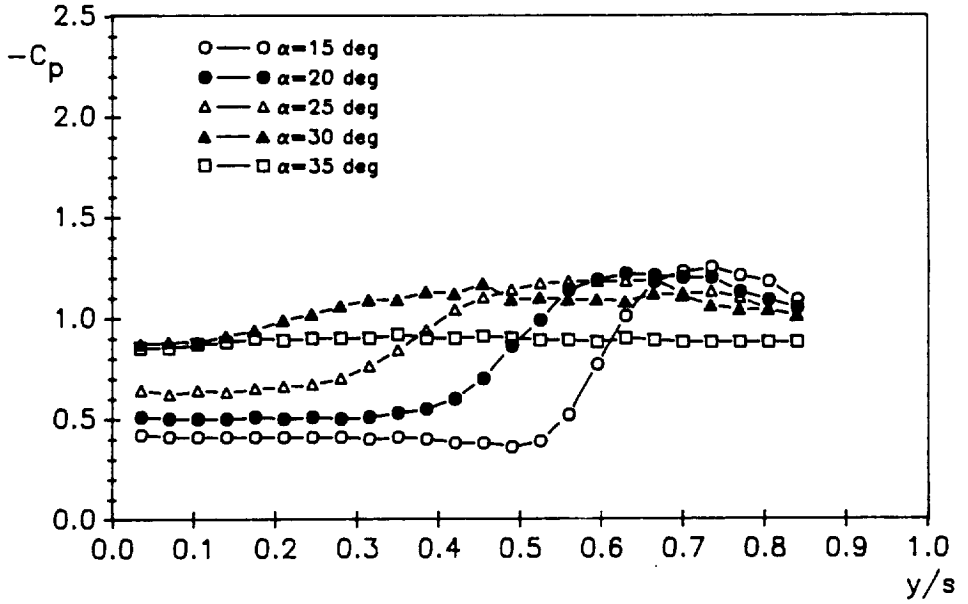

Figure 4.2 Upper surface spanwise pressure distribution without blowing (C_μ -0.0, x/c = 0.545)

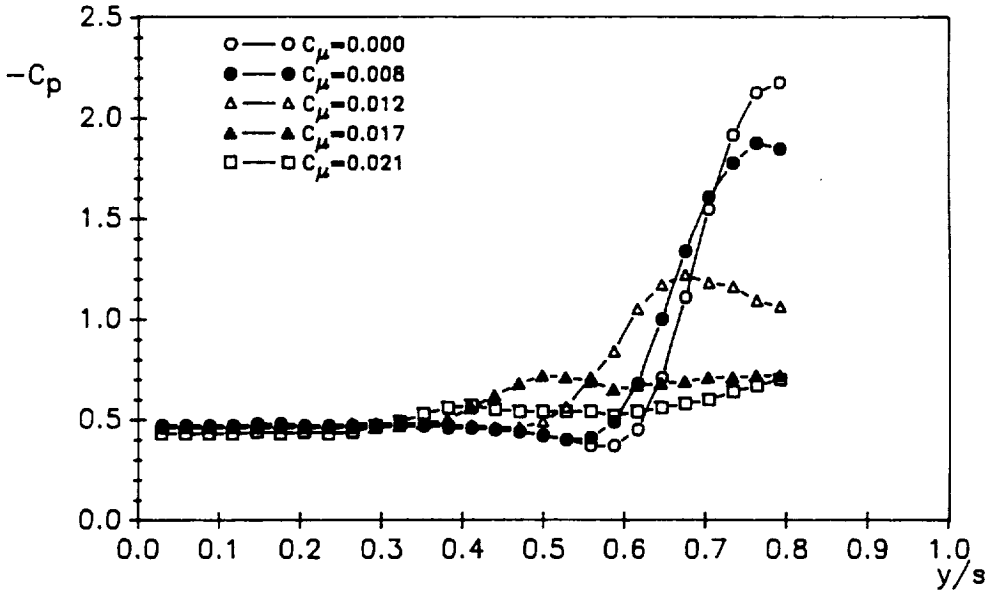

Figure 4.3 Upper surface spanwise pressure distribution with blowing ($\alpha = 15^0$, x/c = 0.325)

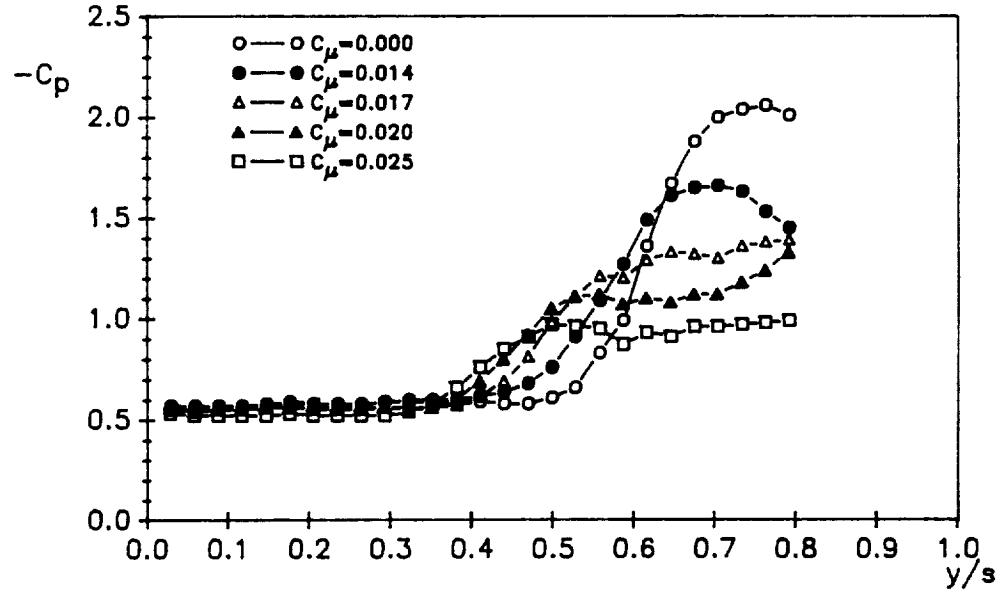

Figure 4.4 Upper surface spanwise pressure distribution with blowing ($\alpha = 20^0$, x/c = 0.325)

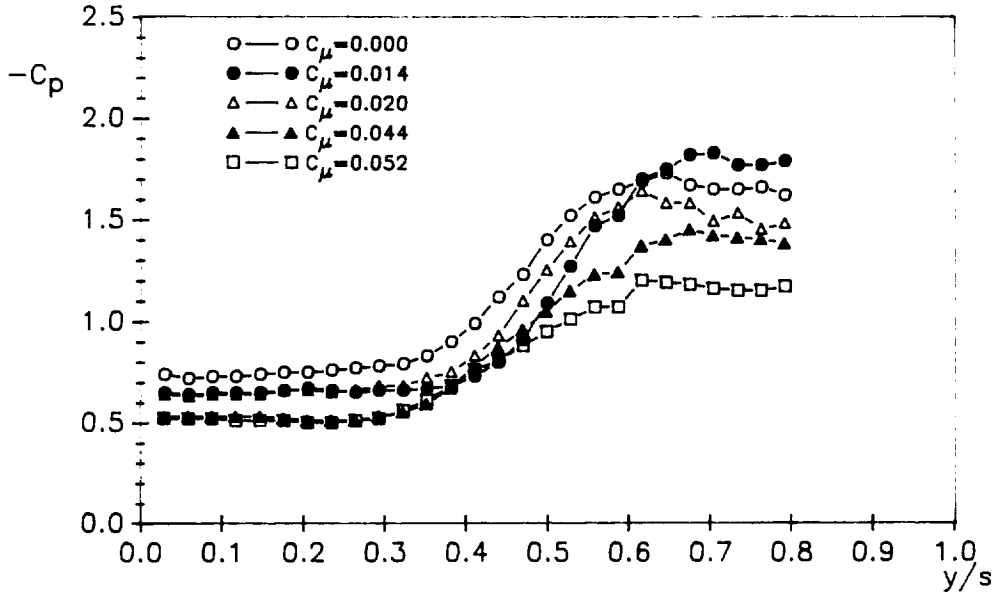

Figure 4.5 Upper surface spanwise pressure distribution with blowing ($\alpha = 25^0$, x/c = 0.325)

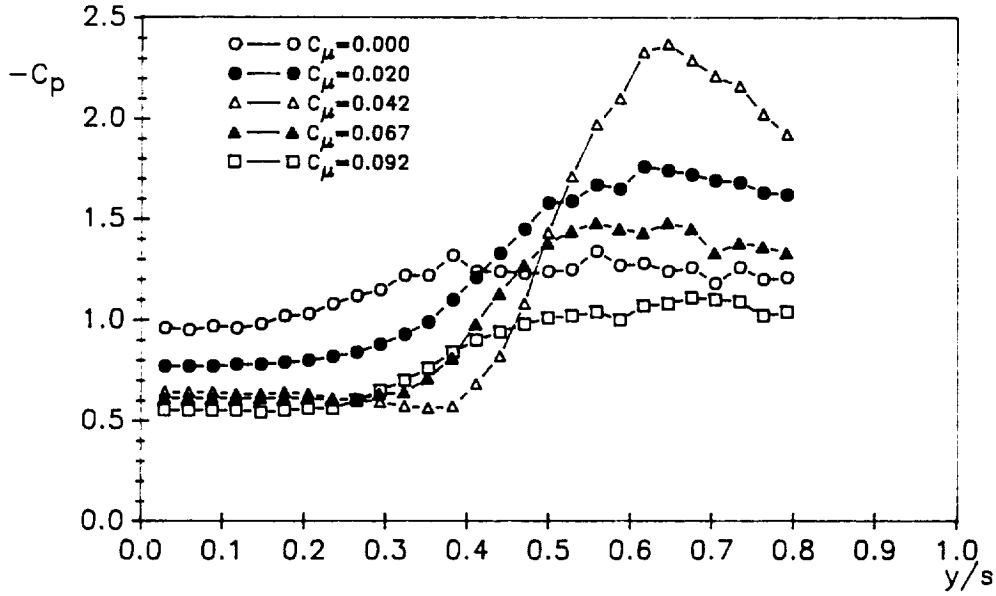

Figure 4.6 Upper surface spanwise pressure distribution with blowing ($\alpha = 30^0$, x/c = 0.325)

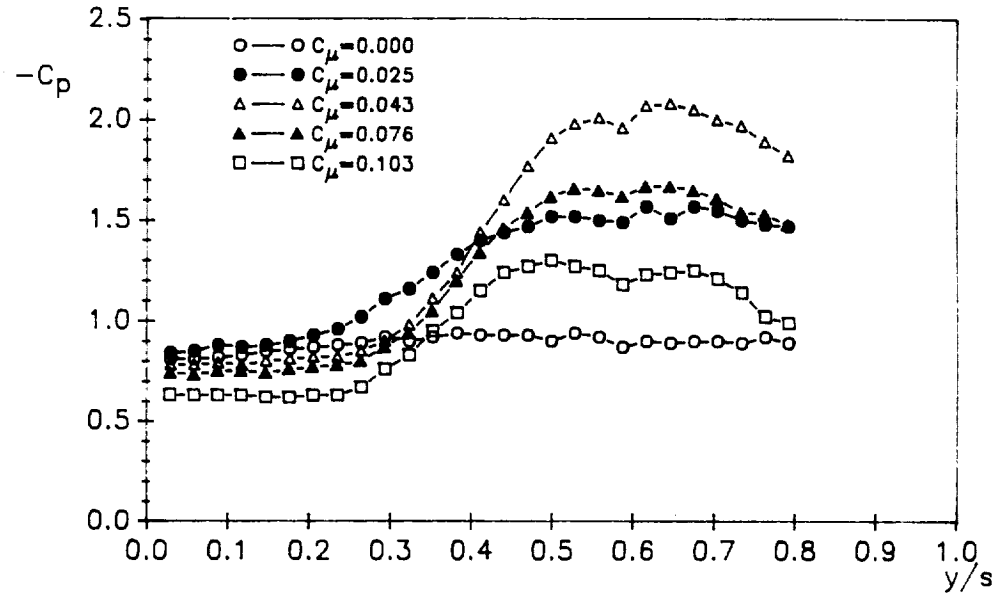

Figure 4.7 Upper surface spanwise pressure distribution with blowing ($\alpha = 35^0$, x/c = 0.325)

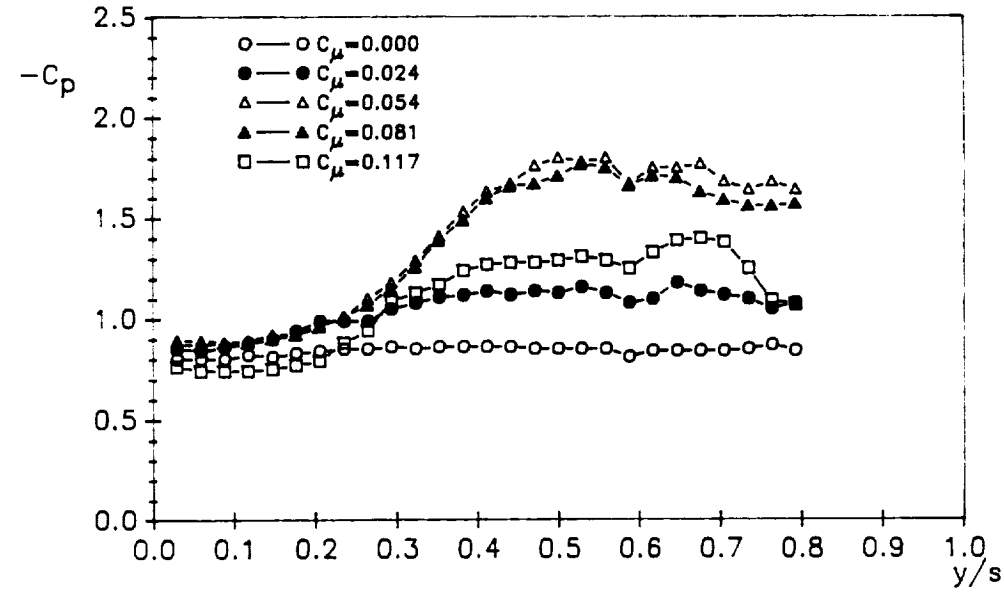

Figure 4.8 Upper surface spanwise pressure distribution with blowing ($\alpha = 40^0$, x/c = 0.325)

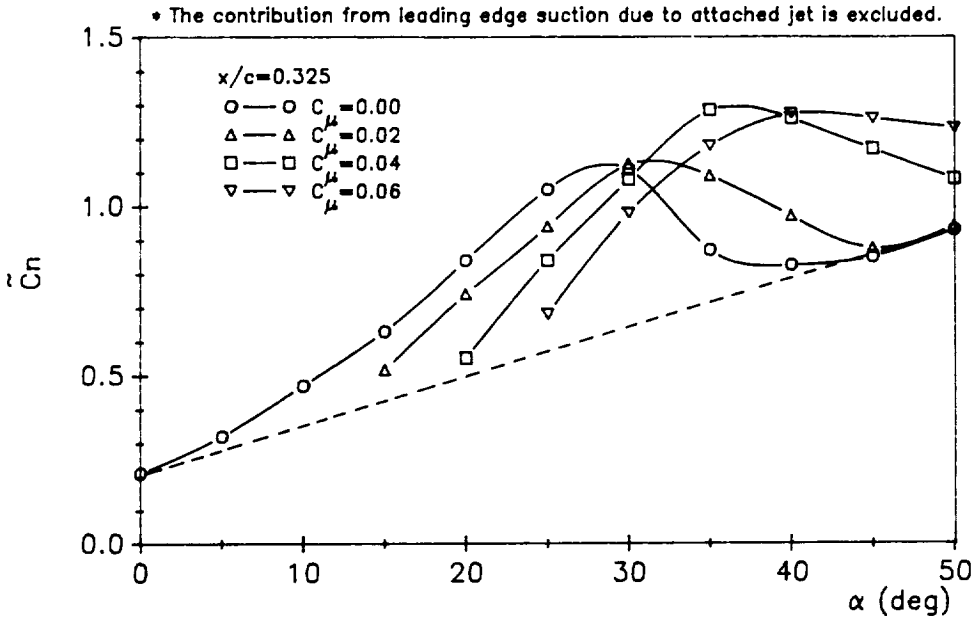

Figure 4.9 Behaviour of upper surface sectional normal force coefficient without/with blowing

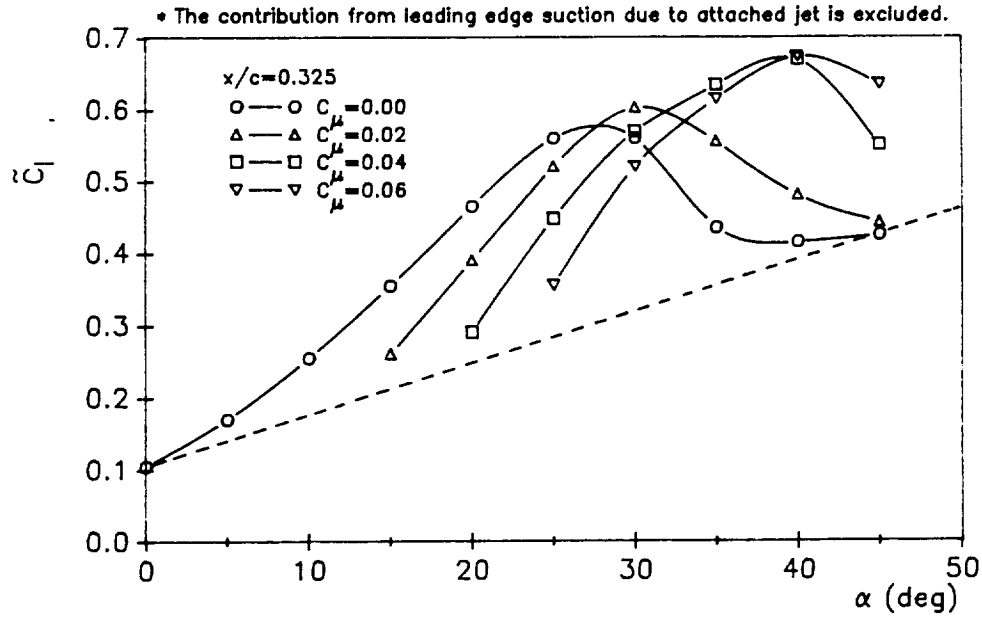

Figure 4.10 Behaviour of upper surface sectional rolling moment coefficient without/with blowing

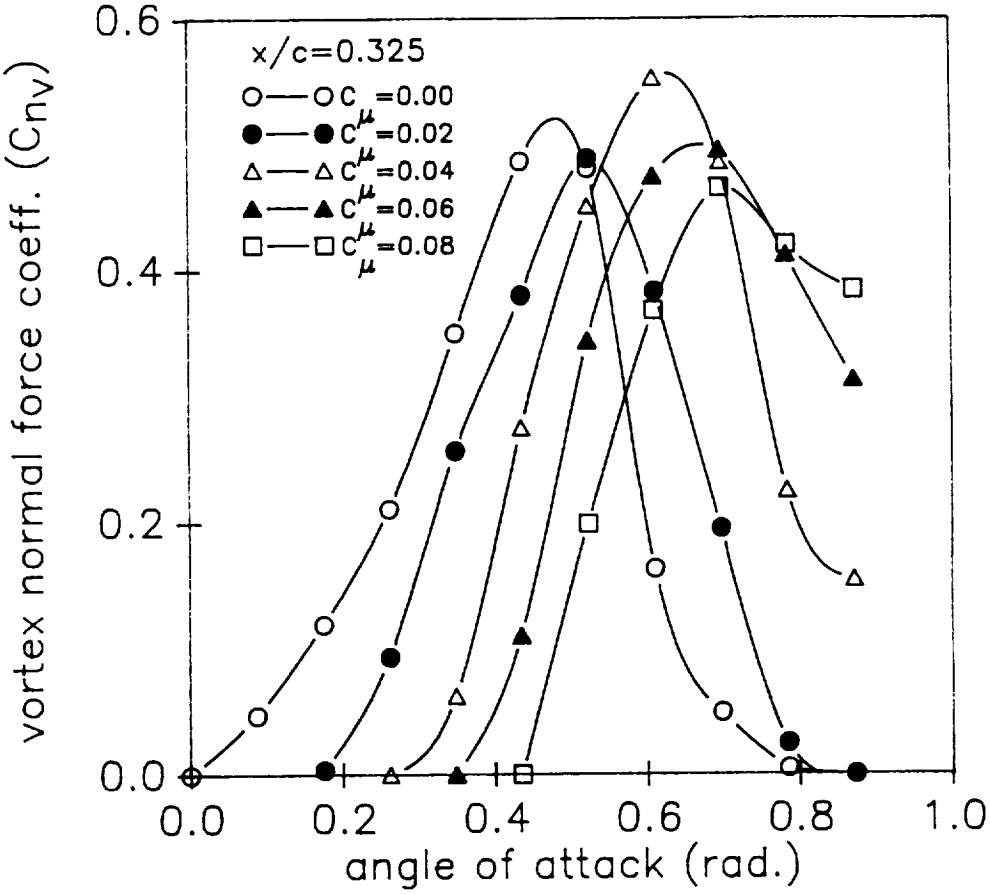

Figure 4.11 Behaviour of vortex normal force coefficient without/with blowing

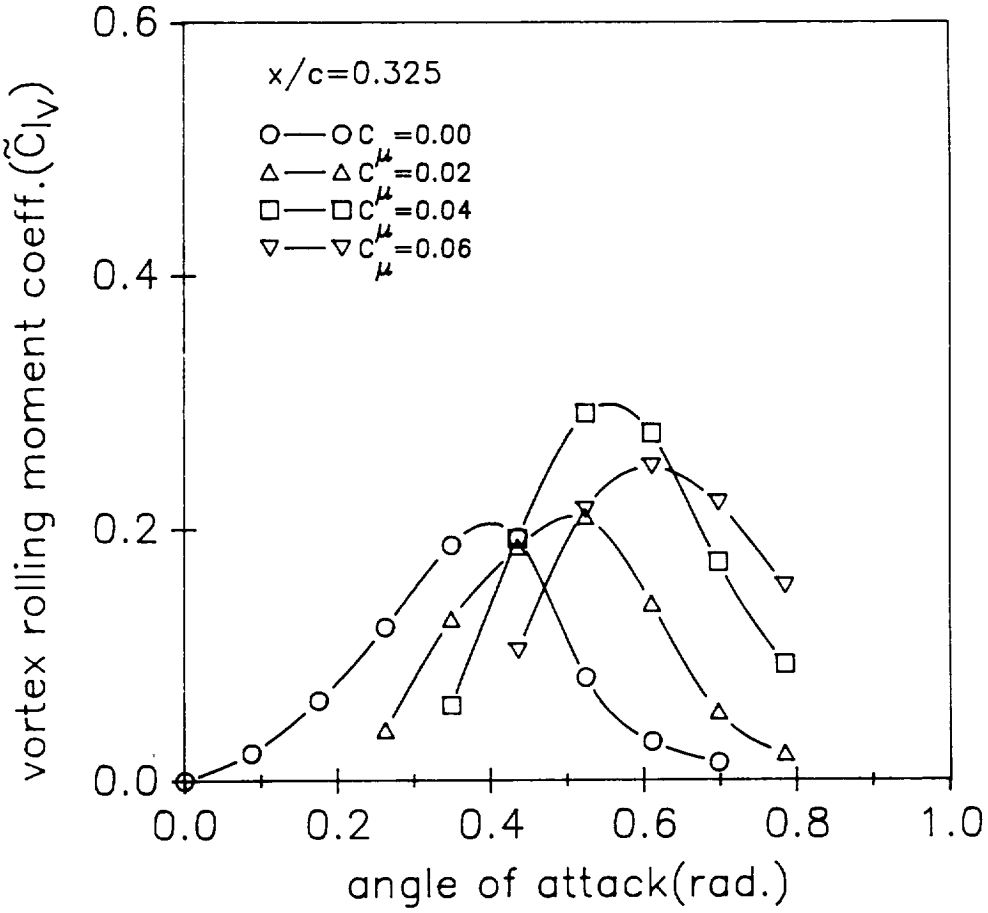

Figure 4.12 Behaviour of vortex rolling moment coefficient without/with blowing

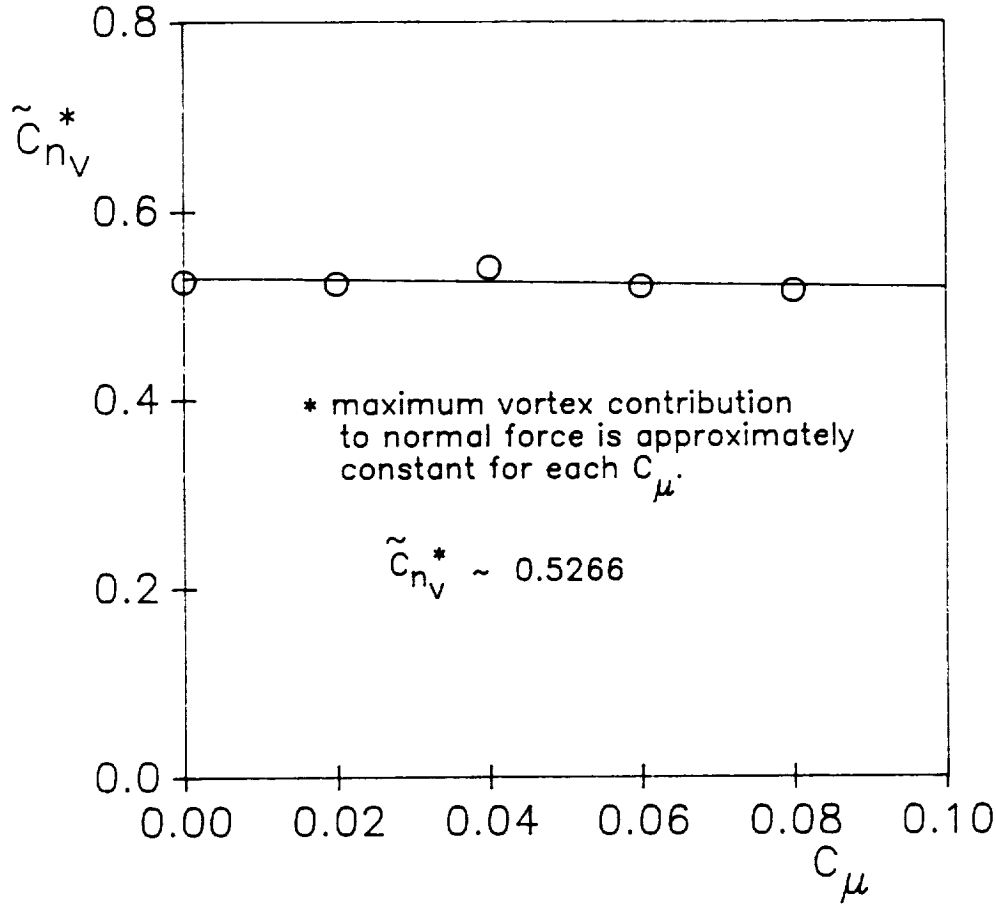

Figure 4.13 Maximum vortex contribution to normal force with respect to C_μ

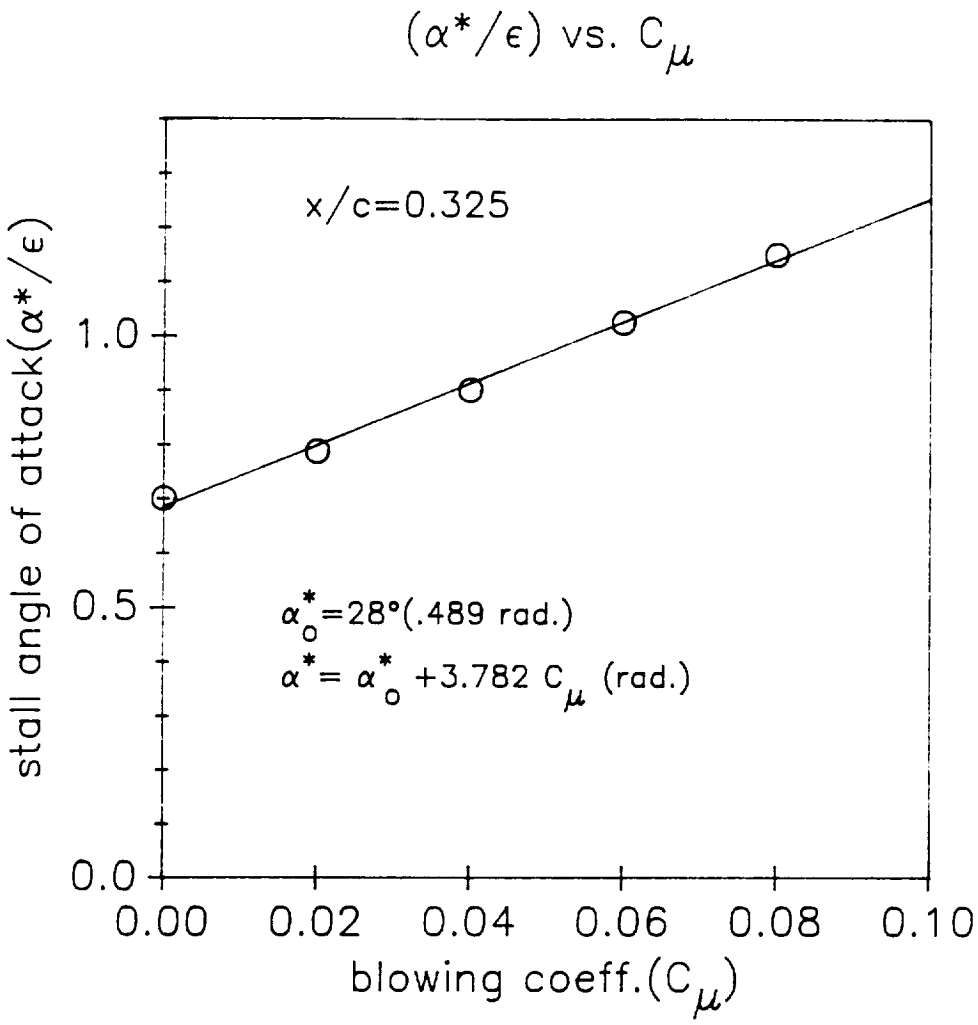

Figure 4.14 Linear variation of the stall angle of attack with respect to blowing strength

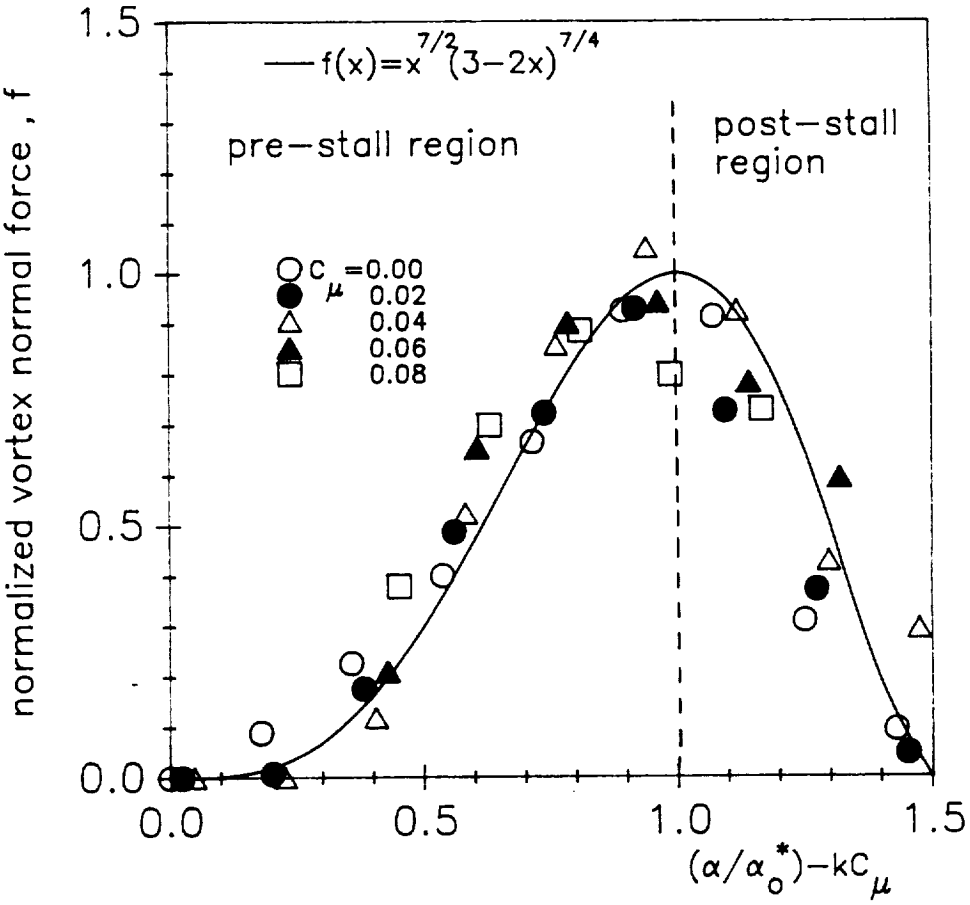

Figure 4.15 Behaviour of vortex contribution to normal force in terms of effective angle of attack

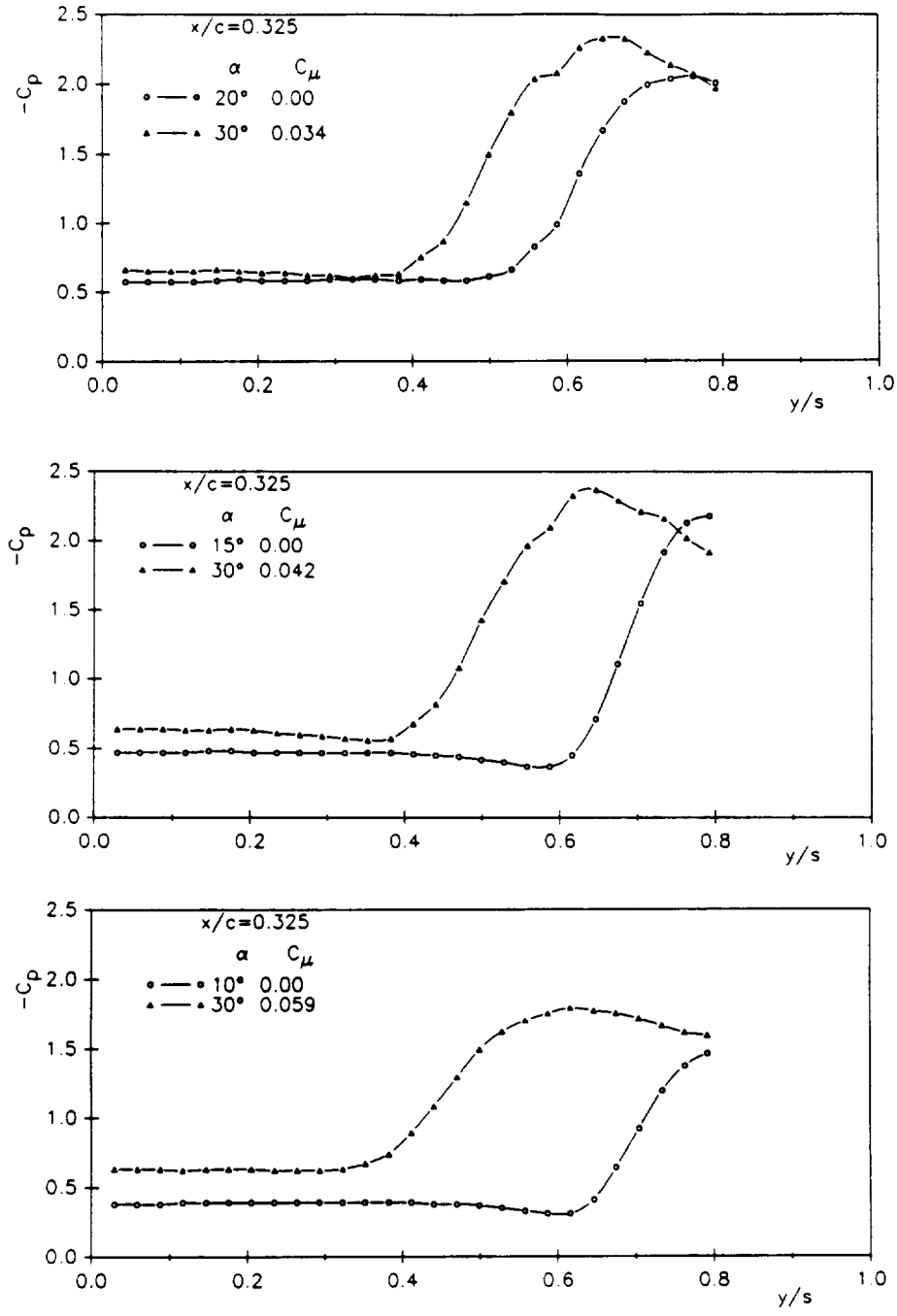

Figure 4.16 The similarity of the vortical flow with/without tangential leading edge blowing

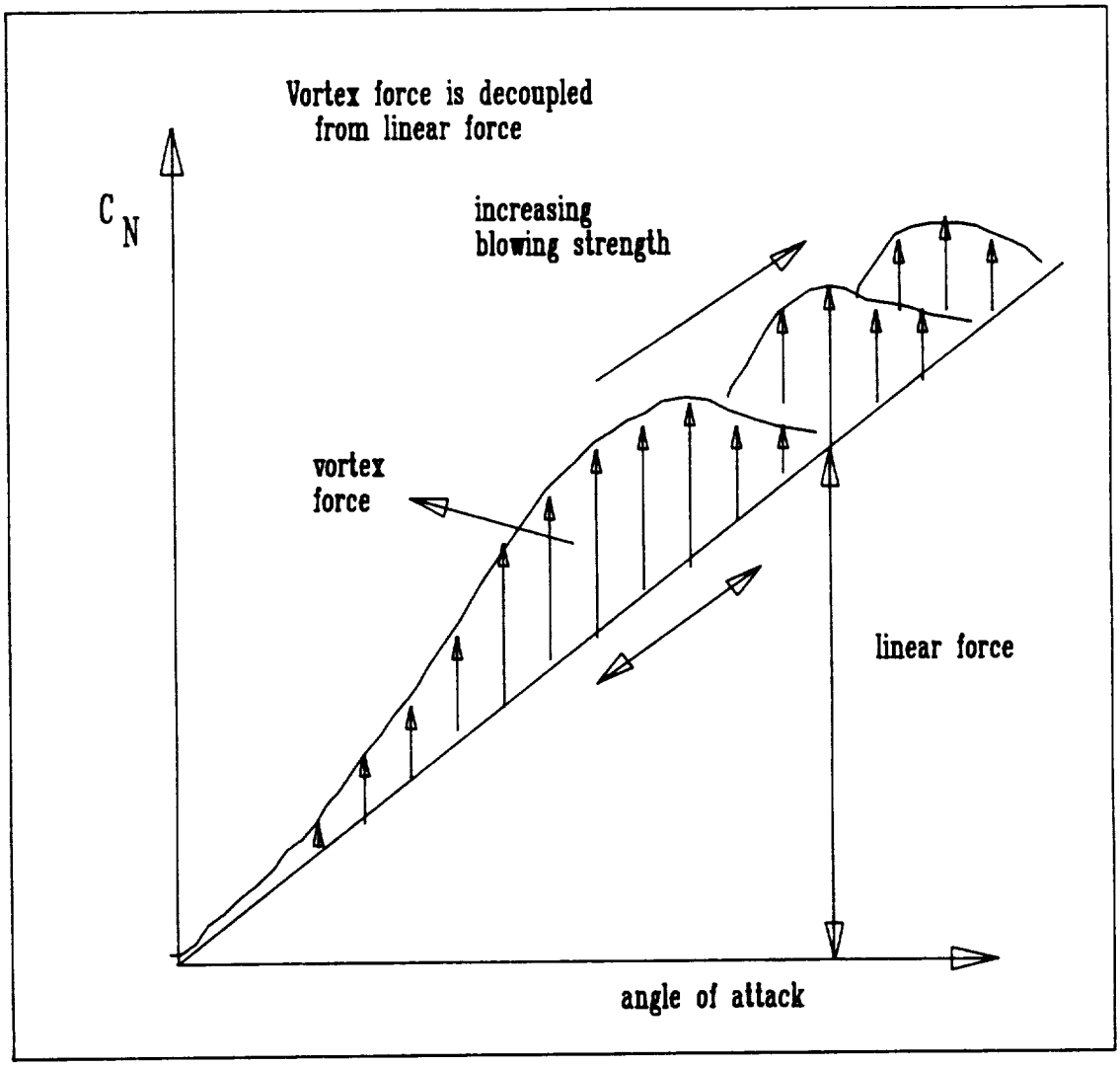

Figure 4.17 The concept of decoupled linear and non-linear lift distribution

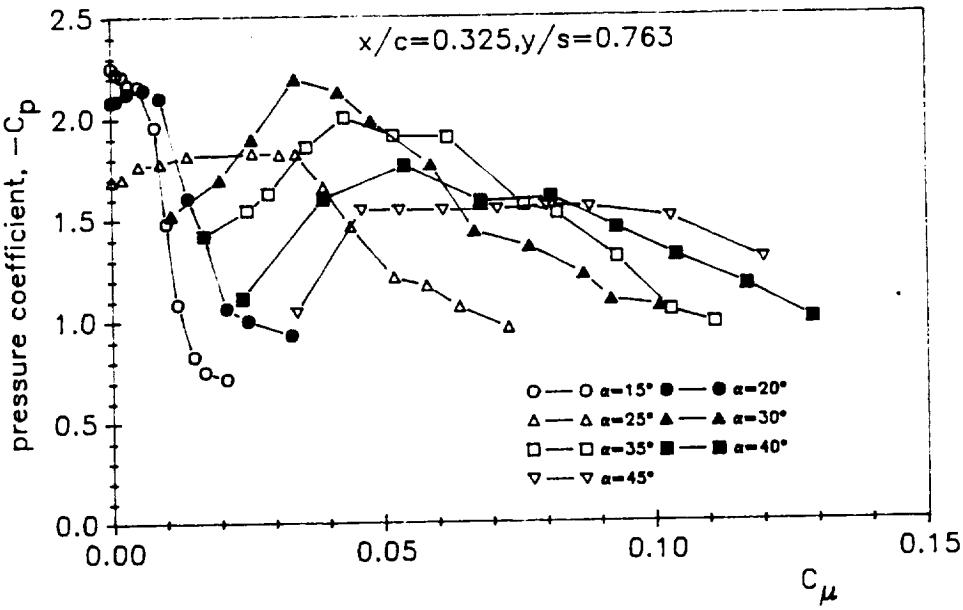

Figure 4.18 Steady surface pressure at single location
(x/c = 0.325, y/s = 0.763)

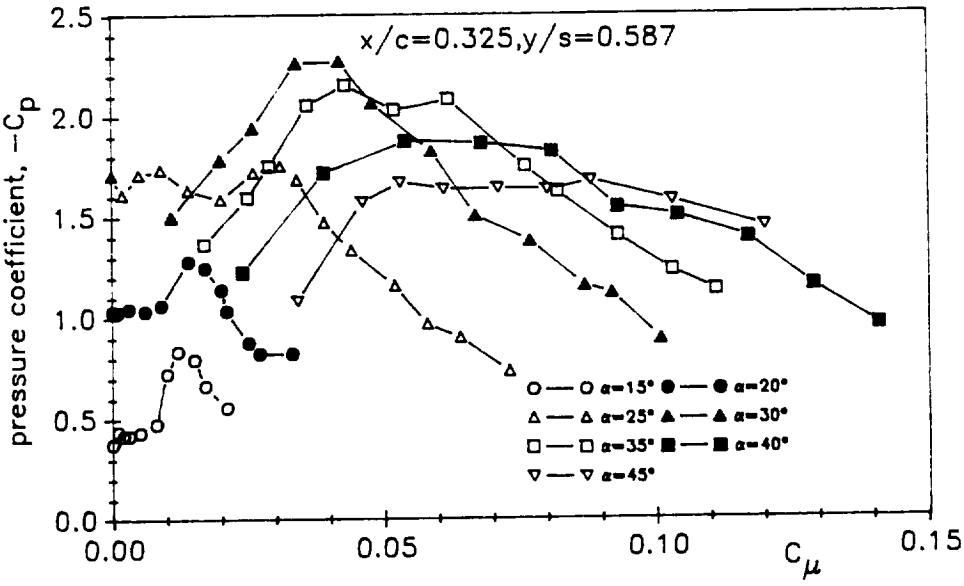

Figure 4.19 Steady surface pressure at single location
(x/c = 0.325, y/s = 0.587)

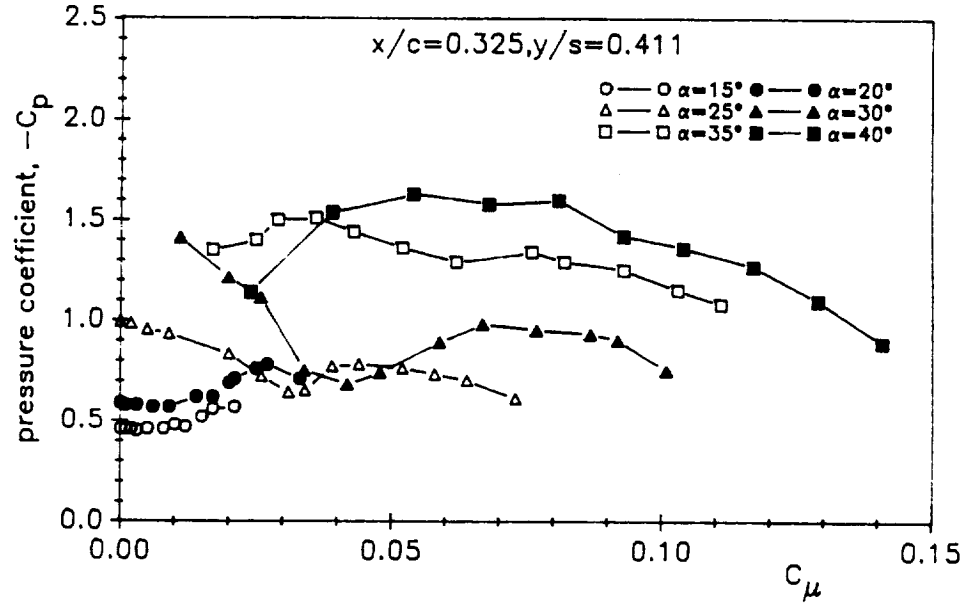

Figure 4.20 Steady surface pressure at single location
(x/c = 0.325, y/s = 0.411)

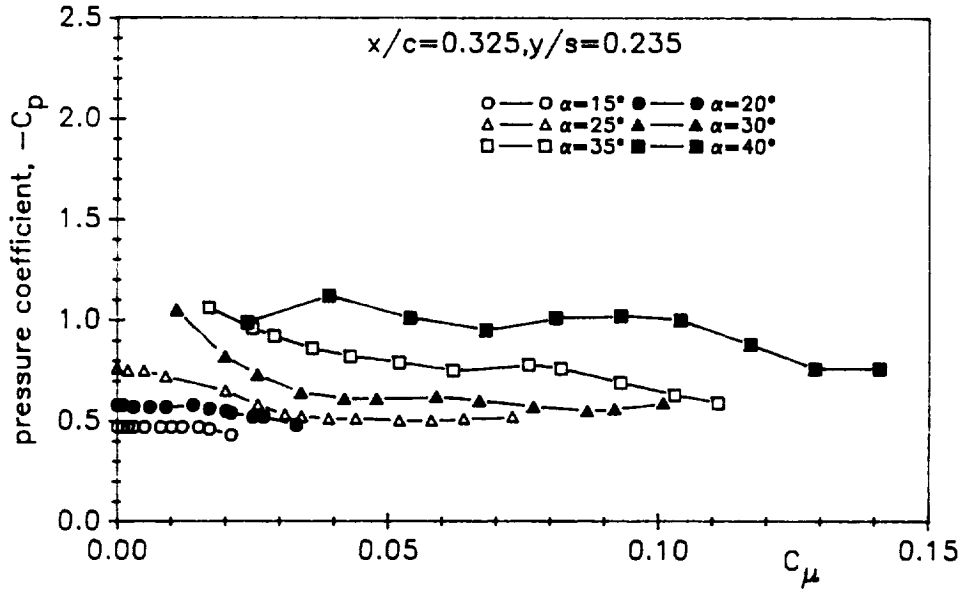

Figure 4.21 Steady surface pressure at single location
(x/c = 0.325, y/s = 0.235)

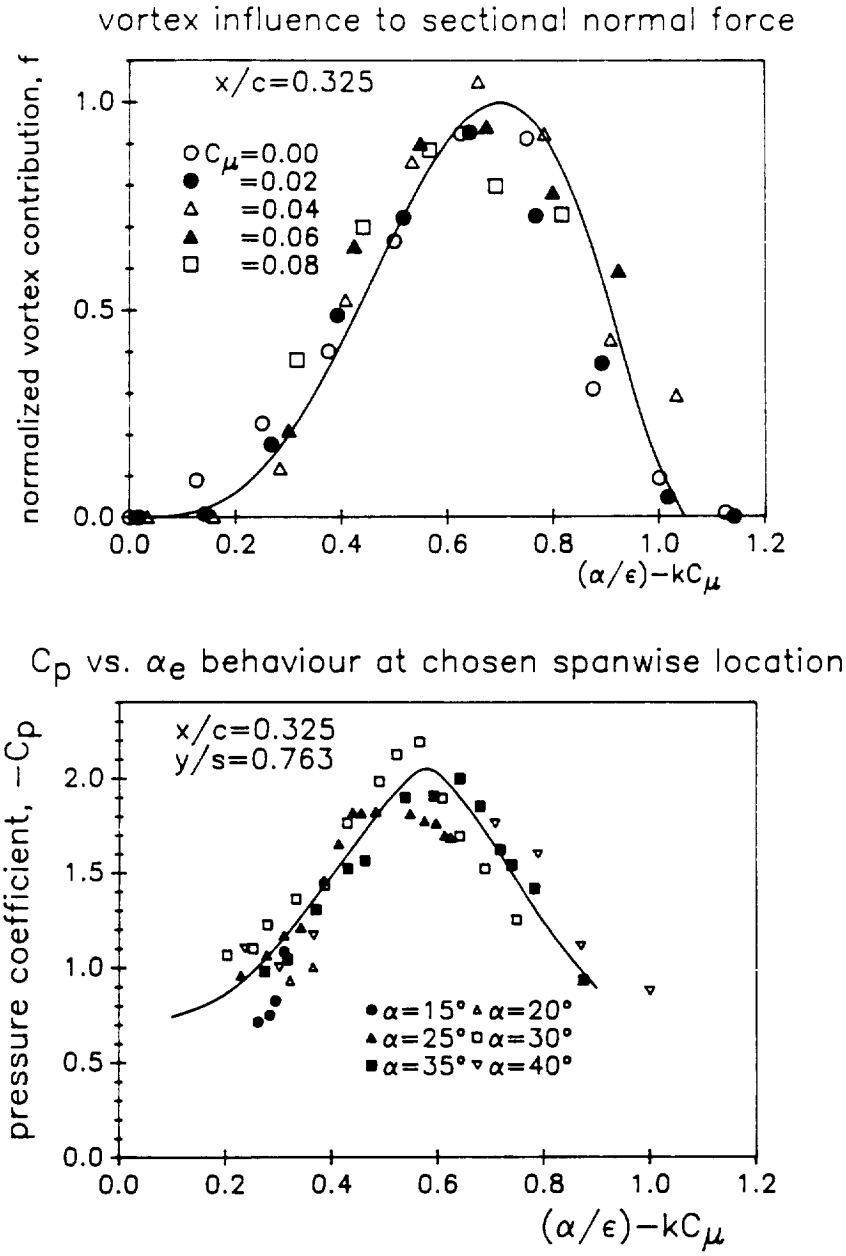

Figure 4.22 Choice of representative sensor location

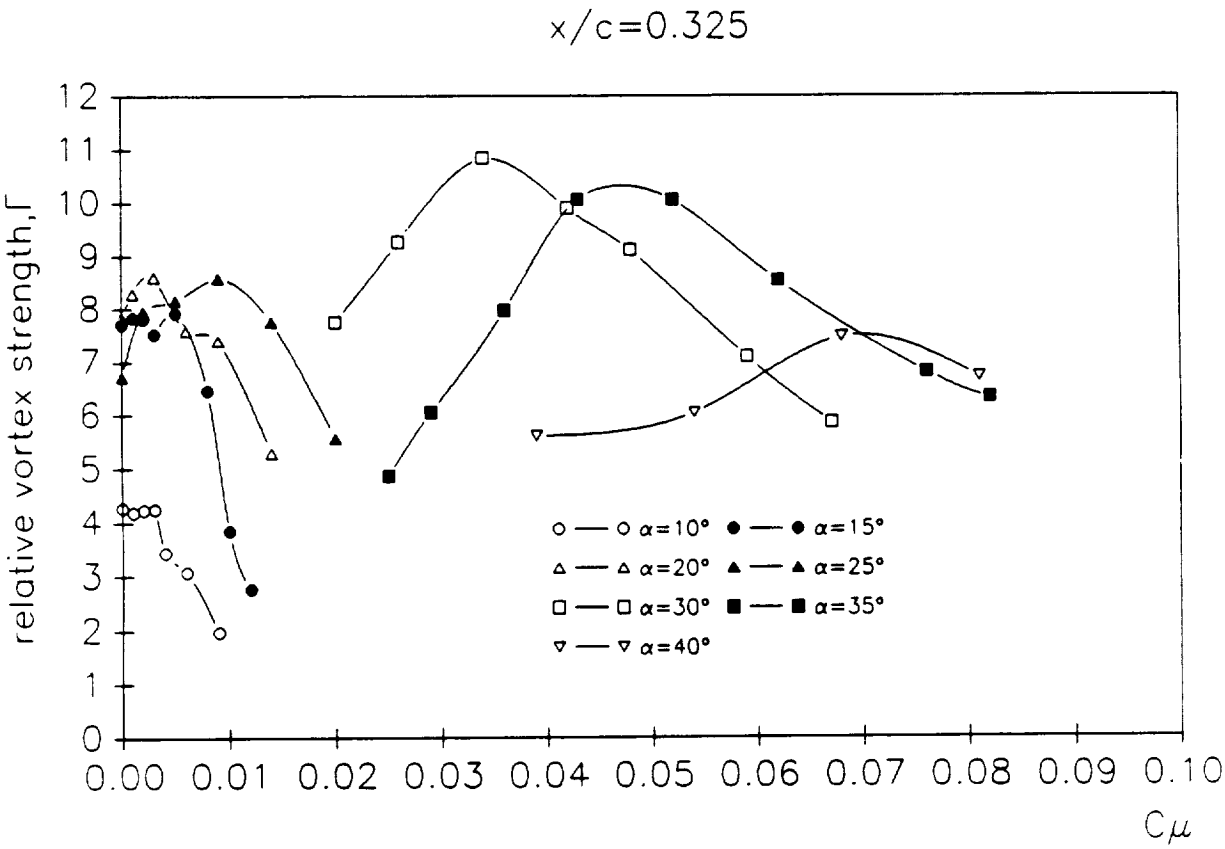

Figure 4.23 Behaviour of local vortex strength

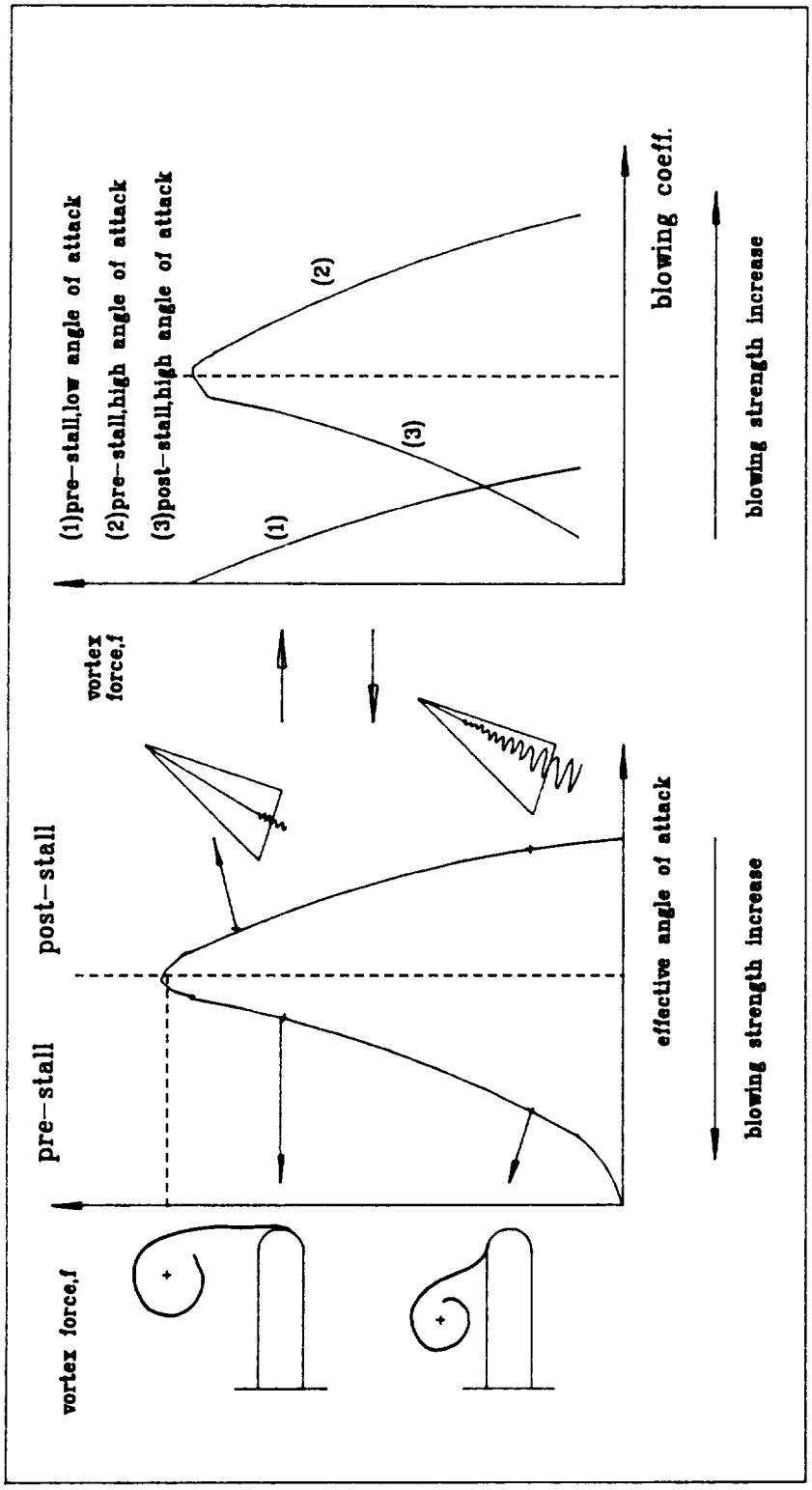

Figure 4.24 Schematic of the vortex flow behaviour for different effective angle of attack regions

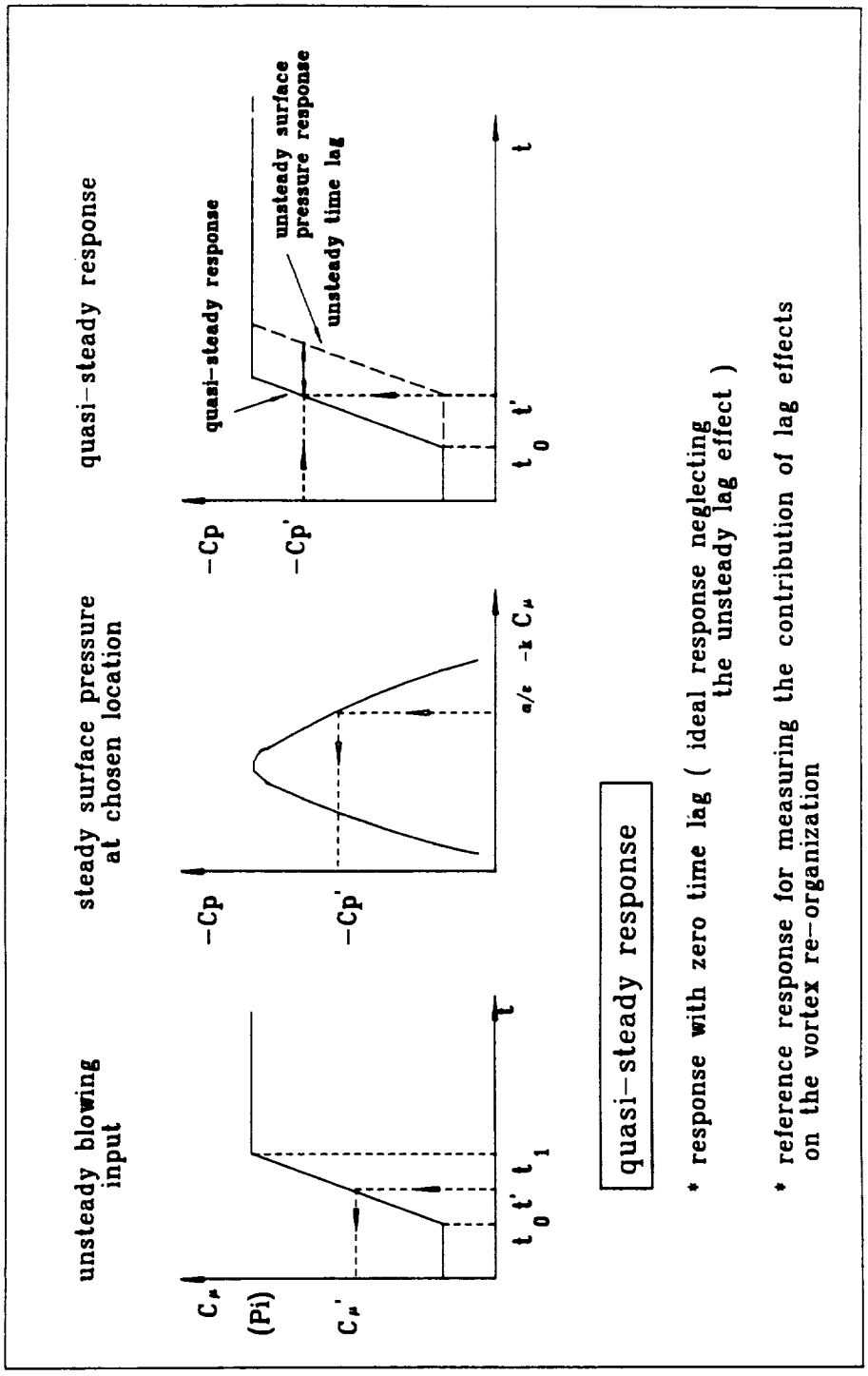

Figure 4.25 Derivation of quasi-steady response

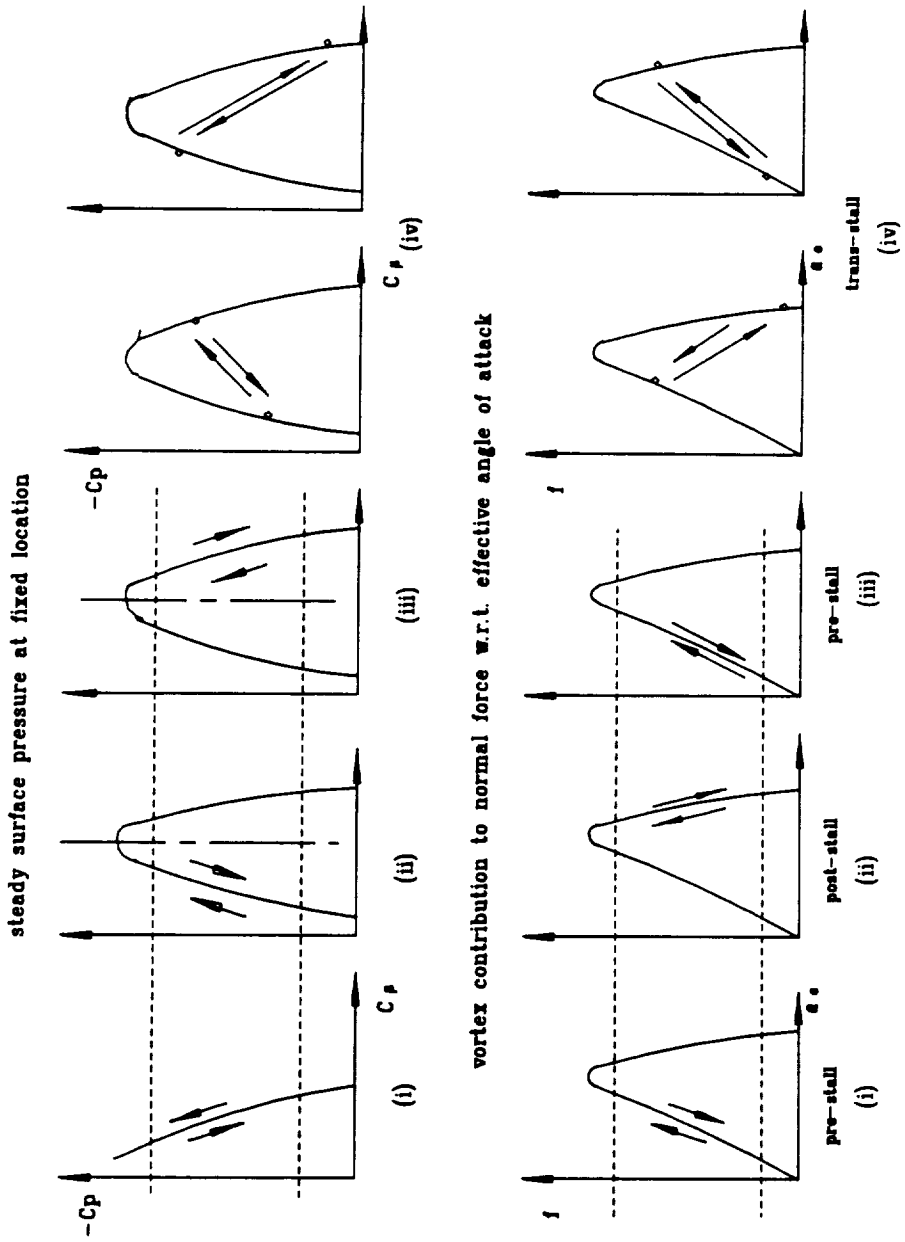

Figure 4.26 Unsteady test conditions based on the steady surface pressure behaviour at fixed location

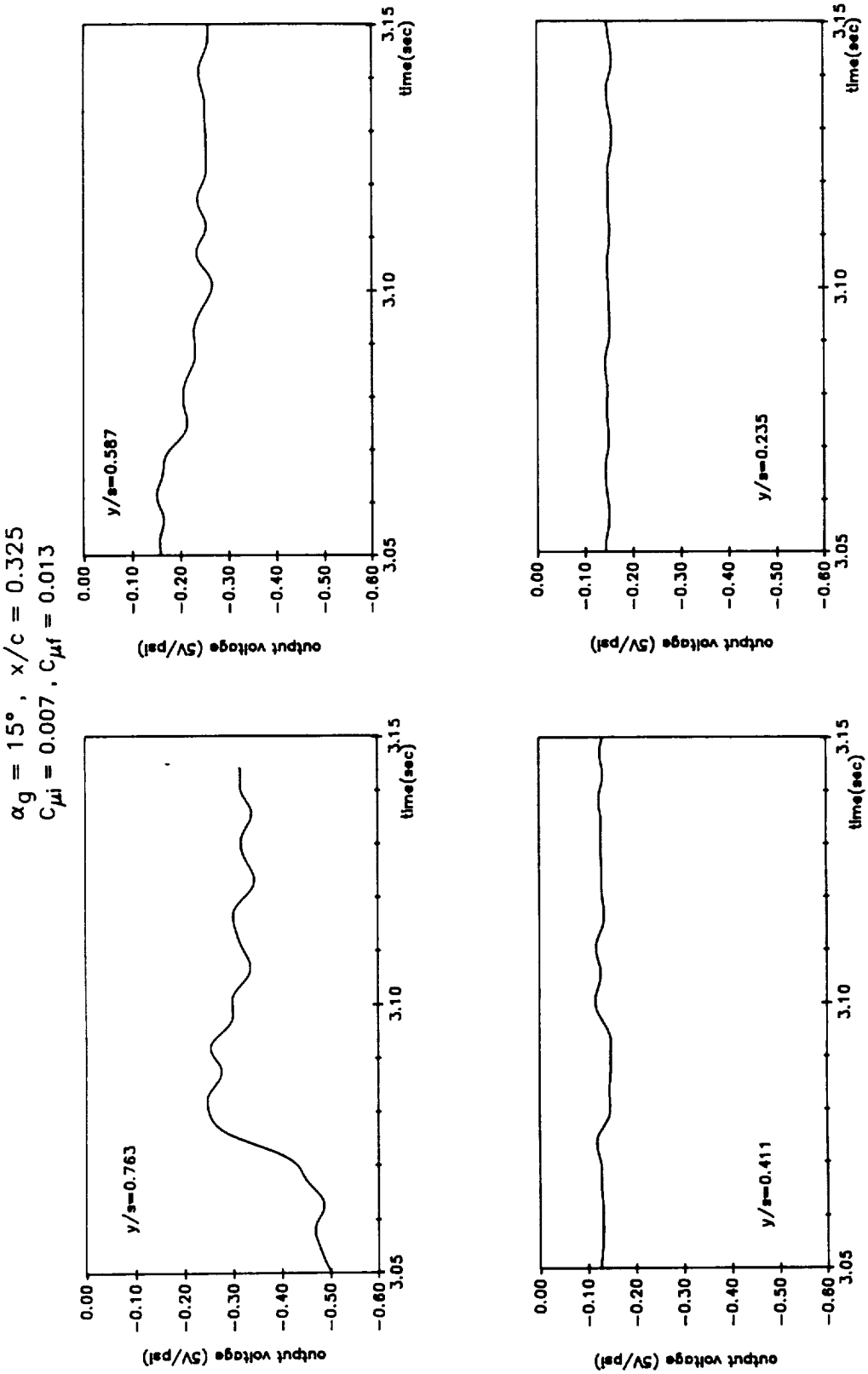

Figure 4.27 Time history of surface pressure at various spanwise locations (pre-stall at low α case)

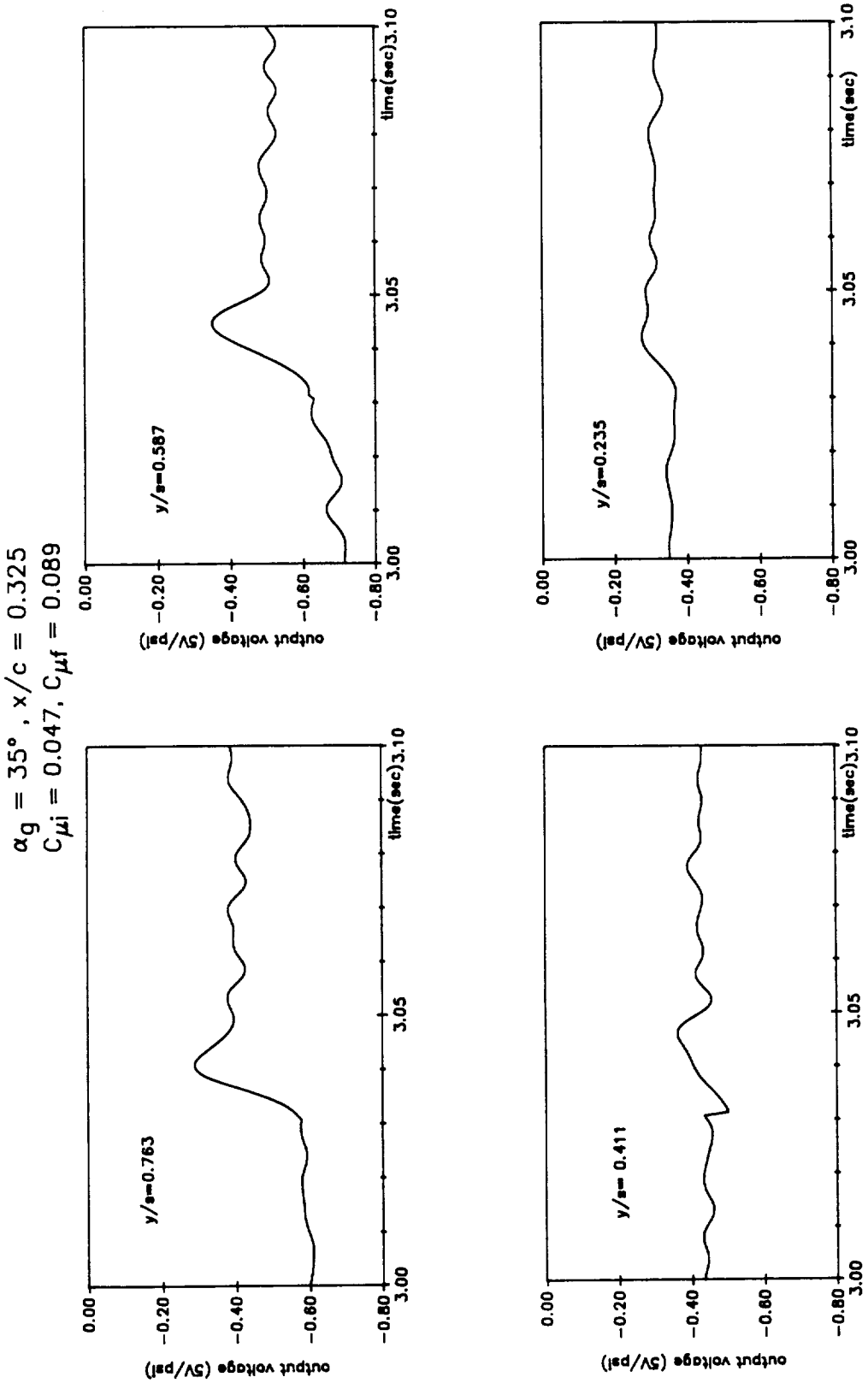

Figure 4.28 Time history of surface pressure at various spanwise locations (pre-stall at high α case)

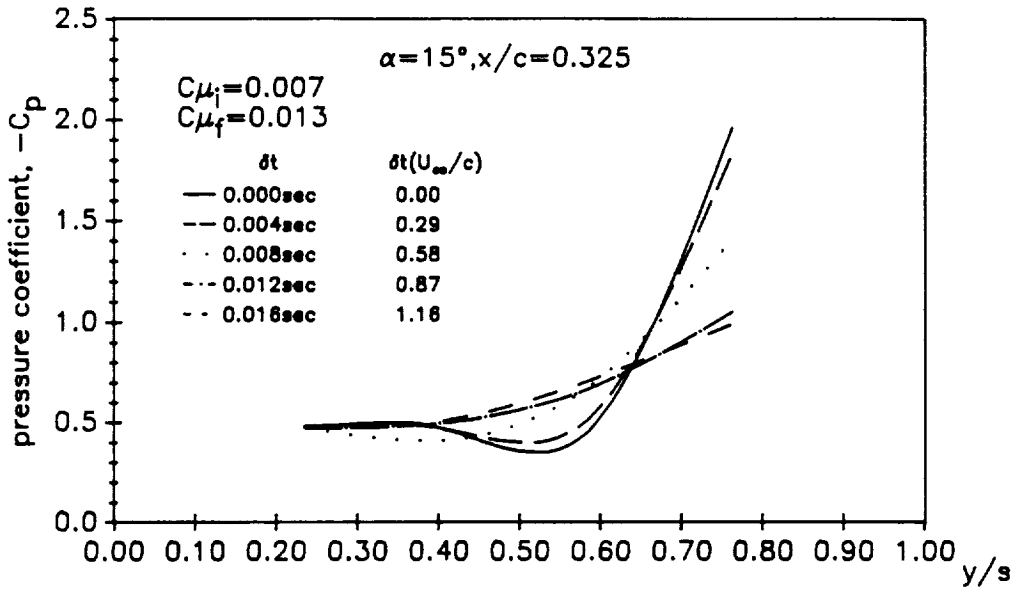

Figure 4.29 Variation of spanwise pressure distribution by transient blowing (pre-stall at low α case)

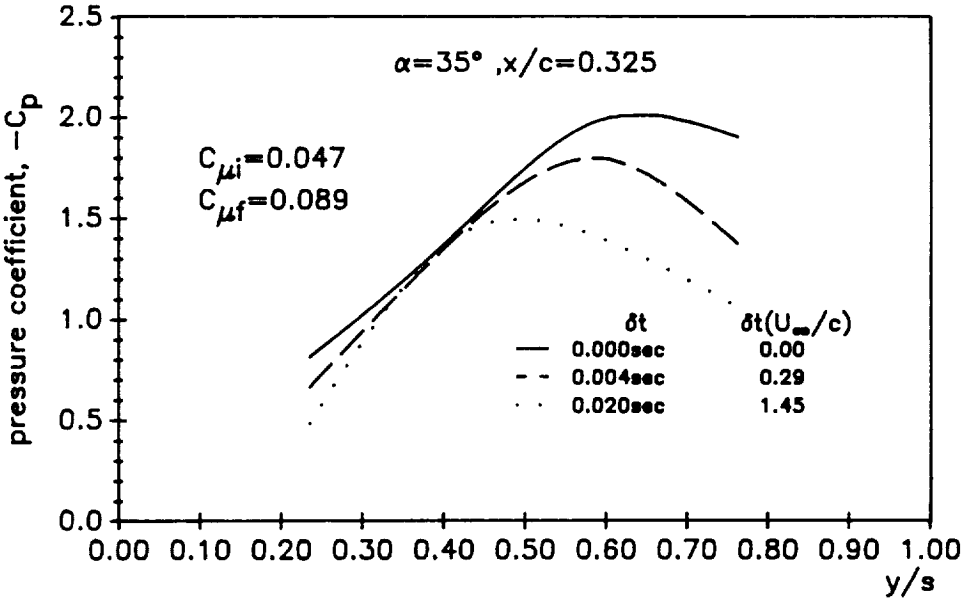

Figure 4.30 Variation of spanwise pressure distribution by transient blowing (pre-stall at high α case)

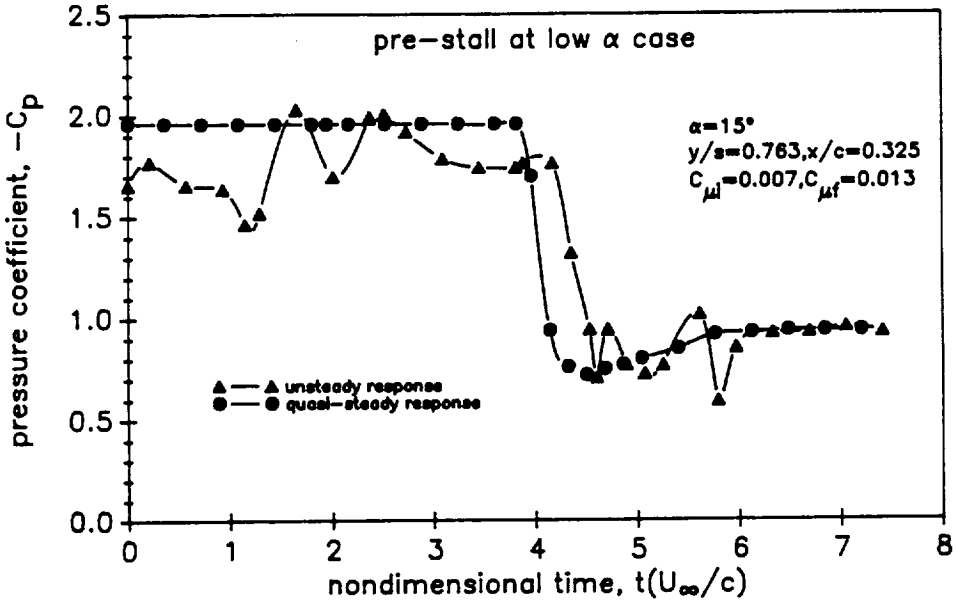

Figure 4.31 Comparison of the unsteady surface pressure and quasi-steady response ($\alpha=15^0, C_{\mu i}=0.007, C_{\mu f}=0.013$)

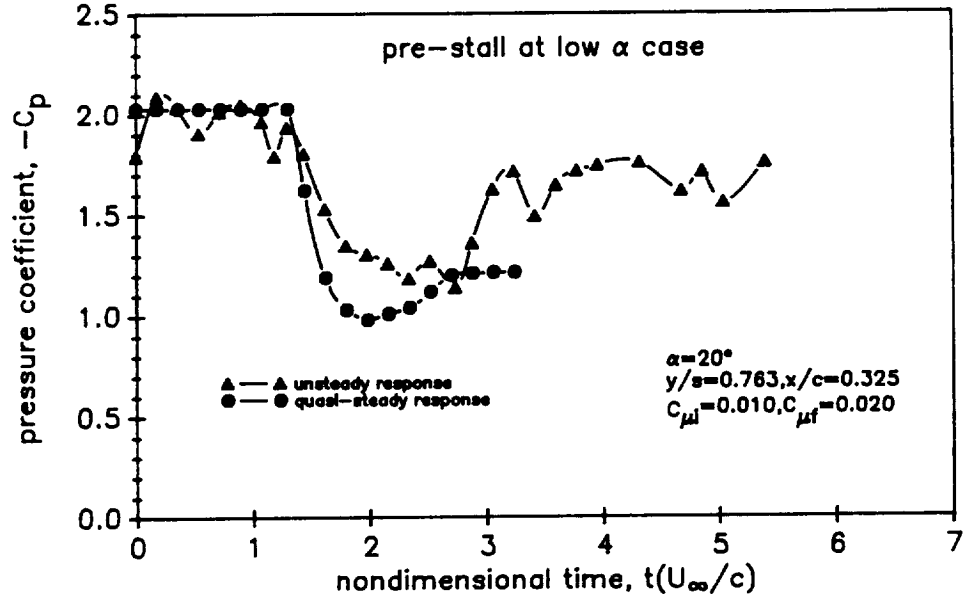

Figure 4.32 Comparison of the unsteady surface pressure and quasi-steady response ($\alpha=20^0, C_{\mu i}=0.010, C_{\mu f}=0.020$)

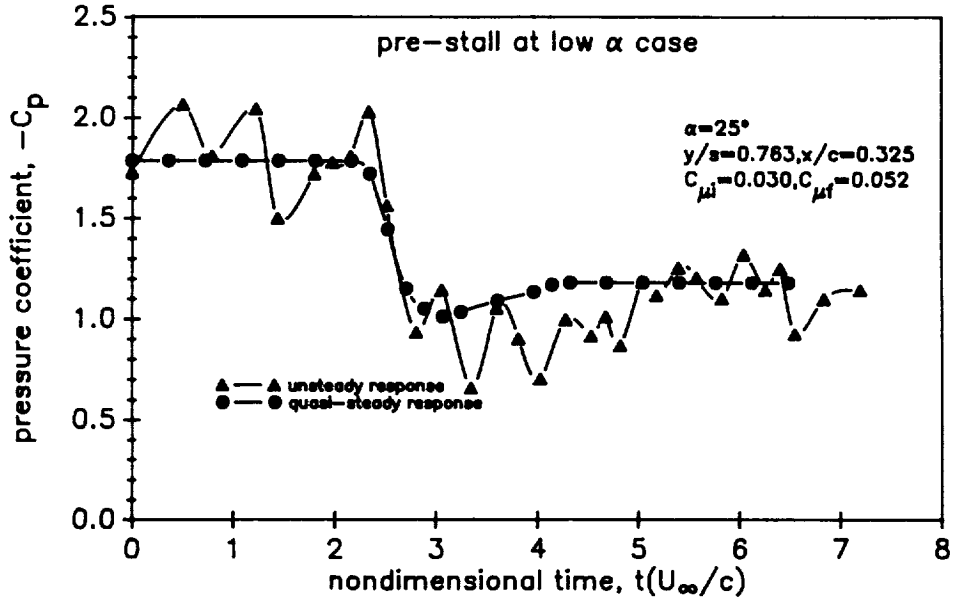

Figure 4.33 Comparison of the unsteady surface pressure and quasi-steady response ($\alpha=25^0, C_{\mu i}=0.030, C_{\mu f}=0.052$)

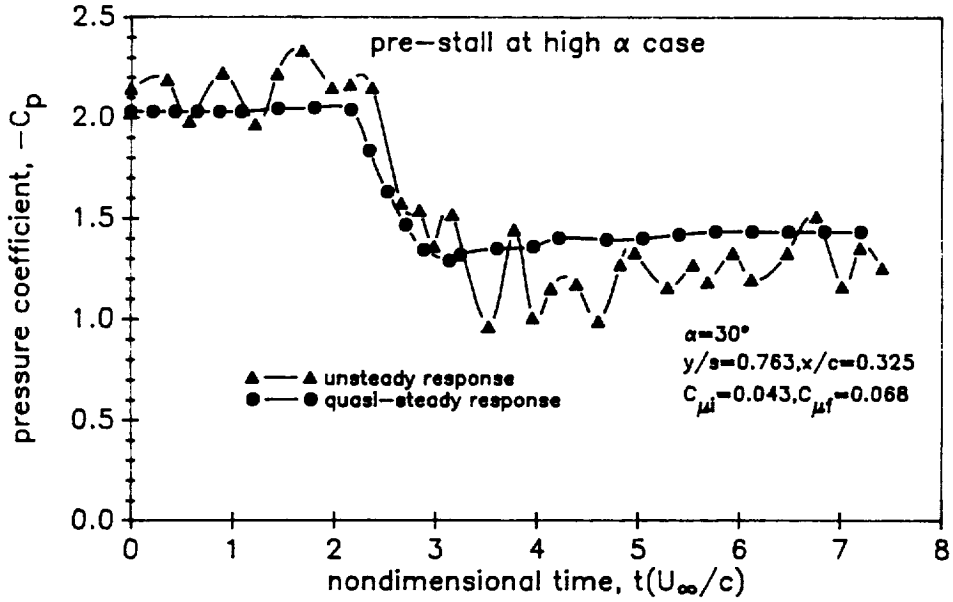

Figure 4.34 Comparison of the unsteady surface pressure and quasi-steady response ($\alpha=30^0, C_{\mu i}=0.043, C_{\mu f}=0.068$)

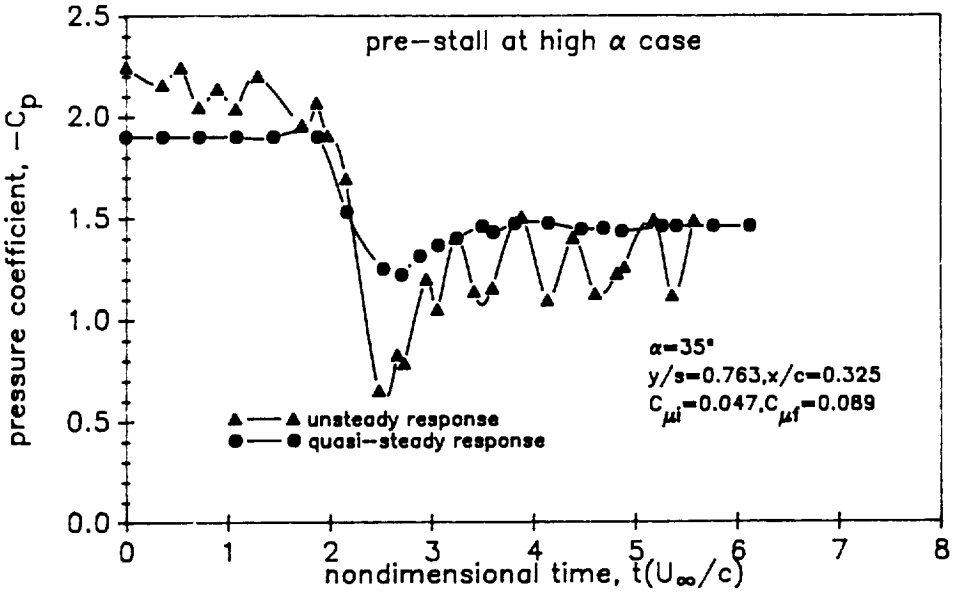

Figure 4.35 Comparison of the unsteady surface pressure and quasi-steady response ($\alpha=35^0, C_{\mu i}=0.047, C_{\mu f}=0.089$)

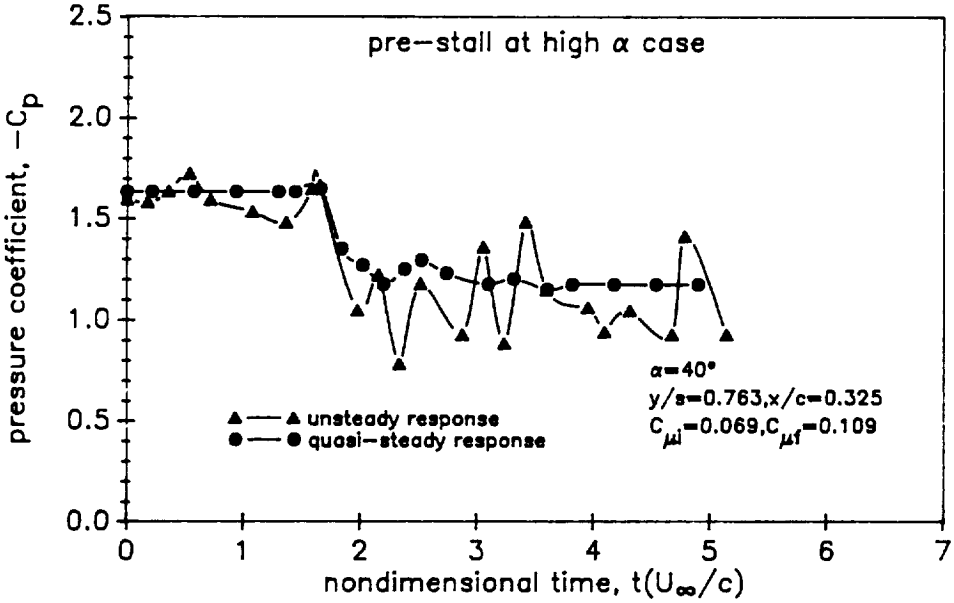

Figure 4.36 Comparison of the unsteady surface pressure and quasi-steady response ($\alpha=40^0, C_{\mu i}=0.069, C_{\mu f}=0.109$)

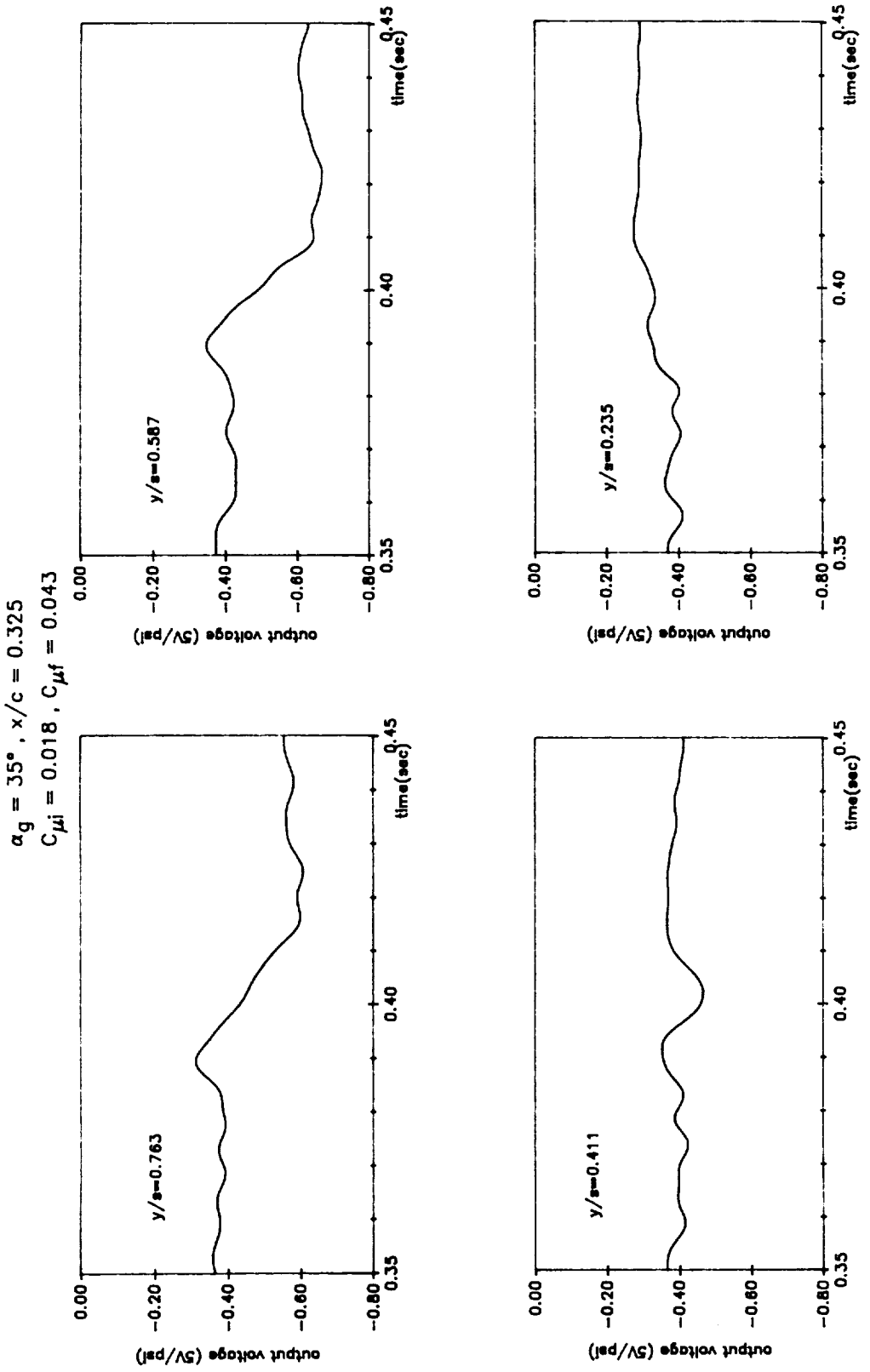

Figure 4.37 Time history of surface pressure at various spanwise locations (post-stall at high α case)

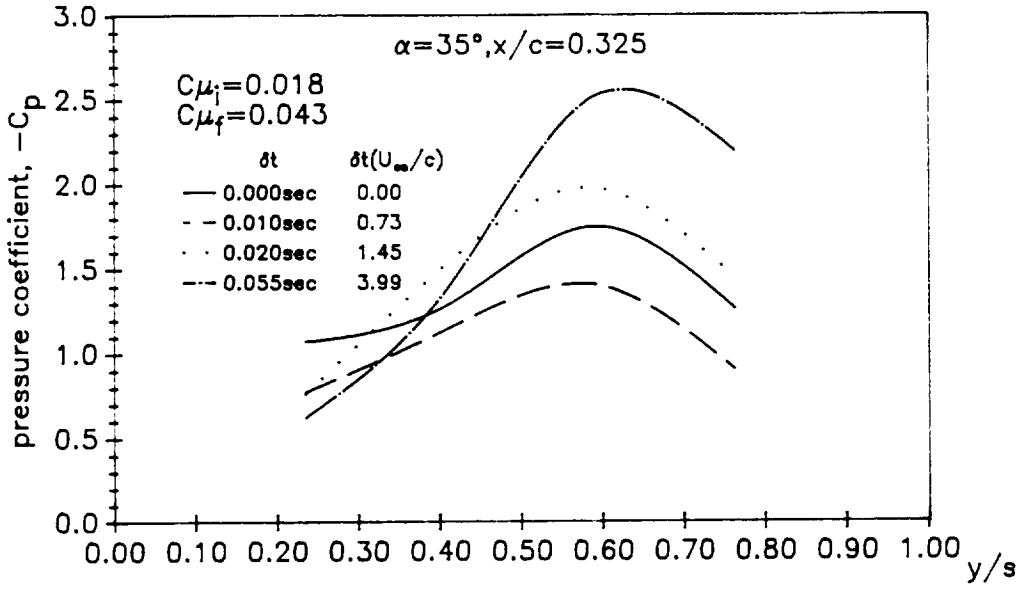

Figure 4.38 Variation of spanwise pressure distribution by transient blowing (post-stall at high α case)

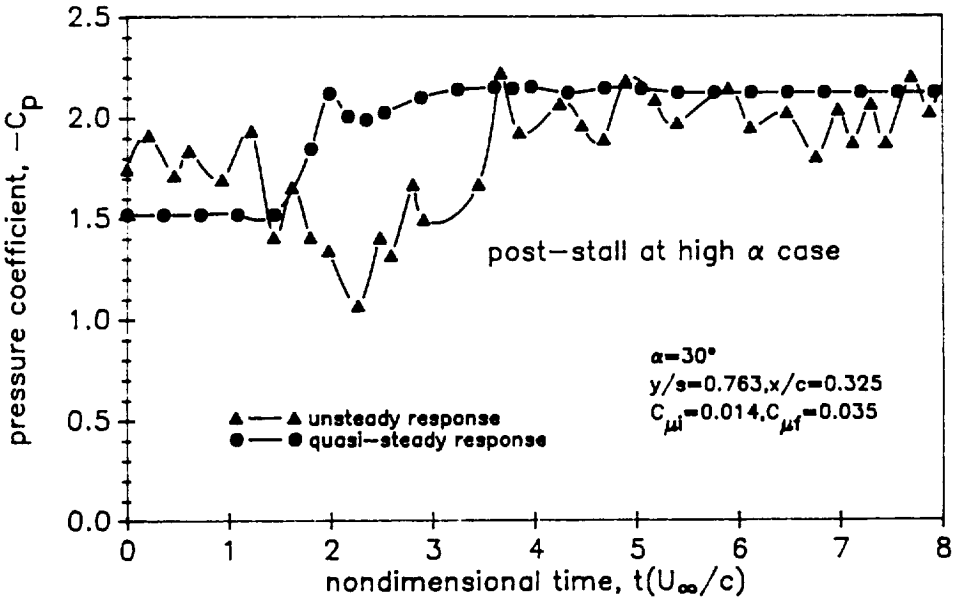

Figure 4.39 Comparison of the unsteady surface pressure and quasi-steady response ($\alpha=30^0, C_{\mu i}=0.014, C_{\mu f}=0.035$)

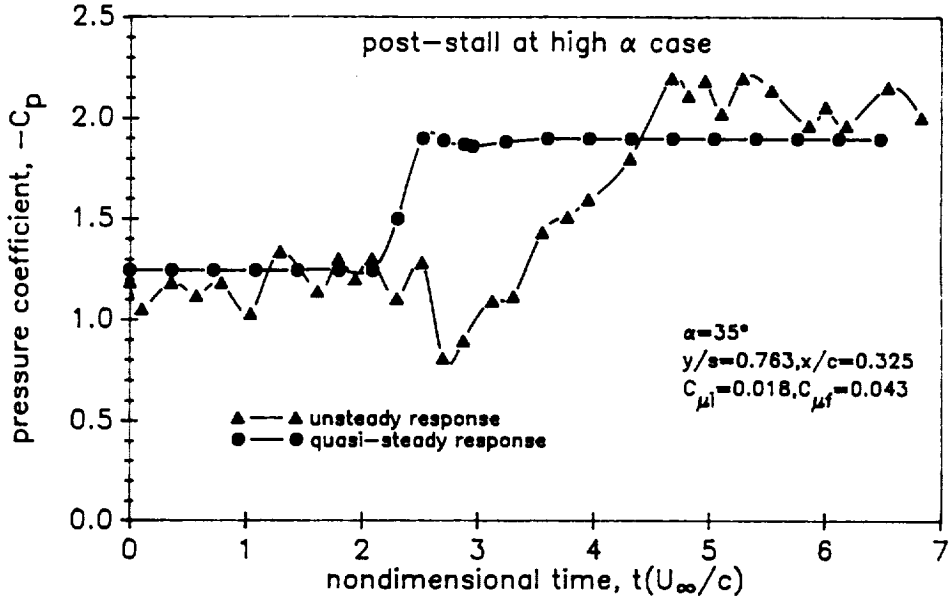

Figure 4.40 Comparison of the unsteady surface pressure and quasi-steady response ($\alpha=35^0, C_{\mu i}=0.018, C_{\mu f}=0.043$)

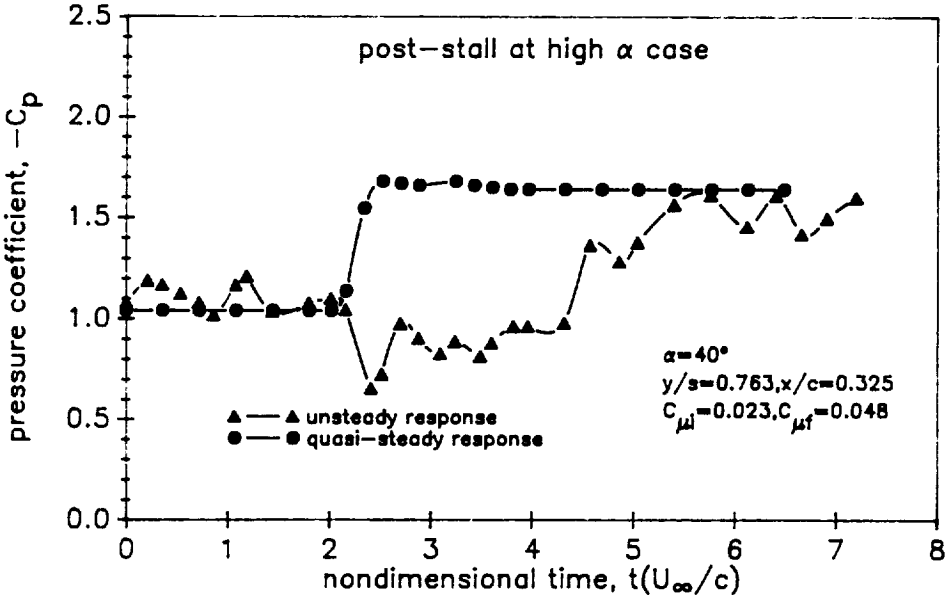

Figure 4.41 Comparison of the unsteady surface pressure and quasi-steady response ($\alpha=40^0, C_{\mu i}=0.023, C_{\mu f}=0.048$)

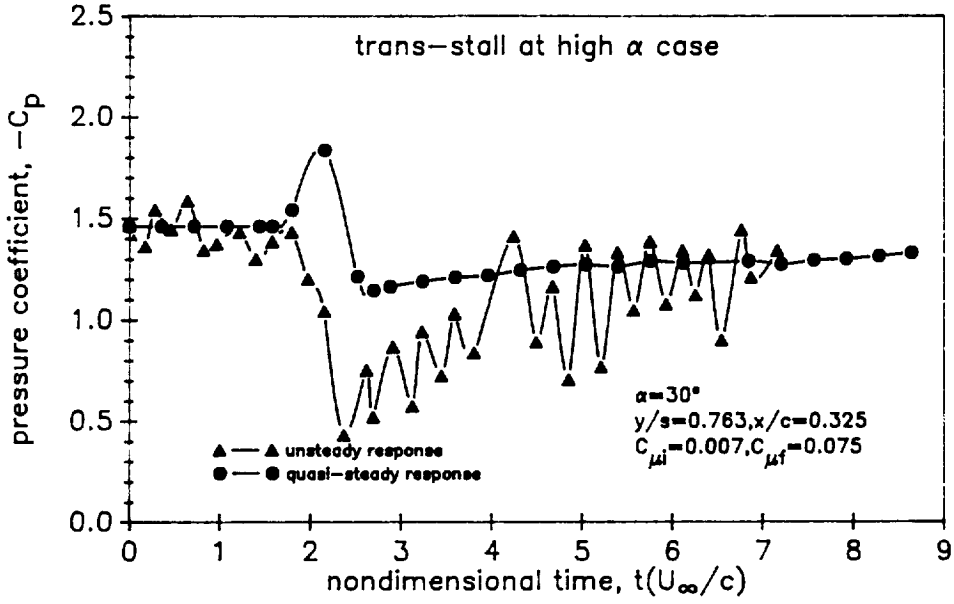

Figure 4.42 Comparison of the unsteady surface pressure and quasi-steady response for trans-stall case ($\alpha=30^0, C_{\mu i}=0.007, C_{\mu f}=0.075$)

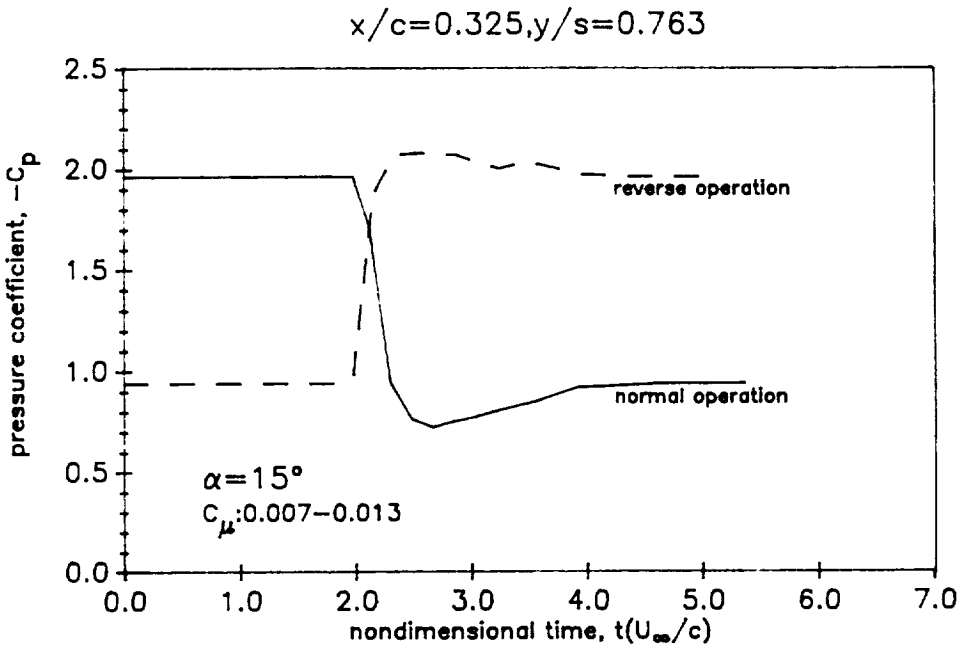

Figure 4.43 Quasi-steady responses for normal and reverse operations (pre-stall at low α case)

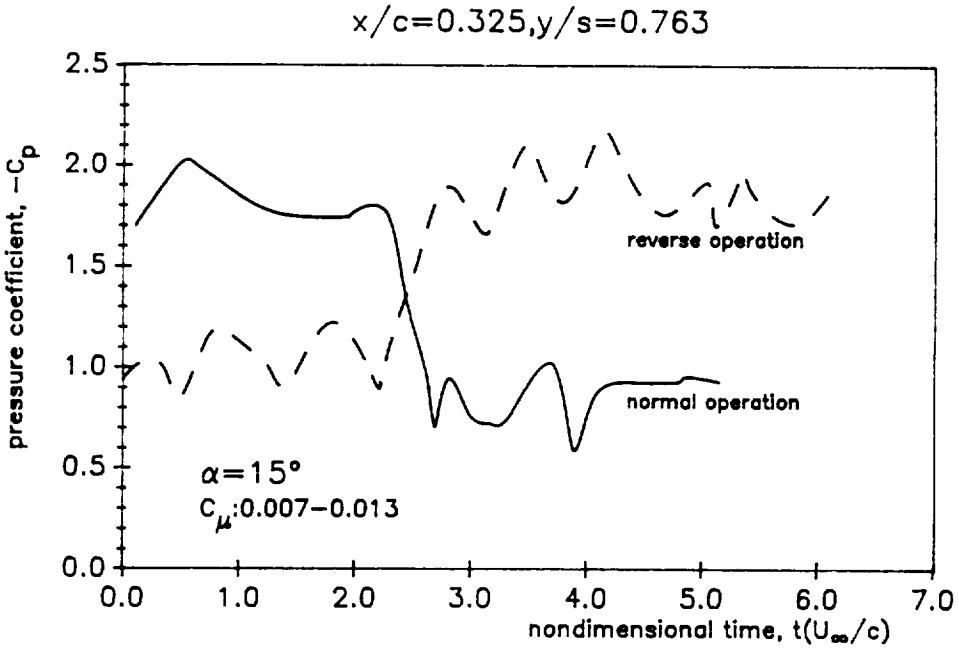

Figure 4.44 Surface pressure responses for normal and reverse operations (pre-stall at low α case)

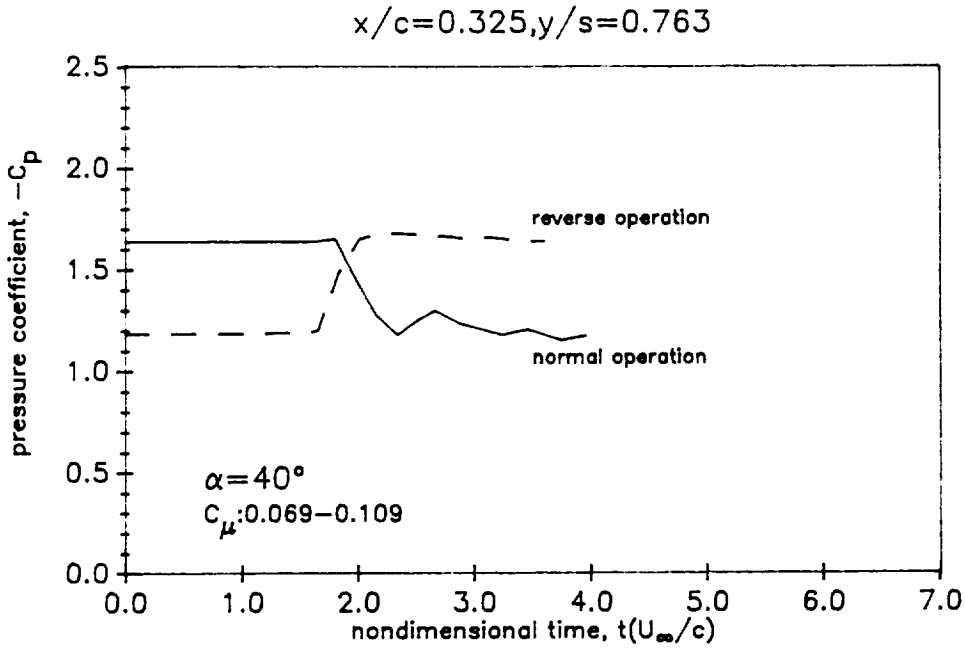

Figure 4.45 Quasi-steady responses for normal and reverse operations (pre-stall at high α case)

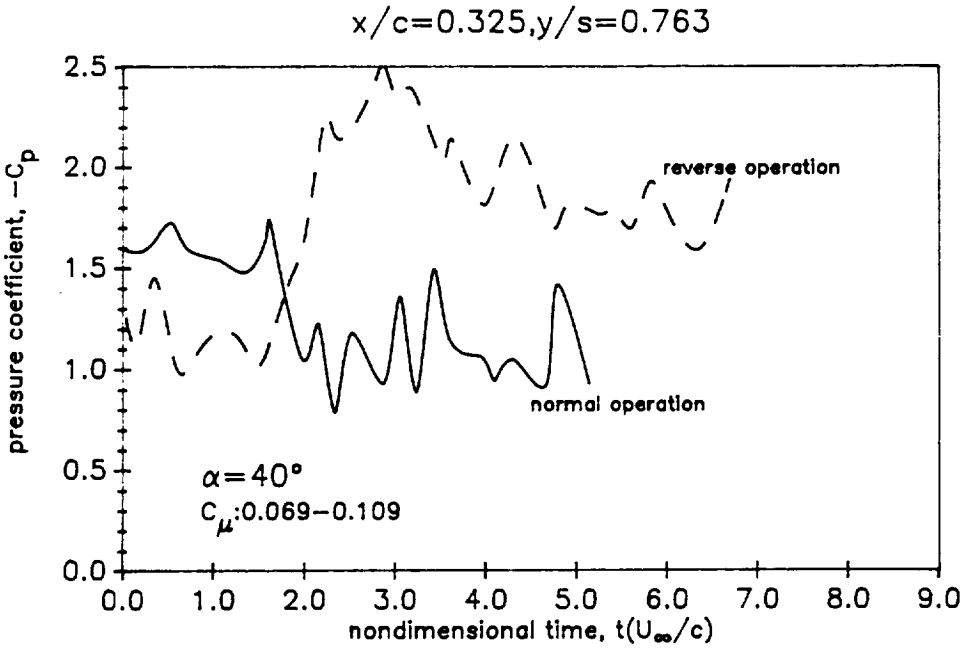

Figure 4.46 Surface pressure responses for normal and reverse operations (pre-stall at high α case)

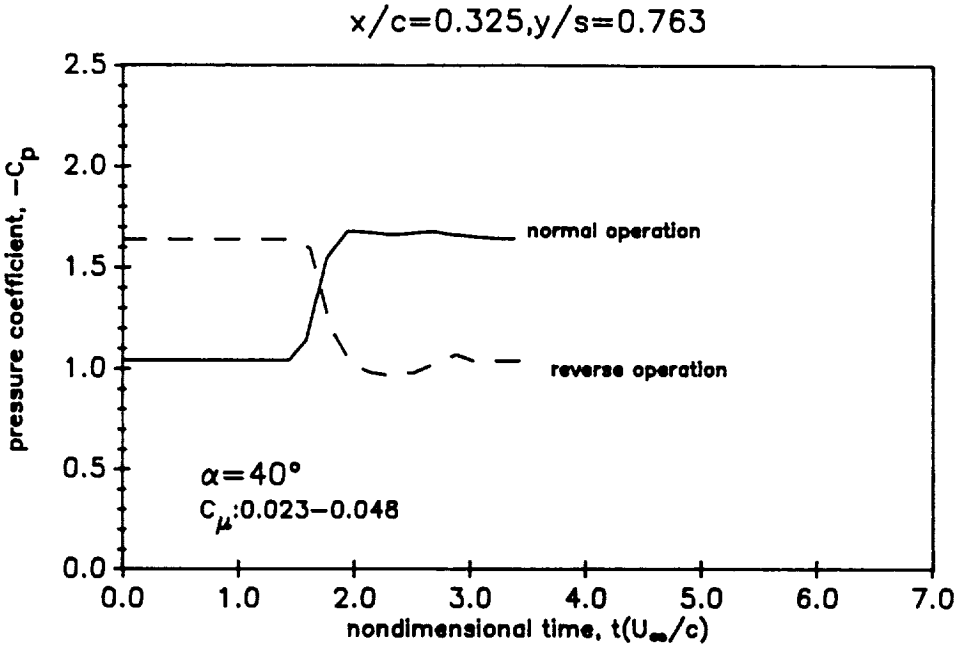

Figure 4.47 Quasi-steady responses for normal and reverse operations (post-stall at high α case)

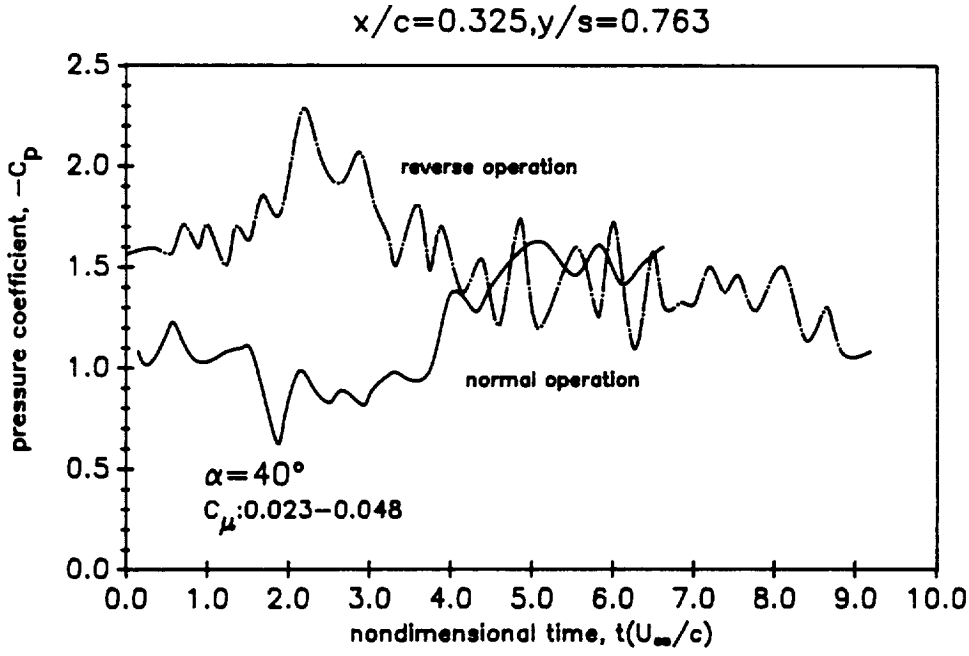

Figure 4.48 Surface pressure responses for normal and reverse operations (post-stall at high α case)

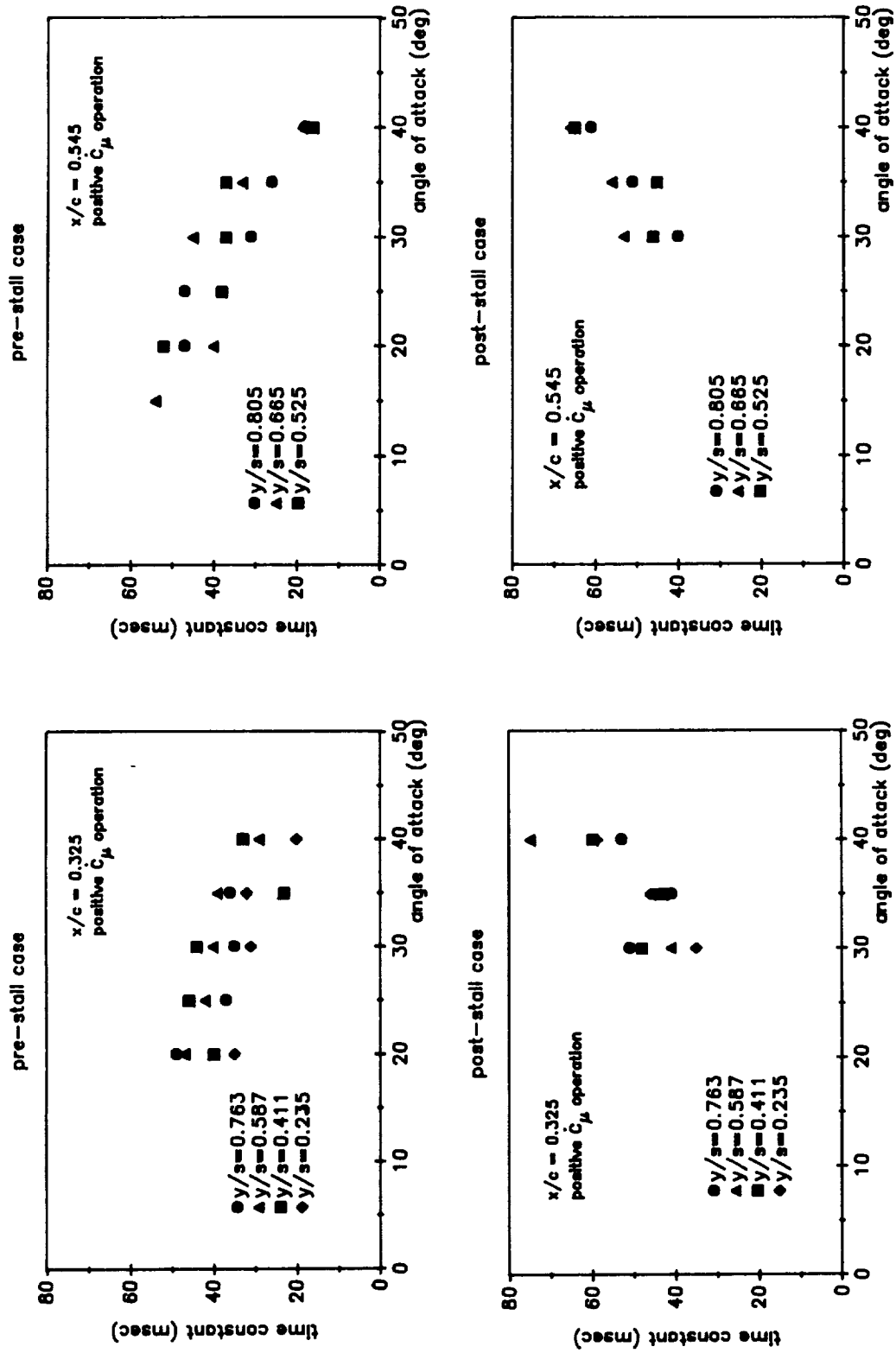

Figure 4.49 Behaviour of time constant for different effective angle of attack regimes

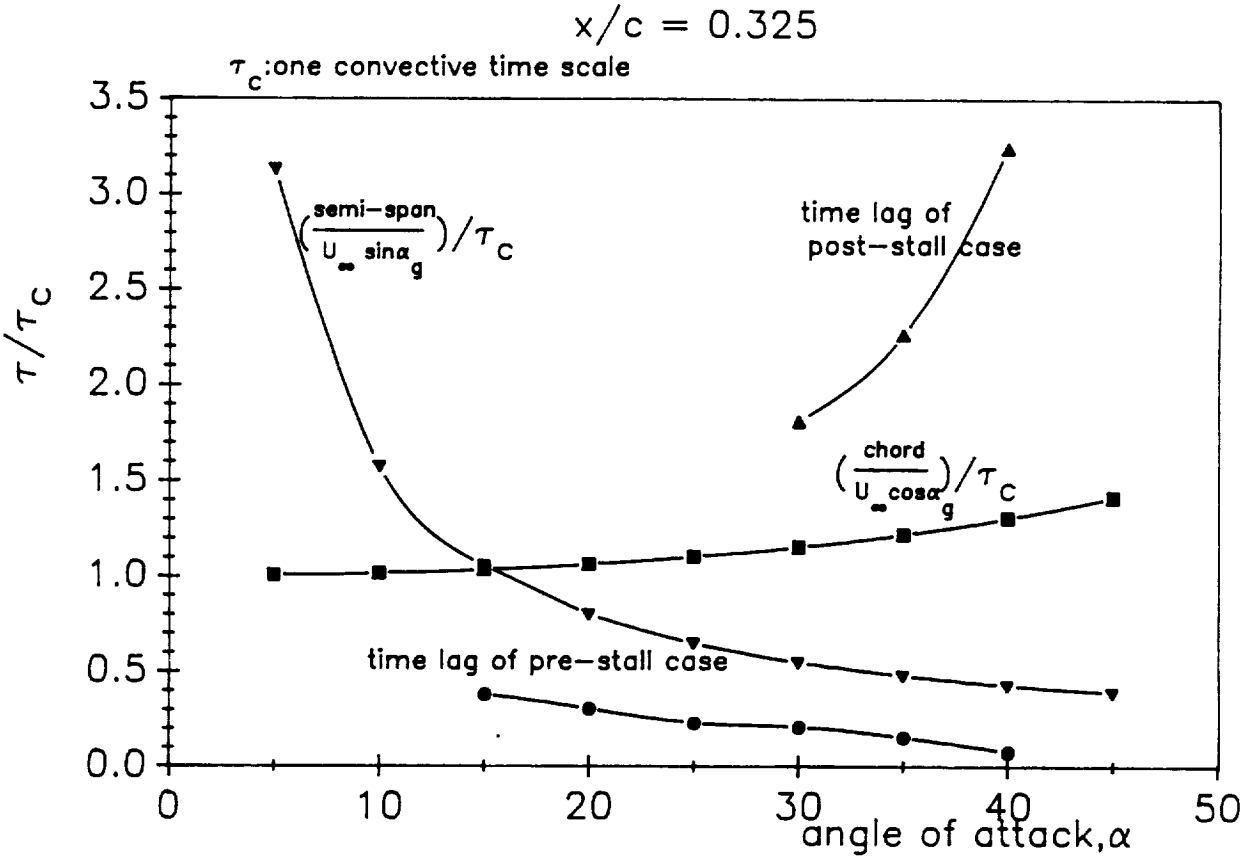

Figure 4.50 Behaviour of time lag in quasi-steady comparison

Chapter 5
Conclusions and Recommendations

5.1 Conclusions

An experimental study of steady and unsteady vortical flow control on delta wings has been successfully carried out by applying "Tangential Leading Edge Blowing(TLEB)" to the rounded leading edge of a delta wing. The main conclusions that have been arrived at in connection with the use of TLEB are as follows:

1. TLEB has been demonstrated as an effective means for controlling the vortical flow over a delta wing over a wide range of angles of attack. TLEB causes a viscous-inviscid interaction since the tangential jet delays primary separation and modifies the vortex equilibrium. That can cause major changes to the vortical flow field.

2. The effect of TLEB on steady vortical flow can be described by introducing the concept of vortex effective angle of attack. The influence of TLEB may be thought of as reducing the vortex effective angle of attack with increasing blowing strength.

3. In regions where the vortical flow is stable and well defined (i.e., pre-stall condition) the flow can be modified by TLEB with time lags of the order of one convective time or less.

4. For the case where a vortex burst is present over the wing surface (i.e., post-stall condition), unsteady TLEB is capable of 'unbursting' the vortex and significantly augmenting the lift although the time lags involved with this vortex re-organization are 3 - 4 times one convective time.

5. The short time scale operation is suggested to be a function of the cross flow parameter and this fast re-organization process is related to the cross flow equilibrium.

6. The long time scale operation is suggested to be a function of the severity of the vortex burst and the modification of the wake in response to the changing lift. This relatively long re-organization process is related to the three-dimensional vortex equilibrium.

7. Required blowing jet momentum to modify the vortical flow is relatively small compared to other "inviscid interaction" type blowing schemes. The efficiency of TLEB device increases with the blowing jet velocity so that reductions in the blowing slot dimensions may further improve the efficiency of TLEB.

In summary, TLEB is particularly useful at high angles of attack to delay vortex breakdown and to restore an orderly vortical flow field. The net result of blowing is to control the vortex, allowing pre-stall conditions at high angles of attack and increases in maximum normal force with angle of attack. It is expected that TLEB is capable of transient operation at rates that will provide both pitch and roll control during extended aircraft maneuvers.

5.2 Recommendations

The following research is suggested to improve and extend the present results;

First, conduct static and dynamic tests of a full-span delta wing with TLEB. From the half-span results, it appears promising to control asymmetric leading edge vortices by applying asymmetric TLEB. In this case, the leading edge vortex is affected by the blowing jet from both leading edges. The interaction between the vortex flow and the blowing jet from both sides cannot be observed with a half-span model configuration due to the implied symmetry. The static and dynamic measurements of force and moment responses with symmetric and asymmetric blowing could provide the input for the formulation of control laws for active control of vortical flows during unsteady maneuvers.

Second, develop a simple model for unsteady vortex re-organization (see Appendix A). It has been shown that the unsteady contribution, including the unsteady lag effect in the vortex re-organization, is related to the function f (section 4.1.2) which describes the steady state vortex contribution. The derivative of the function f with respect to vortex effective angle of attack and rate of change of blowing strength may be important parameters. If unsteady forces and moments data were available, then a simple correlation of unsteady effects with these parameters could be attempted.

Third, study the possible similarities between TLEB and unsteady pitch. A number of researchers have conducted experiments on unsteady

pitching delta wings [36,37,38,39,40]. With TLEB, the geometric angle of attack is fixed but the effective angle of attack is changed by blowing, whereas the geometric angle of attack is changed during unsteady pitching. Despite the modification of the vortex flow being achieved by two different mechanisms, the positive pitching rate corresponds to negative rate of change of blowing strength and vice versa. The unsteady lag effects from those two different vortex re-organization procedures are very similar. If the parameters for unsteady effects are identified then they might be applied to other devices for leading edge vortex flow control.

Concerning the practical application of TLEB, additional recommendations are made.

(1) Reynolds number effects

The present qualitative experimental work was conducted in a very limited range of Reynolds number for low subsonic flow. Primary separation line modification around the rounded leading edge is definitely a viscous phenomenon, so a quantitative study regarding the effects of Reynolds number is suggested.

Futhermore, curvature of the rounded leading edge with blowing coupled with the viscous effects must affect the primary separation line and resulting wing surface pressure. Therefore, the effects of greater leading edge curvature with blowing on the resulting vortical flow should be studied.

(2) Efficiency of TLEB devices

The amount of jet momentum to achieve the required modification of vortical flow is a crucial factor for this kind of scheme. The fact that a large jet velocity can improve the efficiency of the scheme is already verified. But the optimization of the slot geometry and the shape of the rounded leading edge must be investigated for maximum efficiency.

REFERENCES

[1] Herbst,W.B., "Dynamics of Air Combat", Journal of Aircraft, Vol.20, July 1983, pp.594-598.

[2] Orlik-Rückemann,K.J., "Aerodynamic Aspects of Aircraft Dynamics at High Angles of Attack", Journal of Aircraft, Vol.20, Sep.1983, pp.737-752

[3] Ericsson,L.E., "The Fluid Mechanics of Slender Wing Rock", Journal of Aircraft, Vol.21, May 1984, pp.322-328.

[4] Malcolm,G.N. and Skow,A.M., "Flow Visualization Study of Vortex Manipulation of Fighter Configurations at High Angles of Attack", AGARD CP-413, Oct.1986.

[5] Bird,J.D., "Tuft-Grid Surveys at Low Speeds for Delta Wings", NASA TN D-5045, Feb. 1969.

[6] Yeh,D.,Tavella,D.A. and Roberts,L., "Numerical Study of Delta Wing Leading Edge Blowing", JIAA TR-86, Stanford University, July 1988.

[7] Alexander,A.J., "Experiments on a Delta Wing Using Leading Edge Blowing to Remove the Secondary Separation", Report No.161, The College of Aeronautics, Cranfield, May 1963.

[8] Alexander,A.J., "Experimental Investigation on a Cropped Delta Wing with Edge Blowing", Aero. Research Council 25213, June 1963.

[9] Trebble,W.J.B., "Exploratory Investigation of the Effects of Blowing from the Leading Edge of Delta Wing", Aero. Research Council R & M 3518, April 1966.

[10] Spillman,J. and Goodridge,M., "Flow Characteristics about a Delta Wing at 15^0 Incidence with and without Edge Blowing", Cranfield Report Aero. No.9, April 1972.

[11] Bradley,R.G. and Wray,W.O., "A Conceptual Study of Leading-Edge Vortex Enhancement by Blowing", Journal of Aircraft, Vol.11, July 1973, pp.33-38.

[12] Campbell,J.F., "Effect of Spanwise Blowing on the Pressure Field and Vortex Lift Characteristics of a 44^0 Swept Trapezoidal Wing", NASA TN D-7907, 1975.

[13] Campbell,J.F., "Augmentation of Vortex Lift by Spanwise Blowing", Journal of Aircraft, Vol.13, Sep.1976, pp.727-732.

[14] Anglin,E.L. and Satran,D., "Effects of Spanwise Blowing on Two Fighter Airplane Configuration", Journal of Aircraft, Vol.17, Dec.1980, pp.883-889.

[15] Iwanski,K.P.,Ng,T.T. and Nelson,R.C.,"An Investigation of the Vortex Flow over a Delta Wing with and without External Jet Blowing", M.S.Thesis, Dept. of Aerospace and Mechanical Eng.,University of Notre Dame, April 1988.

[16] Visser,K.D.,Nelson,R.C. and Ng,T.T.,"An Investigation of the Effects of an External Jet on the Performance of a Highly Swept Delta Wing", M.S.Thesis, Dept. of Aerospace and Mechanical Eng.,University of Notre Dame, April 1988.

[17] Rao,D.M., "Leading-Edge Vortex Flap Experiments on a 74-Deg. Delta Wing", NASA CR-159161,1979.

[18] Marchman,J.F., Manor,D. and Plentovich,E.B., "Performance Improvement of Delta Wings at Subsonic Speeds Due to Vortex Flaps", AIAA Paper 80-1802, Aug.1980.

[19] Rao,D.M., Moskovitz,C. and Murri,D.G., "Forebody Vortex Management for Yaw Control at High Angles of Attack", Journal of Aircraft, Vol.24, April 1987, pp.248-254.

[20] Wentz,W.H.Jr. and Kohlman,D.L., "Wind Tunnel Investigation of Vortex Breakdown on Slender Sharp-Edged Wings", NASA CR-98737, 1969.

[21] Bartlett,C.E. and Vidal,R.J., "Experimental Investigation of Influence of Edge Shape on the Aerodynamic Characteristics of Low Aspect Ratio Wings at Low Speeds", Journal of Aeronautical Sciences, Vol.22, Aug.1955, pp.517-533,588.

[22] Tosti, Louis P., "Low-Speed Static Stability and Damping in Roll Characteristics of Some Swept and Unswept Low Aspect Ratio Wings", NASA TN 1468, 1947.

[23] Polhamus,E.C., "Charts for Predicting the Subsonic Vortex Lift Characteristics of Arrow, Delta, and Diamond Wings", NASA TN D-6243, April 1971.

[24] Erickson,G.E. and Campbell,J.F., "Flow Visualization of Leading-Edge Vortex Enhancement by Spanwise Blowing", NASA TM X-72702, July 1975.

[25] Wood,N.J. and Nielsen,J., "Circulation Control Airfoils - Past, Present and Future", AIAA Paper 85-0204, 1985.

[26] Wood,N.J. and Roberts,L., "The Control of Vortical Lift on Delta Wings by Tangential Leading Edge Blowing", AIAA Paper 87-0158, 1987.

[27] Wood,N.J., Roberts,L. and Lee,K.T., "The Control of Vortical Flow on Delta Wings at High Angles of Attack", AIAA Paper 87-2278, 1987.

[28] Wood,N.J., Lee,K.T. and Roberts,L., "Dynamic Control of Vortical Flow on Delta Wings at High Angles of Attack", AIAA Paper 88-4333-CP, 1988.

[29] Press,W.H., Flannery,B.P., Teukolsky,S.A. and Vetterling,W.T., Numerical Recipes, Cambridge University Press, 1986, pp.495-497.

[30] Küchemann,D., The Aerodynamic Design of Aircraft, Pergamon Press, Oxford, England, 1978, pp.338-438.

[31] Elle,B.J., "An Investigation at Low Speed of the Flow near the Apex of Thin Delta Wings with Sharp Leading Edges", Aero. Research Council R & M 3176, Jan.1958.

[32] Wood,N.J. and Nielson,J., "Circulation Control Airfoils as Applied to Rotary-Wing Aircraft", Journal of Aircraft, Vol.23, Dec.1986, pp.865-875.

[33] Wood,N.J., "The Aerodynamics of Circulation Control Aerofoils", JIAA TR-41, Stanford University, July 1981.

[34] Hummel,D., "On the Vortex Formation over a Slender Wing at Large Angles of Incidence", High Angle of Attack Aerodynamics, AGARD CP-247, Paper No.15, Jan.1979.

[35] Levin,D. and Katz,J., "Dynamic Load Measurements with Delta Wings Understanding Self-Induced Roll Oscillations", Journal of Aircraft, Vol.21 No.1, Jan.1984, pp.30-36.

[36] Bragg,M.B. and Soltani,M.R., "An Experimental Study of the Effect of Asymmetrical Vortex Bursting on a Pitching Delta Wing"' AIAA Paper 88-4334.

[37] Gad-el-Hak,Mohamed. and Ho,C.M., "The Pitching Delta Wing", AIAA Journal, Vol.23, Nov.1985, pp.1660-1665.

[38] Lemay,S.P., Batill,S.M. and Nelson,R.C., "Leading Edge Vortex Dynamics on a Pitching Delta Wing", AIAA Paper 88--2559-CP, 1988.

[39] Soltani,M.R. and Bragg,M.R., "Experimental Measurements on an Oscillating 70-Degree Delta Wing in Subsonic Flow", AIAA Paper 88-2576-CP, 1988.

[40] Jarrah, Mohammad-Ameen M., "Unsteady Aerodynamics of Delta Wings Performing Maneuvers to High Angle of Attack", Ph.D Thesis, Stanford University, Dept. of Aero. & Astro., Dec.1988.

[41] Brown,C.E. and Michael,W.H.,"On Slender Delta Wings with Leading Edge Separation", NACA TN 3430, April 1955.

APPENDIX A

Simplified Model of Unsteady Blowing Effects

In this simplified model it is assumed that the vortical flow is incompressible and has a velocity potential expressed as

$$\phi = U_\infty x + \phi' \tag{A.1}$$

where ϕ' is the perturbation from the uniform stream potential.

The unsteady pressure may be derived from the Bernoulli equation as

$$\frac{p}{\rho_\infty} = \text{const} - \frac{\partial \phi'}{\partial t} - \frac{1}{2}\left(U_\infty^2 + 2\frac{\partial \phi'}{\partial x} U_\infty\right) \tag{A.2}$$

where terms of $O(\frac{\partial \phi'}{\partial x})^2$ have been neglected.

The disturbance pressure $p' = p - p_\infty$ can therefore be written

$$\frac{p'}{\rho_\infty} = -\left(\frac{\partial \phi'}{\partial t} + U_\infty \frac{\partial \phi'}{\partial x}\right) \tag{A.3}$$

satisfying the condition of no disturbance at infinity.

Although the form of ϕ' is not known, the experimental measurements of the pressure distribution suggest that the following assumed form be assumed

$$\phi' = U_\infty c \left[\left(\frac{\alpha}{\epsilon}\right) F_{att}\left(\frac{x}{c}, \frac{y}{c}, \frac{z}{c}\right) + f\left(\frac{\alpha}{\epsilon} - kC_\mu\right) F_{vor}\left(\frac{x}{c}, \frac{y}{c}, \frac{z}{c}\right)\right] \tag{A.4}$$

reflecting the two contributions due to the attached flow and the vortical flow. Here the time dependence of ϕ' is assumed to be contained only in

the function $f(\frac{\alpha}{\epsilon} - kC_\mu)$ through the unsteady blowing parameter C_μ. From (A.3) and (A.4), therefore the unsteady pressure coefficient may be written

$$C_p = \frac{p'}{\frac{1}{2}\rho_\infty U_\infty^2} = -2 \left[(\frac{\alpha}{\epsilon}) \frac{\partial}{\partial(x/c)} F_{att} + f(\frac{\alpha}{\epsilon} - kC_\mu) \frac{\partial}{\partial(x/c)} F_{vor} \right]_{z=0}$$

(steady pressure perturbation)

$$+ 2 \left[F_{vor} \, k \, \dot{C}_\mu \frac{c}{U_\infty} f'(\frac{\alpha}{\epsilon} - kC_\mu) \right]_{z=0} \qquad (A.5)$$

(unsteady pressure perturbation)

where f' is the derivative of f with respect to the argument and $\dot{C}_\mu \frac{c}{U_\infty}$ is a dimensionless time derivative of C_μ.

If the pressure distribution is now integrated over the wing area the result will be of the form

$$\frac{C_N}{\epsilon^2} = (\frac{\alpha}{\epsilon}) \left[\iint_A \left(\frac{\partial}{\partial(x/c)} F_{att} \right)_{z=0} d(\frac{x}{c}) d(\frac{y}{c}) \right]$$

$$+ f(\frac{\alpha}{\epsilon} - kC_\mu) \left[\iint_A \left(\frac{\partial}{\partial(x/c)} F_{vor} \right)_{z=0} d(\frac{x}{c}) d(\frac{y}{c}) \right]$$

$$- k \frac{c}{U_\infty} \dot{C}_\mu f'(\frac{\alpha}{\epsilon} - kC_\mu) \left[\iint_A (F_{vor})_{z=0} d(\frac{x}{c}) d(\frac{y}{c}) \right] \qquad (A.6)$$

and the square brackets will each give a constant value for a particular configuration of wing. Thus equation (A.6) will take the form

$$\frac{C_N}{\epsilon^2} = k_1 (\frac{\alpha}{\epsilon}) + k_2 f(\frac{\alpha}{\epsilon} - kC_\mu) + k_3 (\frac{c}{U_\infty} \dot{C}_\mu) f'(\frac{\alpha}{\epsilon} - kC_\mu) \qquad (A.7)$$

As can be seen, the first and second terms represent the steady effects of angle of attack and blowing whereas the third term represents the unsteady contribution due to blowing. The constants k_1, k_2, k_3 must be determined experimentally.

Equation (A.7) suggests that the unsteady contribution (i.e. the total less the quasi-steady) should vary as

$$\frac{c}{U_\infty} \dot{C}_\mu \, f'\left(\frac{\alpha}{\epsilon} - kC_\mu\right)$$

or

$$\frac{\Delta\left(\frac{C_N}{\epsilon^2}\right)_{\text{unsteady}}}{\frac{c}{U_\infty} \dot{C}_\mu} \propto f'\left(\frac{\alpha}{\epsilon} - kC_\mu\right) \qquad \text{(A.8)}$$

and it is possible to check this variation using the experimental data. In order to incorporate the effect of a time lag the argument of f' should be evaluated at a time $t - \Delta t$ where Δt must be found experimentally.

An attempt has been made to plot both the steady and unsteady contributions with $\Delta t = 0.5 \frac{c}{U_\infty}$. The results are shown in figures (A.1) and (A.2).

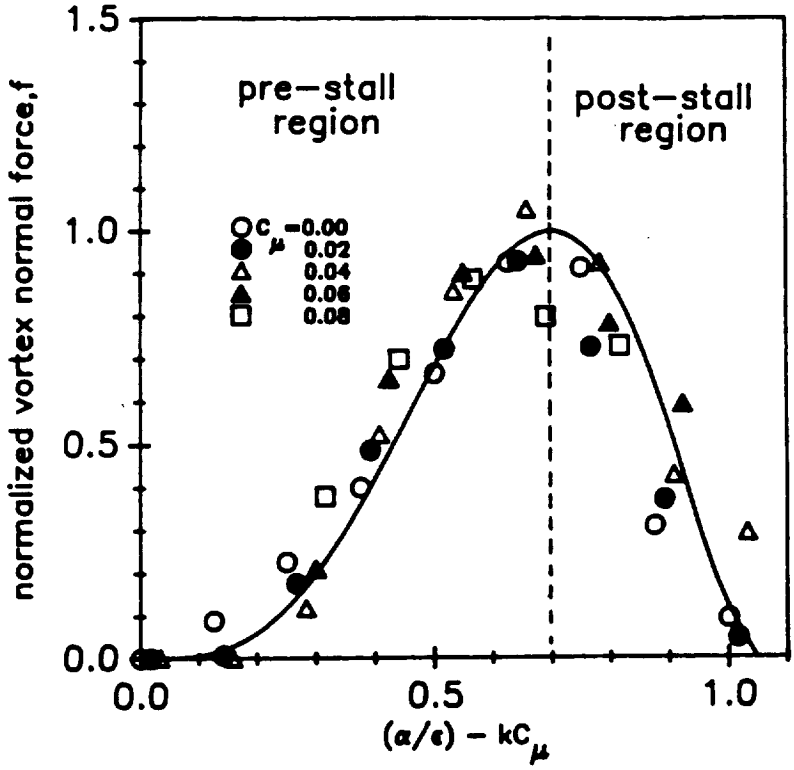

Figure A.1 Quasi-steady vortex contribution to normal force

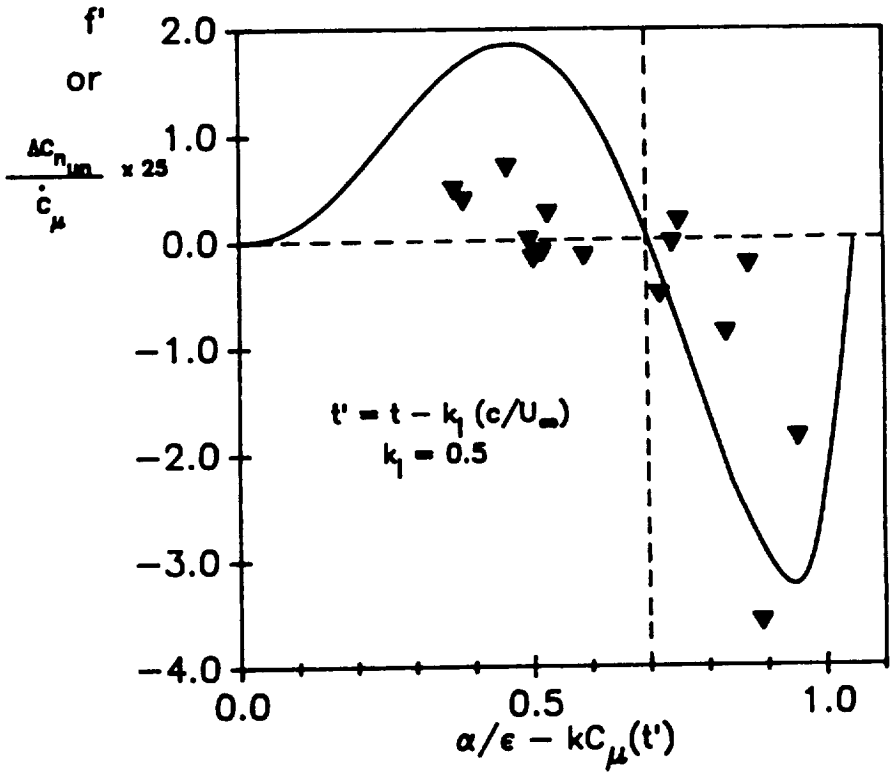

Figure A.2 Unsteady vortex contribution with time delay

The results are in qualitative agreement with the simple theory; however it is concluded that a more detailed analysis, beyond the scope of this thesis, is required. Some of the reasons for the lack of good quantitative agreement for the unsteady results are:

(1) The small disturbance approximation is for thin, slender delta wings. For this case, wing model has 6.25% thickness with respect to the root chord and 40^{o} semi-apex angle. Strictly speaking, it is not a thin, slender body.

(2) The experimental data for unsteady section normal force is not accurate enough due to the integration from the sparse unsteady pressure measurement locations. If the more accurate unsteady force data becomes available, it will be possible to check the validity of the model more precisely.

(3) This simple model assumes the conical leading edge vortex flow implicitly. But the vortical flow at the post-stall condition is not conical and the longitudinal change of three-dimensional vortex flow is an important feature of vortex re-organization. The accuracy and validity of this simple model can be improved if an adequate formulation for the unsteady time lag, Δt , as a function of effective angle of attack is introduced.